Quantum Optics Devices

Les Houches Singapore 2009
Lecture Notes

Christian Kurtsiefer
christian.kurtsiefer@gmail.com
Antía Lamas Linares
antia.lamas@gmail.com

Quantum Optics Group
Centre for Quantum Technologies
National University of Singapore
3 Science Road 2
Singapore 117543

Contents

Chapter 1

Basic field quantization - the foundations

Quantum optics devices require, as a very first step, a reasonable understanding of what a quantum description of light actually covers. In this chapter, we will probably repeat elements of electrodynamics, with some specializations relevant for the optical domain, you may have seen several times already. The intent of this very basic introduction is to establish the notions, so one can perhaps easier distinguish the quantum physics aspects from what is optics or classical electrodynamics.

Specifically, we consider here electromagnetic phenomena which take place on a time scale of $\tau \approx 10^{-15}$ s, or on wave phenomena with a characteristic length scale of $\lambda \approx 10^{-7}$ to 10^{-6} m, corresponding to energy scales of the order $E \approx \hbar/\tau \approx 10^{-19}$ J ≈ 1 eV.

An excellent reference book on the field quantization, which is the basis for the introductory part of this lecture, is Photons and Atoms: Introduction to quantum electrodynamics [1].

1.1 Recap of classical Electrodynamics

1.1.1 Maxwell equations

We begin with understanding of the treatment of time-varying electromagnetic fields in classical physics. In a nonrelativistic context (which will be the case for the scope of the matter interacting with the light field), the electromagnetic field is typically separated to two vectorial quantities with space and time as parameters, the electric and the magnetic field:

$$\mathbf{E}(\mathbf{x}, t) \qquad \mathbf{B}(\mathbf{x}, t) \tag{1.1}$$

Maxwell equations in vacuum

The dynamics of these two fields (in free space) are covered by a set of differential equations, commonly referred to as the Maxwell equations:

$$\nabla \cdot \mathbf{E}(\mathbf{x},t) = \frac{1}{\epsilon_0}\rho(\mathbf{x},t), \tag{1.2}$$

$$\nabla \times \mathbf{E}(\mathbf{x},t) = -\frac{\partial}{\partial t}\mathbf{B}(\mathbf{x},t), \tag{1.3}$$

$$\nabla \cdot \mathbf{B}(\mathbf{x},t) = 0, \tag{1.4}$$

$$\nabla \times \mathbf{B}(\mathbf{x},t) = \frac{1}{c^2}\frac{\partial}{\partial t}\mathbf{E}(\mathbf{x},t) + \frac{1}{\epsilon_0 c^2}\mathbf{j}(\mathbf{x},t) \tag{1.5}$$

Therein, the quantities $\rho(\mathbf{x},t)$ represent a local charge density (this is a scalar quantity), and $\mathbf{j}(\mathbf{x},t)$ a current density (this is a vector property), which describes the motion of charges, and is connected with the charge density through the charge current. Typically, we set $\rho = 0$ and $\mathbf{j} = 0$ in most of the space we consider, which allows us to understand the dynamics of a 'free field'.

Energy content in the electromagnetic field

An important notion for quantizing the electromagnetic field will be the total energy contained in the field of a given volume. For a system without dielectric media, the total energy of the electromagnetic field is given by

$$H = \frac{\epsilon_0}{2}\int d\mathbf{x}\,[E^2 + c^2 B^2]\,. \tag{1.6}$$

Here and subsequently, $\int d\mathbf{x}$ refers to volume integration over the relevant space. This is only the energy of the free field, without any charges and currents present; they can be added later.

1.2 Sorting the mess: Count your degrees of freedom

The Maxwell equations are a set of coupled differential equations where $\mathbf{E}$ and $\mathbf{B}$ (in the case of free space) are the variables describing the state of the system completely. More specifically, each point in the volume of interest has six scalar variables, and the state of the system is determined by describing each of these six field components at each point in space. However, this description is redundant. In the next subsection, we should find out how to eliminate that redundancy, and will arrive at the minimal set of variables we need to describe electromagnetic fields. Then, we will try to decouple the remaining equations of motion by transformation on normal coordinates.

1.2.1 Reducing degrees of freedom: Potentials and gauges

It can be shown that the electric and magnetic fields can always be written as derivatives of two fields $\mathbf{A}(\mathbf{x},t)$ and $U(\mathbf{x},t)$ called vector potential and scalar potential, respectively:

$$\mathbf{E}(\mathbf{x},t) = -\frac{\partial}{\partial t}\mathbf{A} - \nabla U(\mathbf{x},t), \tag{1.7}$$

$$\mathbf{B}(\mathbf{x},t) = \nabla \times \mathbf{A}(\mathbf{x},t) \tag{1.8}$$

We can then rewrite Maxwell equations in term of the potentials by substituting eqns (1.7) and (1.8) into eqns (1.2) and (1.5), leading to

$$\nabla^2 U(\mathbf{x},t) = -\frac{1}{\epsilon_0}\rho(\mathbf{x},t) - \nabla\cdot\frac{\partial}{\partial t}\mathbf{A}(\mathbf{x},t), \tag{1.9}$$

$$\left(\frac{1}{c^2}\frac{\partial^2}{\partial t^2} - \nabla^2\right)\mathbf{A}(\mathbf{x},t) = \frac{1}{\epsilon_0 c^2}\mathbf{j}(\mathbf{x},t) - \nabla\left[\nabla\cdot\mathbf{A}(\mathbf{x},t) + \frac{1}{c^2}\frac{\partial}{\partial t}U\right] \tag{1.10}$$

All of these expressions are derivatives but completely describe the evolution of the field. By this trick, the number of variables describing the free field is already reduced to four scalar values for each point. There can be additive constants to the potentials U and $\mathbf{A}$ which leave the actual fields $\mathbf{E}$ and $\mathbf{B}$ and their dynamics unchanged. With the following transformation on the potentials

$$\mathbf{A}(\mathbf{x},t) \rightarrow \mathbf{A}'(\mathbf{x},t) = \mathbf{A}(\mathbf{x},t) + \nabla F(\mathbf{x},t), \tag{1.11}$$

$$U(\mathbf{x},t) \rightarrow U'(\mathbf{x},t) = U(\mathbf{x},t) - \frac{\partial}{\partial t}F(\mathbf{x},t)\,, \tag{1.12}$$

where $F(\mathbf{x},t)$ is any scalar field. This transformation of potentials has no physically observable consequences: electric and magnetic fields remain unchanged, and they are the quantities necessary to determine the forces on charged particles. Such a transformation is called *gauge transformation*, and the property of the fields $\mathbf{E}$ and $\mathbf{B}$ being invariant under such a transformation is referred to as *gauge invariance*.

Therefore, we are free to choose the gauge function $F(\mathbf{x},t)$ to come up with a particularly simple form of the equations of motion. There are two typical gauges used in electrodynamics. For many occasions, e.g. the free field, the so-called *Lorentz gauge* is very convenient. It is defined by

$$\nabla\cdot\mathbf{A}(\mathbf{x},t) + \frac{1}{c^2}\frac{\partial}{\partial t}U(\mathbf{x},t) = 0. \tag{1.13}$$

Equations (1.9) and (1.10) under Lorentz gauge take a particularly simple and symmetric form:

$$\Box U(\mathbf{x},t) = \frac{1}{\epsilon_0}\rho(\mathbf{x},t)\,, \tag{1.14}$$

$$\Box\mathbf{A}(\mathbf{x},t) = \frac{1}{\epsilon_0 c^2}\mathbf{j}(\mathbf{x},t)\,, \tag{1.15}$$

with the definition of the differential operator $\Box$ referred to as d'Alembert - operator:

$$\Box := \frac{1}{c^2}\frac{\partial^2}{\partial t^2} - \nabla^2. \tag{1.16}$$

This form of the Maxwell equations is particularly suited for problems where a Lorentz invariance of the problem is important. However, for the purpose of optics or interaction with atoms of non-relativistic speed, another gauge is more favorable, the so-called Coulomb gauge:

$$\nabla \cdot \mathbf{A}(\mathbf{x}, t) = 0 \tag{1.17}$$

Equations (1.9) and (1.10) under Coulomb gauge take the form:

$$\nabla^2 U(\mathbf{x}, t) = -\frac{1}{\epsilon_0}\rho(\mathbf{x}, t), \tag{1.18}$$

$$\Box \mathbf{A}(\mathbf{x}, t) = \frac{1}{\epsilon_0 c^2}\mathbf{j}(\mathbf{x}, t) - \frac{1}{c^2}\nabla\frac{\partial}{\partial t}U(\mathbf{x}, t) \tag{1.19}$$

If we operate in a region without free charges, i.e. $\rho(\mathbf{x}, t) = 0$, we have $U(\mathbf{x}, t) = 0$ everywhere, and the free field is completely described by the three components of the vector potential $\mathbf{A}(\mathbf{x}, t)$. Its evolution in time is governed by a single equation of motion, a simplified version of (1.19). Thus, the gauge invariance helps us to identify a redundancy in the combination of scalar and vector potential and their corresponding equations of motion.

1.2.2 Decoupling of degrees of freedom: Fourier decomposition

Now, we have to address another problem - the Maxwell equations form a set of coupled differential equations. The electromagnetic scenery in a region of space is thus described by the potentials $U(\mathbf{x}, t)$ and $\mathbf{A}(\mathbf{x}, t)$, but the values at different points (x, y, z) in space are coupled via the spatial differential operators. We therefore need to sort out this problem before we continue searching for further redundancies.

In order to arrive at the simplest (as in separable) description of the evolution of the field, we try to apply a mode decomposition of the field, very similar to the mode decomposition of mechanical oscillators in coupled systems like the lattice vibration or the vibration of a membrane. There, we try to express the local variables (like local displacement) as a function of normal coordinates, which have a completely decoupled evolution in time.

Such an attempt will be helpful for the field quantization. For most occasions, we choose the most common normal coordinate transformation for a system (as defined by the structure of equations of motion, and the boundary conditions) with translational invariance, namely the *Fourier transformation*. It has to be

kept in mind that this is only a convenient choice, and by no means the only normal coordinate choice to make. There are many occasions in quantum optics where a different mode decomposition is appropriate, we will come back to that later in Section 1.4.

When using the Fourier transformation as the transformation to normal coordinates, plane waves (which are solutions of the homogenous Maxwell equations) form the basis for our solution. The amplitudes of various plane waves, characterized by a wave vector k, will be the new coordinates. We still want to arrive at a description of the electromagnetic field where we keep time as the parameter describing the evolution of the variables; this choice is suited to describe observations in typical non-relativistic lab environments. Therefore, we restrict the Fourier transformation only on the spatial coordinates. The transformation and their inverse for the electrical field reads explicitly:

$$\boldsymbol{\mathscr{E}}(\mathbf{k},t) = \frac{1}{(2\pi)^{3/2}}\int d\mathbf{x}\,\mathbf{E}(\mathbf{x},t)e^{-i\mathbf{k}\cdot\mathbf{r}}, \tag{1.20}$$

$$\mathbf{E}(\mathbf{x},t) = \frac{1}{(2\pi)^{3/2}}\int d\mathbf{k}\,\boldsymbol{\mathscr{E}}(\mathbf{k},t)e^{i\mathbf{k}\cdot\mathbf{r}} \tag{1.21}$$

The quantity $\boldsymbol{\mathscr{E}}(\mathbf{k},t)$ is a set of electric field amplitudes for every $\mathbf{k}$, which we will lead to a decoupled set of equation of motion, and thus form a suitable set of normal coordinates.

Similarly, we have transformations for all the other field quantities we have encountered so far:

$$\mathbf{E}(\mathbf{x},t) \leftrightarrow \boldsymbol{\mathscr{E}}(\mathbf{k},t), \tag{1.22}$$

$$\mathbf{B}(\mathbf{x},t) \leftrightarrow \boldsymbol{\mathscr{B}}(\mathbf{k},t), \tag{1.23}$$

$$\mathbf{A}(\mathbf{x},t) \leftrightarrow \boldsymbol{\mathscr{A}}(\mathbf{k},t), \tag{1.24}$$

$$U(\mathbf{x},t) \leftrightarrow \mathscr{U}(\mathbf{k},t), \tag{1.25}$$

$$\rho(\mathbf{x},t) \leftrightarrow \rho(\mathbf{k},t), \tag{1.26}$$

$$\mathbf{j}(\mathbf{x},t) \leftrightarrow \mathrm{j}(\mathbf{k},t) \tag{1.27}$$

One thing to take note is that, while the actual fields are real, the quantities in Fourier space can be complex. The reality of the electric field in real space, mathematically expressed by $\mathbf{E}^* = \mathbf{E}$, implies that

$$\boldsymbol{\mathscr{E}}^*(\mathbf{k},t) = \boldsymbol{\mathscr{E}}(-\mathbf{k},t) \tag{1.28}$$

for the electric field. This is a redundancy to keep in mind when counting the degrees of freedom of our system.

Two of the few identities that are useful to keep in mind are the Parseval-Plancherel identity and the Fourier transform of convolution product. The first one,

$$\int d\mathbf{x}\,F^*(\mathbf{x})G(\mathbf{x}) = \int d\mathbf{k}\,\mathscr{F}^*(\mathbf{k})\mathscr{G}(\mathbf{k})\,, \tag{1.29}$$

tells us that we can evaluate the integral over the whole space of a product of two functions (e.g. fields) also in a similar way in Fourier space. This will come in handy for evaluating the total field energy.

The convolution product of two functions is defined as

$$F(\mathbf{x}) \otimes G(\mathbf{x}) := \frac{1}{(2\pi)^{3/2}} \int d\mathbf{x}'\, F(\mathbf{x}')G(\mathbf{x}-\mathbf{x}')\,, \tag{1.30}$$

where the integration is carried out over a three-dimensional space. A similar definition of a convolution product can be defined in one dimension, with a properly adjusted normalization constant. Such a product typically appears in the evolution of correlation functions.

It can easily be shown that the Fourier transformation of the convolution product is just the product of the Fourier-transformed versions of the two functions:

$$F(\mathbf{x}) \otimes G(\mathbf{x}) \leftrightarrow \mathscr{F}(\mathbf{k})\mathscr{G}(\mathbf{k}) \tag{1.31}$$

This is a useful relation also in practical situations when correlations between functions need to be evaluated, as the numerical evaluation of a Fourier transformation is extremely efficient.

So far, we have not seen that Fourier transformation helps to decouple the Maxwell equations as the equations of motion for the fields, and that this is therefore actually a transformation to normal coordinates. For this, we use the transformation rules for differential operators,

$$\nabla\cdot \leftrightarrow i\mathbf{k}\cdot \quad , \qquad \nabla\times \leftrightarrow i\mathbf{k}\times \qquad \text{etc.} \tag{1.32}$$

to rewrite the Maxwell equations (1.2) - (1.5) in terms of their Fourier-transformed fields $\boldsymbol{\mathscr{E}}(\mathbf{k},t)$ and $\boldsymbol{\mathscr{B}}(\mathbf{k},t)$:

$$\begin{aligned}
i\mathbf{k}\cdot\boldsymbol{\mathscr{E}}(\mathbf{k},t) &= \frac{1}{\epsilon_0}\rho(\mathbf{k},t) && (1.33)\\
i\mathbf{k}\times\boldsymbol{\mathscr{E}}(\mathbf{k},t) &= -\frac{\partial}{\partial t}\boldsymbol{\mathscr{B}}(\mathbf{k},t) && (1.34)\\
i\mathbf{k}\cdot\boldsymbol{\mathscr{B}}(\mathbf{k},t) &= 0 && (1.35)\\
i\mathbf{k}\times\boldsymbol{\mathscr{B}}(\mathbf{k},t) &= -\frac{1}{c^2}\frac{\partial}{\partial t}\boldsymbol{\mathscr{E}}(\mathbf{k},t) + \frac{1}{\epsilon_0 c^2}\mathbf{j}(\mathbf{k},t) && (1.36)
\end{aligned}$$

This is now a set of coupled differential equations *for each* $\mathbf{k}$, but the coupling extends only over the electric and magnetic field components for a given $\mathbf{k}$, not between those of different $\mathbf{k}$ anymore. Thus, the Fourier transformation helped to arrive at a decoupling between the field amplitudes at different locations $\mathbf{x}$ in space, and thus is a transformation on normal coordinates.

Similarly, the connections between fields and potentials in Fourier space are given by

$$\mathscr{B}(\mathbf{k},t) = i\mathbf{k}\times\mathscr{A}(\mathbf{k},t), \tag{1.37}$$

$$\mathscr{E}(\mathbf{k},t) = -\frac{\partial}{\partial t}\mathscr{A}(\mathbf{k},t) - i\mathbf{k}\mathscr{U}(\mathbf{k},t)\,, \tag{1.38}$$

and the gauge transformations turn into

$$\mathscr{A}(\mathbf{k},t) \rightarrow \mathscr{A}'(\mathbf{k},t) = \mathscr{A}(\mathbf{k},t) + i\mathbf{k}\mathscr{F}(\mathbf{k},t), \tag{1.39}$$

$$\mathscr{U}(\mathbf{k},t) \rightarrow \mathscr{U}'(\mathbf{k},t) = \mathscr{U}(\mathbf{k},t) - \frac{\partial}{\partial t}\mathscr{F}(\mathbf{k},t). \tag{1.40}$$

The equations of motion for the potentials transform into

$$k^2\mathscr{U}(\mathbf{k},t) = \frac{1}{\epsilon_0}\rho(\mathbf{k},t) + i\mathbf{k}\cdot\frac{\partial}{\partial t}\mathscr{A}(\mathbf{k},t), \tag{1.41}$$

$$\frac{1}{c^2}\frac{\partial^2}{\partial t^2}\mathscr{A}(\mathbf{k},t) + k^2\mathscr{A}(\mathbf{k},t) = \frac{1}{\epsilon_0 c^2}\mathbf{j}(\mathbf{k},t) - i\mathbf{k}\frac{1}{c^2}\frac{\partial}{\partial t}\mathscr{U}(\mathbf{k},t)\,. \tag{1.42}$$

Again, these equations are simpler in Fourier space because partial differential equations were transformed into a set of ordinary differential equations for the different $\mathbf{k}$. Thus, the Maxwell equations are strictly local in the Fourier space.

1.2.3 Longitudinal and transverse fields

In an attempt to reduce the degrees of freedom we have to consider for a field quantization further, there is another – more subtle – redundancy we need to address. It is connected with the fact that propagating plane waves of electromagnetic fields are *transverse fields*, and can be decomposed in only two polarization components.

As a mathematical definition, a vector field $\mathbf{V}_\parallel(\mathbf{x})$ is called a *longitudinal* vector field if and only if

$$\nabla\times\mathbf{V}_\parallel(\mathbf{x}) = 0\,. \tag{1.43}$$

This equation can be easier interpreted when written in Fourier space:

$$i\mathbf{k}\times\boldsymbol{\mathscr{V}}_\parallel(\mathbf{k}) = 0 \tag{1.44}$$

The vanishing cross product between $\boldsymbol{\mathscr{V}}_\parallel$ and $\mathbf{k}$ simply means that both vectors are parallel. Thus, a longitudinal vector field has its components aligned with the wave vector $\mathbf{k}$.

Similarly, one can define a *transverse* vector field $\mathbf{V}_\perp(\mathbf{x})$ the following properties:

$$\nabla\cdot\mathbf{V}_\perp(\mathbf{x}) = 0\,, \tag{1.45}$$

$$i\mathbf{k}\cdot\boldsymbol{\mathscr{V}}_\perp(\mathbf{k}) = 0\,. \tag{1.46}$$

This time, the vector $\boldsymbol{\mathscr{V}}_\perp$ is perpendicular to the wave vector of a plane wave.

With these definitions, one may decompose any vector field $\mathbf{V}(\mathbf{x})$ into longitudinal and transverse part. This decomposition can be carried out conveniently from a representation in Fourier space:

$$\boldsymbol{\mathscr{V}}_\parallel(\mathbf{k}) = \boldsymbol{\kappa}[\boldsymbol{\kappa}\cdot\boldsymbol{\mathscr{V}}(\mathbf{k})]\,, \tag{1.47}$$

$$\boldsymbol{\mathscr{V}}_\perp(\mathbf{k}) = \boldsymbol{\mathscr{V}}(\mathbf{k}) - \boldsymbol{\mathscr{V}}_\parallel(\mathbf{k})\,, \tag{1.48}$$

where $\boldsymbol{\kappa}$ is the unit vector in the direction of $\mathbf{k}$. The longitudinal and transverse fields ($\mathbf{V}_\parallel(\mathbf{x})$ and $\mathbf{V}_\perp(\mathbf{x})$) in real space can then be obtained via inverse Fourier transformation. This gives the decomposition of the following:

$$\mathbf{V}(\mathbf{x}) = \mathbf{V}_\parallel(\mathbf{x}) + \mathbf{V}_\perp(\mathbf{x}). \tag{1.49}$$

With the definitions of longitudinal and transverse fields, one can see that that the magnetic field is purely transverse. This is clear from Maxwell equation (1.35) which gives

$$\boldsymbol{\mathscr{B}}_\parallel(\mathbf{k},t) = 0 = \mathbf{B}_\parallel(\mathbf{x},t)^1. \tag{1.50}$$

Similarly, the expression for the source term of electrical field using eqns (1.33) and (1.47), allows to isolate the parallel component of the electrical field $\boldsymbol{\mathscr{E}}_\parallel(\mathbf{k},t)$ in Fourier space:

$$\boldsymbol{\mathscr{E}}_\parallel(\mathbf{k},t) = -\frac{i}{\epsilon_0}\rho(\mathbf{k},t)\frac{\mathbf{k}}{k^2} \tag{1.51}$$

The expression for the electric field in real space can be obtained by an inverse Fourier transformation. The Fourier transformation relating convolution product in real space to product in Fourier space (eqn (1.31)) can be used to arrive at:

$$\mathbf{E}_\parallel(\mathbf{x},t) = \frac{1}{4\pi\epsilon_0}\int d\mathbf{x}'\,\rho(\mathbf{x}',t)\frac{\mathbf{x}-\mathbf{x}'}{|\mathbf{x}-\mathbf{x}'|^3} \tag{1.52}$$

This seemingly innocent expression looks just like an expression known from electrostatics, where the field from a charge distribution is obtained using the Green function of a point charge. However, keep in mind that $\mathbf{E}_\parallel(\mathbf{x},t)$ is the field created by the instantaneous position of charges $\rho(\mathbf{x})$ at time t at all locations $\mathbf{x}$, and no retardation effects are taken into account. However, this *does not* violate causality since $\mathbf{E}_\parallel(\mathbf{x},t)$ itself is not a physically observable quantity on its own. What is meaningful is the total electric field, which gets complemented by the transverse field, which in turn takes care of any information propagating around about charges which may have moved.

The dynamics of the transverse and longitudinal field components are still governed by the Maxwell equations, but we are left only with two equations not vanishing to zero:

[1] This means that $\boldsymbol{\mathscr{B}}(\mathbf{k},t) = \boldsymbol{\mathscr{B}}_\perp(\mathbf{k},t)$.

$$\frac{\partial}{\partial t}\boldsymbol{\mathscr{B}}_\perp(\mathbf{k},t) = \frac{\partial}{\partial t}\boldsymbol{\mathscr{B}}(\mathbf{k},t) = -i\mathbf{k}\times\boldsymbol{\mathscr{E}}(\mathbf{k},t) = -i\mathbf{k}\times\boldsymbol{\mathscr{E}}_\perp(\mathbf{k},t), \quad (1.53)$$

$$\frac{\partial}{\partial t}\boldsymbol{\mathscr{E}}_\perp(\mathbf{k},t) = ic^2\mathbf{k}\times\boldsymbol{\mathscr{B}}(\mathbf{k},t) - \frac{1}{\epsilon_0}\mathbf{j}_\perp(\mathbf{k},t). \quad (1.54)$$

In terms of the transverse vector potential the equation of motion is given by

$$\frac{1}{c^2}\frac{\partial^2}{\partial t^2}\boldsymbol{\mathscr{A}}_\perp(\mathbf{k},t) + k^2\boldsymbol{\mathscr{A}}_\perp(\mathbf{k},t) = \frac{1}{\epsilon_0 c^2}\mathbf{j}_\perp(\mathbf{k},t). \quad (1.55)$$

For the longitudinal component, we are left with

$$k^2\mathscr{U}(\mathbf{k},t) = \frac{1}{\epsilon_0}\rho(\mathbf{k},t) + i\mathbf{k}\cdot\frac{\partial}{\partial t}\boldsymbol{\mathscr{A}}_\parallel(\mathbf{k},t). \quad (1.56)$$

If the Coulomb gauge is chosen, we have $\boldsymbol{\mathscr{A}}_\parallel(\mathbf{k},t) = 0$. Then, the Maxwell equations leave us with two distinct problems: One governs the derivation of a scalar potential $U(\mathbf{x})$ from a given charge density $\rho(\mathbf{x})$, the other one governs the evolution of propagating free fields.

Referring to eqn (1.55), for a given mode index $\mathbf{k}$, we are left with two degrees of freedom corresponding to two perpendicular directions orthogonal to $\mathbf{k}$:

$$\boldsymbol{\mathscr{A}}_\perp(\mathbf{k},t) = \sum_\varepsilon a_\varepsilon(\mathbf{k},t)\boldsymbol{\varepsilon} \quad (1.57)$$

where $\boldsymbol{\varepsilon}$ represents the two independent *polarization* directions. By using the concept of transverse fields, we finally arrived at two variables $a_\varepsilon(\mathbf{k},t)$ for each point $\mathbf{k}$ describing completely the evolution of propagating electromagnetic fields.

1.2.4 Normal coordinates - alternative approach

With the two transverse components of the vector potential for each mode index $\mathbf{k}$ and their corresponding equation of motion (1.55) we have arrived at a minimal description of the electromagnetic field. Alternatively we could arrive to a similar point by recalling eqns (1.53) and (1.54). Together with the assumption that $\mathbf{j}_\perp(\mathbf{k},t) = 0$, the two equations can be combined to:

$$\frac{\partial}{\partial t}(\boldsymbol{\mathscr{E}}_\perp[\mathbf{k},t) \mp c\boldsymbol{\kappa}\times\boldsymbol{\mathscr{B}}(\mathbf{k},t)] = \mp i\omega[\boldsymbol{\mathscr{E}}_\perp(\mathbf{k},t) \mp c\boldsymbol{\kappa}\times\boldsymbol{\mathscr{B}}(\mathbf{k},t)] \quad (1.58)$$

with $\omega = c|\mathbf{k}|$, making use of the time dependency $e^{-i\omega t}$ for the plane waves.

This suggests us to define the following two normal coordinates,

$$\boldsymbol{\alpha}(\mathbf{k},t)) := -\frac{i}{2\mathscr{N}(k)}[\boldsymbol{\mathscr{E}}_\perp(\mathbf{k},t) - c\boldsymbol{\kappa}\times\boldsymbol{\mathscr{B}}(\mathbf{k},t)], \quad (1.59)$$

$$\boldsymbol{\beta}(\mathbf{k},t)) := -\frac{i}{2\mathscr{N}(k)}[\boldsymbol{\mathscr{E}}_\perp(\mathbf{k},t) + c\boldsymbol{\kappa}\times\boldsymbol{\mathscr{B}}(\mathbf{k},t)] \quad (1.60)$$

where the normalization $\mathscr{N}(k)$ is somewhat arbitrary and will be chosen so that the Hamilton function has a nice form.

However, $\boldsymbol{\alpha}(\mathbf{k},t)$ and $\boldsymbol{\beta}(\mathbf{k},t)$ are not independent. Since $\mathbf{E}_\perp(\mathbf{x},t)$ and $\mathbf{B}(\mathbf{x},t)$ are real quantities, we have equations similar to eqn (1.28) for $\boldsymbol{\mathscr{E}}_\perp(\mathbf{k},t)$ and $\boldsymbol{\mathscr{B}}(\mathbf{k},t)$. These equations give the following relation between $\boldsymbol{\alpha}(\mathbf{k},t)$ and $\boldsymbol{\beta}(\mathbf{k},t)$:

$$\boldsymbol{\beta}(\mathbf{k},t) = -\boldsymbol{\alpha}^*(-\mathbf{k},t). \tag{1.61}$$

It is then sufficient to describe the electric and magnetic fields by one complex variable $\boldsymbol{\alpha}(\mathbf{k},t)$ only.

Using eqns (1.61), eqns (1.59) and (1.60) can be solved for $\boldsymbol{\mathscr{E}}_\perp(\mathbf{k},t)$ and $\boldsymbol{\mathscr{B}}(\mathbf{k},t)$

$$\boldsymbol{\mathscr{E}}_\perp(\mathbf{k},t) = i\mathscr{N}(k)[\boldsymbol{\alpha}(\mathbf{k},t) - \boldsymbol{\alpha}^*(-\mathbf{k},t)], \tag{1.62}$$

$$\boldsymbol{\mathscr{B}}_\perp(\mathbf{k},t) = i\frac{\mathscr{N}(k)}{c}[\boldsymbol{\kappa}\times\boldsymbol{\alpha}(\mathbf{k},t) + \boldsymbol{\kappa}\times\boldsymbol{\alpha}^*(-\mathbf{k},t)] \tag{1.63}$$

Therefore, the knowledge of $\boldsymbol{\alpha}(\mathbf{k},t)$ for all $\mathbf{k}$ enables one to derive all physical quantities like $\boldsymbol{\mathscr{E}}_\perp(\mathbf{k},t)$ and $\boldsymbol{\mathscr{B}}(\mathbf{k},t)$. Since there is no restriction to the reality of $\boldsymbol{\alpha}(\mathbf{k},t)$,they are really independent variables. The *complete* field is now described by the variables $\boldsymbol{\alpha}(\mathbf{k},t)$.

Subtracting eqn (1.53) from eqn (1.54), with the definition of $\boldsymbol{\alpha}(\mathbf{k},t)$ in mind, we have

$$\frac{\partial}{\partial t}\boldsymbol{\alpha}(\mathbf{k},t) + i\omega\boldsymbol{\alpha}(\mathbf{k},t) = \frac{i}{2\epsilon_0\mathscr{N}(k)}\mathbf{j}_\perp(\mathbf{k},t) \tag{1.64}$$

This is the equation of motion of the electromagnetic field, which is completely equivalent to eqn (1.55), this time formulated as a first order differential equation in time, and the complex coefficients $\alpha_\varepsilon(\mathbf{k},t)$ are the same as the ones used in the earlier derivation up to a normalization constant.

We note that $\boldsymbol{\alpha}(\mathbf{k},t)$ is a *transverse* field because it is defined as a sum of two transverse fields in eqn (1.59). Therefore, there are only *two degrees of freedom* corresponding to the transverse direction rather than three degrees of freedom. This means that

$$\boldsymbol{\alpha}(\mathbf{k},t) = \sum_\varepsilon \alpha_\varepsilon(\mathbf{k},t)\boldsymbol{\varepsilon} = \alpha_{\varepsilon_1}(\mathbf{k},t)\boldsymbol{\varepsilon}_1 + \alpha_{\varepsilon_2}(\mathbf{k},t)\boldsymbol{\varepsilon}_2\,, \tag{1.65}$$

where the *mutually orthogonal* polarization vectors $\boldsymbol{\varepsilon}_1$ and $\boldsymbol{\varepsilon}_2$ are perpendicular to $\mathbf{k}$ for any given $\mathbf{k}$.

We now have the equation of motion as a decoupled set of equations

$$\frac{\partial}{\partial t}\alpha_\varepsilon(\mathbf{k},t) + i\omega\alpha_\varepsilon(\mathbf{k},t) = \frac{i}{2\epsilon_0\mathscr{N}(k)}\mathbf{j}_\perp(\mathbf{k},t)\cdot\boldsymbol{\varepsilon}\,, \tag{1.66}$$

and the pair $(\boldsymbol{\varepsilon},\mathbf{k})$ is an *index* of the different *modes* of the field.

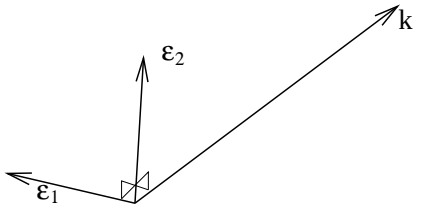

Figure 1.1: Three mutually orthogonal vectors $\boldsymbol{\varepsilon}_1$, $\boldsymbol{\varepsilon}_2$ and $\mathbf{k}$

1.2.5 Hamiltonian of the electromagnetic field

The total electromagnetic field energy in a propagating field[2] is given by

$$H = \frac{\epsilon_0}{2}\int d\mathbf{x}\,[E_\perp^2(\mathbf{x},t) + c^2B^2(\mathbf{x},t)] = \frac{\epsilon_0}{2}\int d\mathbf{k}\,[\mathscr{E}_\perp^2(\mathbf{k},t) + c^2\mathscr{B}^2(\mathbf{k},t)]. \quad (1.67)$$

From eqns (1.62) and (1.63), we find

$$\boldsymbol{\mathscr{E}}_\perp^* \cdot \boldsymbol{\mathscr{E}}_\perp = \mathscr{N}^2(\boldsymbol{\alpha}^* \cdot \boldsymbol{\alpha} + \boldsymbol{\alpha}_- \cdot \boldsymbol{\alpha}_-^* - \boldsymbol{\alpha}^* \cdot \boldsymbol{\alpha}_-^* - \boldsymbol{\alpha}_- \cdot \boldsymbol{\alpha}), \quad (1.68)$$

$$c^2\boldsymbol{\mathscr{B}}_\perp^* \cdot \boldsymbol{\mathscr{B}}_\perp = \mathscr{N}^2(\boldsymbol{\alpha}^* \cdot \boldsymbol{\alpha} + \boldsymbol{\alpha}_- \cdot \boldsymbol{\alpha}_-^* + \boldsymbol{\alpha}^* \cdot \boldsymbol{\alpha}_-^* + \boldsymbol{\alpha}_- \cdot \boldsymbol{\alpha}) \quad (1.69)$$

with $\boldsymbol{\alpha}_-^* = \boldsymbol{\alpha}^*(-\mathbf{k},t)$. The first equation for $\boldsymbol{\mathscr{E}}_\perp^* \cdot \boldsymbol{\mathscr{E}}_\perp$ can be obtained easily. To go from eqn (1.63) to the second equation, the following identity is used, while keeping in mind that $\boldsymbol{\alpha}(\mathbf{k},t)$ is transverse. The expression of the energy becomes[3]

$$H = \epsilon_0 \int d\mathbf{k}\,\mathscr{N}^2[\boldsymbol{\alpha}^* \cdot \boldsymbol{\alpha} + \boldsymbol{\alpha}_- \cdot \boldsymbol{\alpha}_-^*]. \quad (1.70)$$

The normalization coefficient $\mathscr{N}(k)$ is chosen to be $\sqrt{\frac{\hbar\omega}{2\epsilon_0}}$. A change of variable is performed for the second term in the equation above, where $\mathbf{k}$ is changed to $-\mathbf{k}$. Finally, we have

$$H = \int d\mathbf{k} \sum_\varepsilon \frac{\hbar\omega}{2}[\alpha_\varepsilon^*(\mathbf{k},t)\alpha_\varepsilon(\mathbf{k},t) + \alpha_\varepsilon(\mathbf{k},t)\alpha_\varepsilon^*(\mathbf{k},t)]. \quad (1.71)$$

Let's summarize the expression for electric field, magnetic field and vector potential before we proceed to consider the quantization of the radiation field:

$$\mathbf{E}_\perp(\mathbf{x},t) = i\int d\mathbf{k} \sum_\varepsilon \mathscr{E}_\omega[\alpha_\varepsilon(\mathbf{k},t)e^{i\mathbf{k}\cdot\mathbf{x}} - \alpha_\varepsilon^*(\mathbf{k},t)e^{-i\mathbf{k}\cdot\mathbf{x}}]\boldsymbol{\varepsilon}, \quad (1.72)$$

$$\mathbf{B}(\mathbf{x},t) = i\int \frac{d\mathbf{k}}{c} \sum_\varepsilon \mathscr{E}_\omega[\alpha_\varepsilon(\mathbf{k},t)e^{i\mathbf{k}\cdot\mathbf{x}} - \alpha_\varepsilon^*(\mathbf{k},t)e^{-i\mathbf{k}\cdot\mathbf{x}}]\boldsymbol{\kappa}\times\boldsymbol{\varepsilon}, \quad (1.73)$$

$$\mathbf{A}_\perp(\mathbf{x},t) = \int d\mathbf{k} \sum_\varepsilon \frac{\mathscr{E}_\omega}{\omega}[\alpha_\varepsilon(\mathbf{k},t)e^{i\mathbf{k}\cdot\mathbf{x}} + \alpha_\varepsilon^*(\mathbf{k},t)e^{-i\mathbf{k}\cdot\mathbf{x}}]\boldsymbol{\varepsilon} \quad (1.74)$$

[2]Assume the region is far away from the source and we can neglect the contribution of the source, which is the longitudinal part of the energy

[3]The order of multiplication is retained for quantization purposes.

with $\mathscr{E}_\omega = \sqrt{\frac{\hbar\omega}{2\epsilon_0(2\pi)^3}}$[4].

1.3 The works: Canonical quantization for dummies

Let's recall one form of the equation of motion (1.64) for the electromagnetic field in complex variables:

$$\frac{\partial}{\partial t}\boldsymbol{\alpha}(\mathbf{k},t) + i\omega\boldsymbol{\alpha}(\mathbf{k},t) = \frac{i}{2\epsilon_0\mathscr{N}(k)}\mathbf{j}_\perp(\mathbf{k},t) \tag{1.75}$$

This equation resembles a set of equations of motion for a simple harmonic oscillators, each of the form

$$\frac{\partial}{\partial t}\alpha(t) + i\omega\alpha(t) = f(t)\,. \tag{1.76}$$

Its quantization is well known, and this analogy suggests that a field quantization could be performed by interpretation of each single mode of the field as a harmonic oscillator following the standard harmonic oscillator quantization. This is however, is not completely according to the book. The proper way (as you probably have seen it in your quantum mechanics textbooks) would be to

1. Start with a Lagrange-density or a complete Langrage function,
2. Identify the coordinates of the system,
3. Find the canonically conjugated momenta,
4. Use the Hamilton-Jacobi formalism to express the energies of the field in terms of coordinates and conjugated momenta,
5. Express the physical quantities like **E** and **B** as a function of coordinates and momenta,
6. Use the Schroedinger or Heisenberg equation to describe the dynamics of the system in various pictures.

This procedure will lead to exactly the same result as the simple quantization approach obtained by simply using the analogy in the normal coordinates which shall be done in this section.

[4]No quantization has been performed yet, even though the expression for $\mathscr{E}_\omega$ contains $\hbar$. This is a purely arbitrary choice of a normalization factor for the normal coordinates

1.3.1 Quantization

Now let's perform the quantization as according to the simple method outlined in previous section. We use the transition

$$\alpha \to \hat{a}, \qquad \alpha^* \to \hat{a}^\dagger \tag{1.77}$$

similar to the case of harmonic oscillator. The field then turns into field operators as shown below:

$$\hat{\mathbf{A}}_\perp = \sum_j \mathscr{A}_{\omega_j} \left[\hat{a}_j \boldsymbol{\varepsilon}_j e^{i\mathbf{k}_j \cdot \mathbf{x}} + \hat{a}_j^\dagger \boldsymbol{\varepsilon}_j e^{-i\mathbf{k}_j \cdot \mathbf{x}} \right], \tag{1.78}$$

$$\hat{\mathbf{E}}_\perp = i \sum_j \mathscr{E}_{\omega_j} \left[\hat{a}_j \boldsymbol{\varepsilon}_j e^{i\mathbf{k}_j \cdot \mathbf{x}} - \hat{a}_j^\dagger \boldsymbol{\varepsilon}_j e^{-i\mathbf{k}_j \cdot \mathbf{x}} \right], \tag{1.79}$$

$$\hat{\mathbf{B}}_\perp = i \sum_j \mathscr{B}_{\omega_j} \left[\hat{a}_j (\boldsymbol{\kappa}_j \times \boldsymbol{\varepsilon}_j) e^{i\mathbf{k}_j \cdot \mathbf{x}} - \hat{a}_j^\dagger (\boldsymbol{\kappa}_j \times \boldsymbol{\varepsilon}_j) e^{-i\mathbf{k}_j \cdot \mathbf{x}} \right]. \tag{1.80}$$

The Hamilton operator of the field is given by

$$\hat{H} = \sum_j \frac{\hbar \omega_j}{2} (\hat{a}_j^\dagger \hat{a}_j + \hat{a}_j \hat{a}_j^\dagger) \tag{1.81}$$

which, as expected, resembles that of harmonic oscillators.

1.3.2 Harmonic oscillator physics

The individual terms $\hat{H}_j$ of the Hamilton operator in eqn (1.81),

$$\hat{H} = \sum_j \hat{H}_j \,, \quad \hat{H}_j = \frac{\hbar \omega_j}{2} (\hat{a}_j^\dagger \hat{a}_j + \hat{a}_j \hat{a}_j^\dagger) \,, \tag{1.82}$$

define the dynamics for the field state in each mode. We will come back to a few field states later, but mention that each mode j is associated with a Hilbert space $\mathcal{H}_j$ to capture every possible single-mode state $|\Psi_j\rangle$. A convenient way to characterize a in that space is its decomposition into the spectrum of energy eigenstates. We re-write the $\hat{H}_j$ in the form

$$\hat{H}_j = \hbar \omega_j (\hat{n} + \frac{1}{2}) \quad \text{with} \quad \hat{n} = \hat{a}^\dagger \hat{a} \tag{1.83}$$

with the so-called number operator $\hat{n}$ and using the commutator relation $[\hat{a}, \hat{a}^\dagger] = 1$. The energy eigenstates of the harmonic oscillator are given by the discrete set of eigenstates $|n\rangle$ of the number operator,

$$\hat{n}|n\rangle = n|n\rangle \,, n = 0, 1, 2, \ldots \tag{1.84}$$

Any state in this mode can now be expressed as a superposition of number states:

$$|\Psi\rangle = \sum_{n=0}^{\infty} c_n |n\rangle \quad \text{with coefficients} \quad c_n \in \mathbb{C}\,, \quad \sum_{n=0}^{\infty} |c_n|^2 = 1 \tag{1.85}$$

It is useful to see the analogy of a harmonic oscillator with a mass and a restoring force to the harmonic oscillator associated with an electromagnetic field mode. For the first case, we have a Hamilton operator of the form

$$\hat{H} = \frac{\hat{p}^2}{2m} + \frac{1}{2} m\omega^2 \hat{x}^2 \tag{1.86}$$

with operator $\hat{x}$ and $\hat{p}$ for position and momentum of the mass m. These operators can be expressed as sum and difference of the ladder operators $\hat{a}$ and $\hat{a}^\dagger$:

$$\hat{x} = \sqrt{\frac{\hbar}{2m\omega}} \left(\hat{a}^\dagger + \hat{a}\right) \tag{1.87}$$

$$\hat{p} = \sqrt{\frac{\hbar m\omega}{2}}\, i \left(\hat{a}^\dagger - \hat{a}\right) \tag{1.88}$$

Since the position (or momentum) probability amplitude $\phi(x)$ is well known for some common harmonic oscillator states (e.g. the number states), this analogy can help to derive a distribution corresponding field quantities we will see in the next section.

1.3.3 Field operators

Often the field operators are again split up into

$$\hat{E} = \hat{E}^{(+)} + \hat{E}^{(-)} \tag{1.89}$$

where

$$\hat{E}^{(+)}(\mathbf{x}, t) = i \sum_j \mathscr{E}_{\omega_j} \boldsymbol{\varepsilon}_j \hat{a}_j e^{i\mathbf{k}\cdot\mathbf{x}}, \tag{1.90}$$

$$\hat{E}^{(-)}(\mathbf{x}, t) = -i \sum_j \mathscr{E}_{\omega_j} \boldsymbol{\varepsilon}_j \hat{a}_j^\dagger e^{-i\mathbf{k}\cdot\mathbf{x}}. \tag{1.91}$$

They are referred to as positive and negative frequency contributions, corresponding to the evolutions in a Heisenberg picture; there $\hat{E}$ becomes time dependent, as well as the raising and lowering operators $\hat{a}$ and $\hat{a}^\dagger$.

For the lowering operator, it can be shown by remembering $[\hat{N}, \hat{a}] = -\hat{a}$ and $\hat{N} = \frac{1}{\hbar\omega}\hat{H} - \frac{1}{2}$ that

$$i\hbar \frac{\partial}{\partial t} \hat{a}(t) = \left[\hat{a}(t), \hat{H}\right] = \hbar\omega \hat{a}(t). \tag{1.92}$$

Solving this equation will result in

$$\hat{a}(t) = \hat{a}(0)e^{-i\omega t}. \tag{1.93}$$

The same can be done for the raising operator that leads us to the following equation of motion for the raising operator and its solution:

$$\begin{aligned} i\hbar\frac{\partial}{\partial t}\hat{a}^\dagger(t) &= \left[\hat{a}^\dagger(t), \hat{H}\right] = -\hbar\omega\hat{a}^\dagger(t), & (1.94)\\ \hat{a}^\dagger(t) &= \hat{a}^\dagger(0)e^{i\omega t}. & (1.95) \end{aligned}$$

In the Heisenberg picture, the electric field operator becomes time-dependent and takes the form

$$\hat{E}_\perp(\mathbf{x}, t) = i\sum_j \mathscr{E}_{\omega_j}\boldsymbol{\varepsilon}_j \left\{\hat{a}_j e^{i(\mathbf{k}\cdot\mathbf{x}-\omega t)} - \hat{a}_j^\dagger e^{-i(\mathbf{k}\cdot\mathbf{x}-\omega t)}\right\} \tag{1.96}$$

Next, we consider the following definitions of two operators,

$$\begin{aligned} \hat{a}_Q &:= \frac{1}{2}\left(\hat{a} + \hat{a}^\dagger\right), & (1.97)\\ \hat{a}_P &:= \frac{1}{2i}\left(\hat{a} - \hat{a}^\dagger\right). & (1.98) \end{aligned}$$

These two operators corresponds to the $\hat{x}$ and $\hat{p}$ operators of the harmonic oscillator which was discussed earlier. They are often referred to as *quadrature amplitudes*.

The two quadrature amplitudes are Hermitian operators, as can be shown:

$$\begin{aligned} \hat{a}_Q^\dagger &= \frac{1}{2}\left(\hat{a}^\dagger + \hat{a}\right) = \hat{a}_Q, & (1.99)\\ \hat{a}_P^\dagger &= -\frac{1}{2i}\left(\hat{a}^\dagger - \hat{a}\right) = \frac{1}{2i}\left(\hat{a} - \hat{a}^\dagger\right) = \hat{a}_P. & (1.100) \end{aligned}$$

This means that the two operators can be associated with *observables*. In fact, they are associated with the sine and the cosine component of a particular field amplitude, as can be seen from the expression of the field operator in terms of these operators.

$$\hat{\mathbf{E}}(\mathbf{x}, t) = -\sum_j 2\mathscr{E}_{\omega_j}\boldsymbol{\varepsilon}_j \left\{\hat{a}_{Q,j}\sin(\mathbf{k}\cdot\mathbf{x} - \omega_j t) + \hat{a}_{P,j}\cos(\mathbf{k}\cdot\mathbf{x} - \omega_j t)\right\}. \tag{1.101}$$

The commutation relation between $\hat{a}_P$ and $\hat{a}_Q$ can be shown easily as follow:

$$[\hat{a}_P, \hat{a}_Q] = \frac{1}{4i}\left[\hat{a} - \hat{a}^\dagger, \hat{a} + \hat{a}^\dagger\right] = \frac{1}{4i}\left(\left[\hat{a}, \hat{a}^\dagger\right] - \left[\hat{a}^\dagger, \hat{a}\right]\right) = \frac{1}{2i} \tag{1.102}$$

The reader can verify that for a single mode field, the Hamilton operator can be written in terms of the quadrature amplitude as

$$\hat{H} = \hbar\omega\left(\hat{a}_Q^2 + \hat{a}_P^2\right) \tag{1.103}$$

1.4 Different mode decompositions

So far, we have been using plane waves to decouple the partial differential equations, and to arrive at independent complex amplitudes $\alpha_{k,\epsilon}$ as independent variables. This is a convenient choice if we don't have any conductors or dielectrics in our volume of interest, but it is not the only possible mode decomposition. Before performing the quantization, let us review the case where we have a different set of boundary conditions.

For geometries where one wants to look at the interaction with an atom resting at the origin of a coordinate system, a set of spherical modes is more appropriate. Such a mode decomposition is e.g. useful for the understanding the spontaneous emission of light from an excited atom, or when dealing with spherical resonator geometries as sometimes found for microwaves.

Other common mode decompositions involve a cylindrical geometry, which will be important for describing the electromagnetic field e.g. in optical fibers. There, the boundary conditions for guided modes lead to a field which is centered in the vicinity of a core in the fiber with high refractive index, while electric field decays with the radial distance according to a Bessel function or something similar, depending on the profile for the refractive index in the optical fiber.

A very common mode decomposition in experimental setups involves Gaussian beams, which have a radial field distribution following a Gaussian, and a well-defined dependency of the characteristic width along a light beam. These modes are eigensolutions for the paraxial wave equation, and are typically found in laser physics as eigenfunctions for arrangements of concave mirror cavities.

Many field geometries limit the volume of interest, thus leading to a modified mode structure altogether. A confinement of all three dimensions of space is typically referred to as a *cavity*. For simplicity, let's consider the simplest case and postulate a periodic boundary condition.

1.4.1 Periodic boundary conditions

The simplest step to make a transition from continuous variables to cavities is to enforce periodic boundary conditions. There, the wave vector $\mathbf{k}$ can only have integer multiples of the form:

$$k_x = \frac{2\pi n_x}{L}, \qquad k_y = \frac{2\pi n_y}{L}, \qquad k_z = \frac{2\pi n_z}{L}. \tag{1.104}$$

where L is the period[5]. Here, k_i refers to the component of the wave vector in the i direction.

[5]For simplicity, we consider this to be the same in all directions

We can write down the following correspondence between the sum in continuous case for the infinite space and the sum in discrete case for the finite cavities:

$$\int d\mathbf{k}\, f(\mathbf{k}) \leftrightarrow \sum_{k_{x,y,z}} \left(\frac{2\pi}{L}\right)^3 f(k_{x,y,z}) \tag{1.105}$$

We then arrive at expressions

$$\begin{aligned}
H_{free,\perp} &= \sum_{j=(k_{x,y,z},\boldsymbol{\varepsilon})} \frac{\hbar\omega_j}{2}(\alpha_j^*\alpha_j i + \alpha_j\alpha_j^*), && (1.106)\\
\mathbf{A}_\perp &= \sum_j \mathscr{A}_{\omega_j}\left[\alpha_j\boldsymbol{\varepsilon}_j e^{i\mathbf{k}_j\cdot\mathbf{x}} + \alpha_j^*\boldsymbol{\varepsilon}_j e^{-i\mathbf{k}_j\cdot\mathbf{x}}\right], && (1.107)\\
\mathbf{E}_\perp &= i\sum_j \mathscr{E}_{\omega_j}\left[\alpha_j\boldsymbol{\varepsilon}_j e^{i\mathbf{k}_j\cdot\mathbf{x}} - \alpha_j^*\boldsymbol{\varepsilon}_j e^{-i\mathbf{k}_j\cdot\mathbf{x}}\right], && (1.108)\\
\mathbf{B}_\perp &= i\sum_j \mathscr{B}_{\omega_j}\left[\alpha_j(\boldsymbol{\kappa}_j\times\boldsymbol{\varepsilon}_j) e^{i\mathbf{k}_j\cdot\mathbf{x}} - \alpha_j^*(\boldsymbol{\kappa}_j\times\boldsymbol{\varepsilon}_j) e^{-i\mathbf{k}_j\cdot\mathbf{x}}\right] && (1.109)
\end{aligned}$$

with

$$\mathscr{E}_{\omega_j} = \left[\frac{\hbar\omega_j}{2\epsilon_0 L^3}\right]^{1/2}, \qquad \mathscr{B}_{\omega_j} = \frac{\mathscr{E}_{\omega_j}}{c}, \qquad \mathscr{A}_{\omega_j} = \frac{\mathscr{E}_{\omega_j}}{\omega_j} \tag{1.110}$$

The mode index j now points to a discrete (but still infinite) set of modes, and the integration over all modes to obtain the electrical field strength $\mathbf{E}$ at any location $\mathbf{x}$ turns into a discrete sum.

For the particular case of periodic boundary conditions we still can get away with the simple exponentials describing plane waves; however, for realistic boundary conditions, this is not the case anymore.

1.5 Realistic boundary conditions: Modes beyond plane waves

In a slightly more generalized mode decomposition, the operator for the electric field may be written as

$$\hat{\mathbf{E}}(\mathbf{x},t) = i\sum_j \mathscr{E}_{\omega_j}\left(\mathbf{g}_j(\mathbf{x})\hat{a}_j(t) - \mathbf{g}_j^*(\mathbf{x})\hat{a}_j^\dagger(t)\right), \tag{1.111}$$

where the spatial dependency and polarization property of a mode is covered by a mode function $\mathbf{g}_j(\mathbf{x})$, the time dependency is transferred into the ladder operators $\hat{a}, \hat{a}^\dagger$, and the dimensional components, together with some normalization of the mode function, is contained in the constant $\mathscr{E}_{\omega_j}$. The corresponding operator for

the magnetic field can just be derived out of this quantity via one of the Maxwell equations, (1.4), taking into account the time dependency of the ladder operators:

$$\partial \hat{a}_j/\partial t = -i\omega_j \hat{a}_j\,, \quad \partial \hat{a}_j^\dagger/\partial t = i\omega_j \hat{a}_j^\dagger\,. \tag{1.112}$$

With this, we end up with a magnetic field operator

$$\hat{\mathbf{B}}(\mathbf{x},t) = \sum_j \mathscr{B}_{\omega_j} \left(\nabla \times \mathbf{g}(\mathbf{x})\hat{a}(t) + \nabla \times \mathbf{g}^*(\mathbf{x})\hat{a}^\dagger(t)\right)\,, \quad \text{with} \quad \mathscr{B}_{\omega_j} = \mathscr{E}_{\omega_j}/\omega_j\,. \tag{1.113}$$

In practice, the mode functions $\mathbf{g}_j(\mathbf{x})$ and the dispersion relation ω_j are known or chosen as an ansatz, and it remains to find the normalization constant $\mathscr{E}_{\omega_j}$ to make sure that the Hamilton operator, given as a volume integral in the form of eqn (1.67), corresponds to the standard harmonic oscillator Hamiltonian in eqn (1.81).

For a given mode function $\mathbf{g}(\mathbf{x})$ and dispersion relation compatible with the Maxwell equations, the normalization constant is given by:

$$\mathscr{E}_j = \sqrt{\frac{\hbar\omega_j}{\epsilon_0 V}} \quad \text{with} \quad V := \int d\mathbf{x} \left[|\mathbf{g}(\mathbf{x})|^2 + \frac{c^2}{\omega^2}\,|\nabla \times \mathbf{g}(\mathbf{x})|^2\right] \tag{1.114}$$

The choice of the mode function can now easily adapted to the symmetry of the problem or boundary condition. Depending on the problem, the mode indices j may be discrete, continuous, or a combination of both. In the following, we give a set of examples for various geometries.

Occasionally, it may be helpful to include a finite length or volume, artificially discretizing some continuous mode indices. This may be helpful when evaluating the normalization constant $\mathscr{E}$ and keeping track of state densities for transition rates, but should not affect the underlying physics.

1.5.1 Square wave guide

This refers to very simple boundary conditions: The electromagnetic field is confined into a square pipe with ideally conducting walls (see Fig. 1.2a). It is a mode decomposition suitable for TE modes as found in microwave waveguides. While not exactly of concern in the optics regime, it may become an important set of boundary condition in the context of quantum circuit dynamics.

The generalized mode index $j \equiv (n, m, k)$ is formed by two discrete mode indices $n, m = 0, 1, 2, \ldots; n \cdot m \neq 0$ characterizing the nodes in the transverse direction across the waveguide, and a continuous mode index k characterizing the wave vector along the waveguide.

The mode function $\mathbf{g}(\mathbf{x})$ of a TE_{nm} mode is given by

$$\mathbf{g}(\mathbf{x}) = \hat{e}_y e^{ikz} \sin\left(\frac{n\pi}{a}x\right) \cos\left(\frac{m\pi}{b}y\right)\,, \tag{1.115}$$

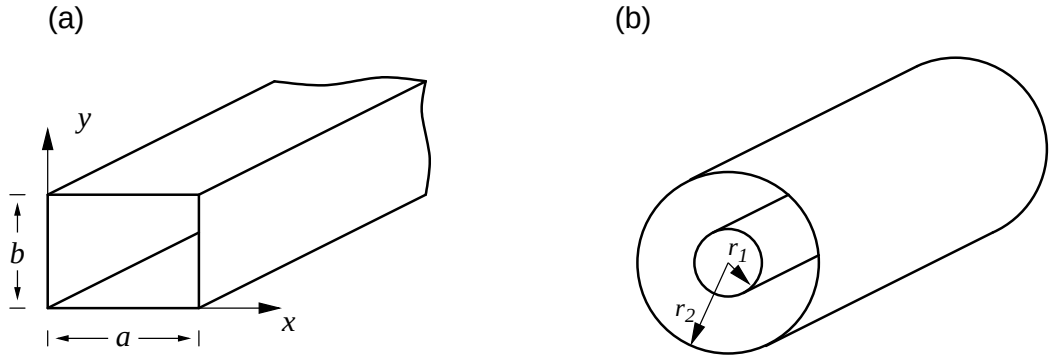

Figure 1.2: Two simple boundary conditions for electromagnetic waves. (a) A waveguide with ideally conducting walls, as used in the microwave domain; (b) a coaxial waveguide, as found at low frequencies. Both geometries illustrate how to carry out field quantization in uncommon mode geometries.

and the dispersion relation is by

$$\omega_j^2 = c_0^2 \left(k^2 + n^2\pi^2/a^2 + m^2\pi^2/b^2\right) . \tag{1.116}$$

This dispersion relation is characteristic for waveguides, which in general have some discretized transverse mode structure and a continuous parameter k, which resembles the wave vector of the plane wave solution. The second part poses a confinement term, leading to a dispersion just due to the geometry of the mode[6].

To carry out the normalization, we introduce a "quantization length" L in the z direction. This discretizes the mode index k to $k = 2\pi l/L, l = 0, 1, 2, \ldots$. The normalization constant for this mode is given by

$$\mathscr{E}_j = \sqrt{\frac{\hbar\omega_j}{\epsilon_0 V}}, \quad V = \frac{Lba}{2} \cdot \begin{cases} 1 & , m = 0 \\ 1/2 & , m > 0 \end{cases} \tag{1.117}$$

1.5.2 Gaussian beams

Many optical experiments work with light beams with a transverse Gaussian beam profile under a paraxial approximation. Such modes typically represent eigenmodes of optical resonators formed by spherical mirrors.

In a typical experiment, the transverse mode parameter (*waist*, w_0) is fixed, and the longitudinal mode index is a continuous wave number k. In a regime where there is no significant wavefront curvature, the mode function is given by

$$\mathbf{g}(\mathbf{x}) = \boldsymbol{\varepsilon} e^{-\rho^2/w_0^2} e^{ikz} , \tag{1.118}$$

[6]Keep in mind that this is not a complete set of modes, it just covers the ones with the lowest cutoff frequencies for $a > b$. There is also another field mode type, the TM modes. See e.g. Jackson [2] for a comprehensive list of modes.

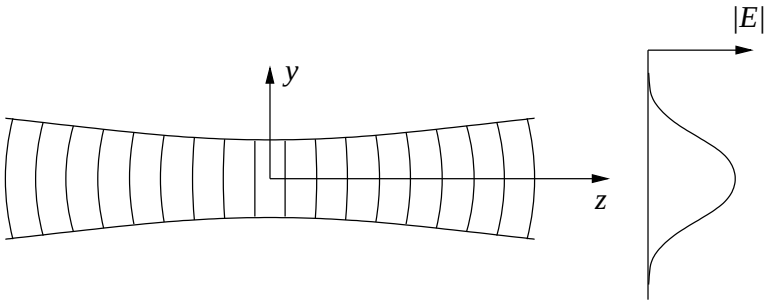

Figure 1.3: Wave fronts and electrical field distribution of a Gaussian beam.

with a radial distance $\rho = \sqrt{x^2 + y^2}$, a transverse polarization vector $\boldsymbol{\varepsilon}$, and a position z along the propagation direction. The dispersion relation for this mode is given by

$$\omega^2 = \frac{c_0^2}{\epsilon_r}\left(k^2 + \frac{2}{w^2}\right) . \tag{1.119}$$

This expression contains already the permittivity ϵ_r if the field is present in a dielectric medium. To cover the vacuum case, just set $\epsilon_r = 1$. The normalization constant $\mathscr{E}$ for the electric field operators is given by

$$\mathscr{E} = \sqrt{\frac{\hbar\omega}{\pi w^2 L \epsilon_0 \epsilon_r}} . \tag{1.120}$$

Herein, we introduced a "quantization length" L, assuming a periodic boundary condition in the propagation direction z. While not necessary, it avoids some confusion when counting over target modes.

This particular mode decomposition is also a good approximation when single mode optical fibers are used to support the electromagnetic field. While the specific dielectric boundary conditions in optical fibers are more complicated and depend on the doping structure, the most common optical fibers have a transverse mode structure which resembles closely a Gaussian mode.

A discretized longitudinal mode index is actually a very common condition for optical resonators, assuming the leakage to the environment is relatively small. If the transition to a continuum is desired, the relevant observable quantity can be first evaluated with a discrete mode spectrum, followed by a transition $L \to \infty$. We will see an example of such a procedure in Chapter 3.

A generalization of this mode function is obtained once the divergence of the Gaussian beam is taken into account. This is typically present in optical resonators with moderate focusing. There, the mode function becomes

$$\mathbf{g}(\mathbf{x}) = \varepsilon \frac{w_0}{w(z)} e^{-\rho^2/2w^2(z)} e^{ikz + ik\frac{\rho^2}{2R(z)} + i\zeta(z)} \tag{1.121}$$

with a beam waist w_0 other commonly used quantities

$$\begin{array}{lrcl} \text{beam parameter:} & w(z) & = & w_0\sqrt{1+(z/z_R)^2} \\ \text{radius of curvature:} & R(z) & = & z + z_R^2/z \\ \text{Guoy phase:} & \zeta(z) & = & \tan^{-1} z/z_R \\ \text{Raleigh range:} & z_R^2 & = & \pi w_0^2/\lambda \end{array} \tag{1.122}$$

Further extension of this concept includes higher order transverse modes; similarly to the waveguides with conductive walls, these modes are characterized by the nodes in radial and angular components, or by nodes in a rectangular geometry (See e.g. Saleh/Teich [3]).

1.5.3 Spherical Harmonics

This mode decomposition is particularly suited to adapt to electrical multipole transitions in atoms and molecules, since the problem has a rotational symmetry around the center, which contains the atom.

These modes fall into two classes, the transverse electrical (TE) or magnetic multipole fields, and the transverse magnetic (TM) or electrical multipole fields, each of them forming a complete set of modes for the electromagnetic field similarly to the plane waves we have seen earlier. Mode indices are given by a combination of two discrete indices L, M addressing the angular momentum, with $L = 0, 1, 2, \ldots$ and $M = -L, -L+1, \ldots, L-1, L$ and a radial wave index $k \in [-\infty, +\infty]$.

Their angular dependency involves the normalized vector spherical harmonics,

$$\mathbf{X}_{LM}(\theta,\phi) := \frac{1}{\sqrt{L(L+1)}}\frac{1}{i}(\mathbf{r}\times\nabla)Y_{LM}(\theta,\phi)\,, \tag{1.123}$$

with the usual spherical harmonics Y_{LM} known from atomic physics. For TM modes, associated with electrical multipole radiation, the mode function for the electrical field is given by

$$\mathbf{g}(\mathbf{x}) = \frac{i}{k}\nabla\times(h_L(kr)\mathbf{X}_{LM}(\theta,\phi)) \tag{1.124}$$

with the spherical Hankel functions

$$h_L(kr) = \sqrt{\pi/2kr}\left[J_{L+1/2}(kr) \pm iN_{L+1/2}(kr)\right] \tag{1.125}$$

governing the radial dependency. For electrical dipole modes, which are the most important modes for atomic transitions in the optical domain, $L = 1$, and $M = 0, \pm 1$ corresponding to π and $\sigma^{\pm}$ polarized light. There, the radial part becomes

$$h_1(kr) = -\frac{e^{ikr}}{kr}\left(\pm 1 + \frac{i}{kr}\right)\,, \tag{1.126}$$

where the $\pm$ reflects the sign of k, distinguishing between asymptotically incoming or outgoing solutions. The dispersion relation is simply $\omega = ck$, and asymptotically (i.e. for $r \gg \lambda$) the field resembles a locally transverse spherical wave. A comprehensive description of these modes can e.g. be found in Jackson [2].

Such modes are used to connect the spontaneous emission rate of atoms with their induced electrical dipole moment or susceptibility [4].

1.5.4 Coaxial cable

This is a somewhat textbook-like mode decomposition, which does not really reach into the optical domain, but is simple to solve analytically. It refers to the propagating modes in the usual cables used for signal transmission. These cables are formed by two concentric cylinders with radii r_1, r_2 which confine the electrical field as depicted in Fig. 1.2(b). The most common (low frequency) mode function is indexed by a wave vector k and has a radial electrical field dependency:

$$\mathbf{g}(\mathbf{x}) = \begin{cases} \mathbf{e}_\rho \frac{e^{ikz}}{\rho} & \text{for} \quad r_1 < r < r_2\,, \\ 0 & \text{elsewhere} \end{cases} \tag{1.127}$$

with the radial unit vector $\mathbf{e}_\rho$. The dispersion relation has no confinement correction, i.e., $\omega = ck$. For a finite length L of the cable (periodic boundary conditions, i.e. $k = n \cdot 2\pi L, n \in \mathbb{N}$), one can simply calculate the "mode volume" V of the cable according to eqn (1.114) as

$$V = \int d\mathbf{x} \left[|\mathbf{g}|^2 + \frac{c^2}{\omega^2} |\nabla \times \mathbf{g}|^2 \right] = 4\pi L \log \frac{r_2}{r_1} \tag{1.128}$$

leading to a normalization constant

$$\mathscr{E}_k = \sqrt{\frac{\hbar\omega_k}{\epsilon_0 V}} = \sqrt{\frac{\hbar\omega_k}{4\pi\epsilon_0 L \log(r_2/r_1)}} \tag{1.129}$$

Keep in mind that the dimension of $\mathscr{E}_k$ is not the one of the field strength, only the combined product of the mode function $\mathbf{g}$ and $\mathscr{E}_k$. Just for getting a feeling for orders of magnitude, we evaluate the normalization constant for a cable of length L=1 m and $k = 10\pi/L$, corresponding to $\omega/2\pi = 1.5\,\mathrm{GHz}$. With $\log r_2/r_1 = 1$, this results in a normalization constant $\mathscr{E} \approx$100 nV - a quantity just about too small for contemporary microwave measurement, but not too far either. The currently developing area of quantum circuit dynamics is starting to explore this parameter regime.

Chapter 2

A silly question: What is a photon?

So far, we only payed attention to the general field quantization - and did not consider specific states of the field. The intent of this lecture is to look at a few states of light, and attempt to get an idea what we mean when we talk about photons. This is not as clean of a question to answer as one would desire: much of the confusion and sometimes arguments between different camps in the community are based on different definitions, or perhaps conceptions which are carried over from a traditional mechanistic view.

To approach this problem, we quickly visit the history of how the concept of a photon came about. Then, we continue with the standard way of introducing field states in finite-size spaces, which perhaps allow the formally cleanest definition of what a photon is in the sense that these field states are energy eigenstates, and thus are stable excitations of a field. Such a set of boundary conditions is provided in practice by optical cavities or other resonators. This also allows a clean definition of typical field states, very similar to simple harmonic oscillator modes.

Another important approach of what a photon could be is inspired by the detection process, based on the photoelectric effect. Such a detection process is able to witness the smallest amount of energy, and usually results in a "detection event" localized in time. This is perhaps the most particle-like definition, and matches a wide range of experiments.

Another common definition of a photon is tied to a generation process, the most prominent one being the spontaneous emission of an excited state of an atom. Again, this leads to a field localized in time and space, not exactly reflecting an energy eigenstate.

2.1 History: The photon of Lewis and Lamb's rage

A somewhat polemic article of W.E. Lamb with a brief historical overview is not only entertaining, but helpful to get an idea where the problem lies [5].

An investigation on the external photoelectric effect by Lenard in 1902 [6] and others lead to the observation that the maximal kinetic energy of the electrons emitted from metals under illumination with light did not depend on the intensity of the light, but only on its frequency. The simple interpretation of this observation by Einstein, namely that the absorption of light can only take place in discrete quanta, and that the dependency of the electron's kinetic energy with frequency should be given by the Planck constant, is sometimes seen as the 'birth' of the photon concept, assigning a corpuscular character to light in the framework of quantum physics [7]. The predicted linear dependency was then verified experimentally with a high accuracy by R. Millikan [8].

The explanation of the photoelectric effect, however, does not really require a quantized treatment of the electromagnetic field, but can be understood by a quantum description of the electron with time-dependent electrical fields and first-order perturbation theory [9].

The original notion of a photon as a particle was introduced by G.N. Lewis in 1926 [10] in a slightly different context, as a carrier for transmitting radiation between atoms which should obey a conservation law. That concept has long vanished.

2.2 Tying it to energy levels: Cavity QED

The perhaps cleanest situation can be found where one has a discrete set of modes: The electromagnetic field in each mode can be described as a harmonic oscillator, and many of the system states (e.g. states of the electromagnetic field) can be understood in terms of harmonic oscillator states.

To be in a situation with a discrete set of modes, we need to have the electromagnetic field confined to a finite volume, preferably with distinct frequencies for the different modes. This is realized with optical cavities, or more recently with electronic resonators of a sufficiently high quality factor such that a coupling to an environment becomes only a small perturbation.

To understand the consequences of quantization of the electric and magnetic fields, we need to look into the expectation values and the variance of the fields using the tools of quantum mechanics. To simplify the treatment, we restrict the treatment to states which only involve a single mode, come back to multi-mode fields later.

Here we briefly review a few harmonic oscillator states most relevant for quantum optics in cavities, namely the number states (or energy eigenstates, also

known as Fock states), the thermal states, and the coherent states.

2.2.1 Number states

The number states (as energy eigenstates of the harmonic oscillator) have been discussed before. We now consider the expectation values and variance of the electric field for a single mode in a number state.

Assuming we focus our attention to the mode indexed by l, we find

$$\langle n|\hat{\mathbf{E}}_l|n\rangle = i\mathscr{E}_l\langle n|\hat{a}_l e^{i\mathbf{k}\cdot\mathbf{x}} - \hat{a}_l^\dagger e^{-i\mathbf{k}\cdot\mathbf{x}}|n\rangle = 0\,. \tag{2.1}$$

The equality is due to property of raising/lowering operator and the orthogonality of the number states:

$$\begin{aligned}\langle n|\hat{a}_l|n\rangle &= \langle n|n-1\rangle\sqrt{n} = 0, &(2.2)\\ \langle n|\hat{a}_l^\dagger|n\rangle &= \langle n|n+1\rangle\sqrt{n+1} = 0 &(2.3)\end{aligned}$$

With this, the expectation value of $\hat{\mathbf{E}}_l^2$ can easily be obtained:

$$\langle n|\hat{E}_l^2|n\rangle = \mathscr{E}_l^2(2n+1) \tag{2.4}$$

Here, for the ground state $|0\rangle$ which we can identify as the vacuum state, the average of the field is zero, but there is fluctuations of the field, since

$$\langle \hat{E}_l^2\rangle = \mathscr{E}_l^2 \tag{2.5}$$

which is nonzero.

The *spread* or uncertainty of the electric field in a number state is given by

$$\Delta\hat{E}_l = \sqrt{\langle \hat{E}_l^2\rangle - \langle \hat{E}_l\rangle^2} = \mathscr{E}_l\sqrt{2n+1} \tag{2.6}$$

Similarly, the expectation values of the quadrature amplitudes can be obtained:

$$\begin{aligned}\langle n|\hat{a}_Q|n\rangle = \langle n|\hat{a}_P|n\rangle &= 0, &(2.7)\\ \langle n|\hat{a}_Q^2|n\rangle = \langle n|\hat{a}_P^2|n\rangle &= \frac{2n+1}{4}. &(2.8)\end{aligned}$$

2.2.2 Thermal states

In many cases, the exact state of a quantum mechanical system is not known, but can be described by an ensemble of possible states following a classical probability distribution; the classical thermal ensembles are a very typical example where one has a certain lack of classical knowledge about the exact state.

Such a partial knowledge about the state of a system can be expressed using a so-called density matrix ρ, which may be composed of projectors for a set of pure quantum states $|\psi\rangle_n$, where the probability of such a realization (of the system in state $|\psi_n\rangle$) is p_n:

$$\hat{\rho} = \sum_n p_n |\psi_n\rangle\langle\psi_n| \tag{2.9}$$

The expectation values of operators $\hat{A}$ is a weighted average over the expectation values of the constituting states in the density matrix definition above, and may be obtained by tracing over these operators:

$$\langle\hat{A}\rangle = \sum_n p_n \langle\psi_n|\hat{A}|\psi_n\rangle \sum_n \langle\Psi_n|\hat{A}|\Psi_n\rangle =: tr\left(\hat{\rho}\hat{A}\right) \tag{2.10}$$

where the sum is taken over a complete set of base vectors $|\Psi_n\rangle$. By definition, the trace of a meaningful density matrix has to be 1:

$$tr\left(\hat{\rho}\right) = 1 \tag{2.11}$$

Sometimes, the definition

$$\langle\hat{A}\rangle = tr\left(\hat{\rho}^{1/2}\hat{A}\hat{\rho}^{-1/2}\right) \tag{2.12}$$

is used, where the operator $\hat{\rho}^{1/2}$ is defined by the MacLaurin series expansion for operators.

For thermal states, the probability distribution is determined by the energy of each state, i.e.

$$p_n = \frac{1}{Z} e^{-\beta E_n} \tag{2.13}$$

where E_n is the energy of the state $|\psi_n\rangle$, $\beta = (k_B T)^{-1}$, and Z a normalization constant (partition function) so that the sum of probabilities equals to 1:

$$Z = \sum_n e^{-\beta E_n}. \tag{2.14}$$

For the harmonic oscillator in particular, we find

$$\begin{aligned} Z &= \sum_{n=0}^{\infty} e^{-\beta E_n} = \sum_{n=0}^{\infty} e^{-\beta\hbar\omega(n+\frac{1}{2})} = e^{-\beta\hbar\omega/2} \sum_{n=0}^{\infty} e^{-\beta\hbar\omega n} \\ &= \frac{e^{-\beta\hbar\omega/2}}{1 - e^{-\beta\hbar\omega}}. \end{aligned} \tag{2.15}$$

The probability p_n of being in the energy eigenstate $|psu_n\rangle$ can then be written as

$$p_n = \frac{e^{\beta\hbar\omega n}}{(1 - e^{-\beta\hbar\omega})^{-1}} = \frac{A^n}{(1-A)^{-1}}, \qquad \text{with } A = e^{-\beta\hbar\omega}. \tag{2.16}$$

In the density matrix formulation, one can write the thermal state as

$$\hat{\rho} = \sum_n \frac{1}{Z} e^{-\beta E_n} |n\rangle\langle n| = \sum_{n=0}^{\infty} \frac{A^n}{(1-A)^{-1}} |n\rangle\langle n| \tag{2.17}$$

Coming back to the expectation values for the electrical field of a single mode and its variance, we now find

$$\langle \hat{\mathbf{E}}_l \rangle_{\text{thermal}} = 0, \tag{2.18}$$

$$\langle \hat{\mathbf{E}}_l^2 \rangle_{\text{thermal}} = \mathscr{E}_l^2 \frac{1+A}{1-A} \tag{2.19}$$

In the high temperature limit ($k_B T \gg \hbar\omega$) we have

$$A = e^{-\beta\hbar\omega} \approx 1 - \beta\hbar\omega. \tag{2.20}$$

This means that the variance of the electrical field is given by

$$\langle \hat{\mathbf{E}}_l^2 \rangle_{\text{thermal}} \approx \mathscr{E}_l^2 \frac{2}{\beta\hbar\omega} = \frac{k_B T}{(2\pi)^3 \epsilon_0} \tag{2.21}$$

On the other hand, for low temperature limit where $k_B T \ll \hbar\omega$, $A \ll 1$ we have

$$\langle \hat{\mathbf{E}}_l^2 \rangle_{\text{thermal}} \approx \mathscr{E}_l^2 \,, \tag{2.22}$$

indicating that for low temperatures, the vacuum fluctuations dominate the distribution of possible measurement results for the electric field.

This is an important point for finding out at which temperatures experiments can be carried out. At room temperature ($T = 300\,\text{K}$), the characteristic thermal frequency to decide upon high- or low temperature limit is given by

$$\omega_{RT} = \frac{k_B T}{\hbar} \approx 2\pi \cdot 6.25\,\text{THz}\,, \tag{2.23}$$

corresponding to a vacuum wavelength of about $48\,\mu$m. Thus, in the optical domain with frequencies on the order of $10^{14}\,$Hz or wavelengths on the order of $1\,\mu$m, electromagnetic fields are typically in the ground state or in close approximation thereof, while for experiments in the microwave domain (frequencies from a few 1 GHz to a few 100 GHz), thermal occupation of mode is a problem, and the structures coupling to a thermal environment due to losses need to be cooled down to very low temperatures.

2.2.3 Coherent states

One of the perhaps most important class of states in quantum optics were introduced by Roy Glauber in 1963 [11]. They are the closest quantum mechanical

analogon to classical motion of a harmonic oscillator, and – as any other pure oscillator state – are coherent superpositions of energy eigenstates of the oscillator.

For a formal approach to these states, consider the lowering operator $\hat{a}$ and one of its eigenstates $|\alpha\rangle$ corresponding to the eigenvalue α:

$$\hat{a}|\alpha\rangle = \alpha|\alpha\rangle \tag{2.24}$$

There exists actually such a state for every $\alpha \in \mathbb{C}$. We leave it as an exercise to the reader to derive a representation of $|\alpha\rangle$ in the energy eigenbasis $\{|n\rangle\}$ in the form

$$|\alpha\rangle = \sum_{n=0}^{\infty} c_n |n\rangle \,. \tag{2.25}$$

The (normalized) result for that representation for a given α is given by

$$|\alpha\rangle = \sum_{n=0}^{\infty} e^{-|\alpha|^2/2} \frac{\alpha^n}{\sqrt{n!}} |n\rangle \tag{2.26}$$

One particular state is obtained for $\alpha = 0$: all contributions but of the ground state of the oscillator vanish, so the corresponding coherent state is the ground state itself:

$$|\alpha = 0\rangle = |n = 0\rangle \,. \tag{2.27}$$

We now can find the expectation values for the electric field and its variance, as we have done before for number states and thermal states:

$$\langle\alpha|\hat{\mathbf{E}}_l|\alpha\rangle = i\mathscr{E}_l\boldsymbol{\varepsilon}_l \left(\alpha e^{i\mathbf{k}\cdot\mathbf{x}} - \alpha^* e^{-i\mathbf{k}\cdot\mathbf{x}}\right) \tag{2.28}$$

Here, the expression of $\hat{\mathbf{E}}$ in terms of $\hat{a}_Q$ and $\hat{a}_P$ comes in handy. With

$$\langle\alpha|\hat{a}_Q|\alpha\rangle = \frac{1}{2}\langle\alpha|(\hat{a} + \hat{a}^\dagger)|\alpha\rangle = \frac{1}{2}(\alpha + \alpha^*) = \mathrm{Re}(\alpha), \tag{2.29}$$

$$\langle\alpha|\hat{a}_P|\alpha\rangle = \frac{1}{2i}\langle\alpha|(\hat{a} - \hat{a}^\dagger)|\alpha\rangle = \frac{1}{2i}(\alpha - \alpha^*) = \mathrm{Im}(\alpha)\,, \tag{2.30}$$

we can write the expectation value of the electrical field operator as

$$\begin{aligned} \langle\hat{\mathbf{E}}_l\rangle &= -\mathscr{E}_l\boldsymbol{\varepsilon}_l \left\{2\langle\hat{a}_Q\rangle \sin(\mathbf{k}\cdot\mathbf{x} - \omega t) + \langle\hat{a}_P\rangle \cos(\mathbf{k}\cdot\mathbf{x} - \omega t)\right\} \\ &= -2\mathscr{E}_l\boldsymbol{\varepsilon}_l \left\{\mathrm{Re}(\alpha)\sin(\mathbf{k}\cdot\mathbf{x} - \omega t) - \mathrm{Im}(\alpha)\cos(\mathbf{k}\cdot\mathbf{x} - \omega t)\right\} \,. \end{aligned} \tag{2.31}$$

Real and imaginary part of α are the expectation values of the sine and cosine component of something which looks like a classical field, e.g. an expectation value of the field strength that oscillates sinusoidally in time. Therefore, these states are also called quasi-classical states. Note that this property applies not only to the harmonic oscillators associated with an electromagnetic field mode, but any harmonic oscillator following a Hamiltonian with the same structure.

Let's now have a closer look at the variance of the electrical field, expressed both in the variance of $\langle\hat{\mathbf{E}}\rangle$ itself and its quadrature components. We start by finding the expectation value of the square of the electric field,

$$\begin{aligned}\langle\hat{\mathbf{E}}_l^2\rangle &= \langle\alpha|\left\{i\mathscr{E}_l\boldsymbol{\varepsilon}_l\left(\hat{a}_l e^{i\mathbf{k}\cdot\mathbf{x}} - \hat{a}_l^\dagger e^{-i\mathbf{k}\cdot\mathbf{x}}\right)\right\}^2|\alpha\rangle \\ &= -\mathscr{E}_l^2\left\{\alpha^2 e^{2i\mathbf{k}\cdot\mathbf{x}} - (2\alpha\alpha^* + 1) + \alpha^{*2}e^{-2i\mathbf{k}\cdot\mathbf{x}}\right\}.\end{aligned} \tag{2.32}$$

For the variance, we also need

$$\begin{aligned}\langle\hat{\mathbf{E}}_l\rangle^2 &= \left\{i\mathscr{E}_l\left(\alpha e^{i\mathbf{k}\cdot\mathbf{x}} - \alpha^* e^{-i\mathbf{k}\cdot\mathbf{x}}\right)\right\}^2 \\ &= -\mathscr{E}_l^2\left\{\alpha^2 e^{2i\mathbf{k}\cdot\mathbf{x}} - 2\alpha\alpha^* + \alpha^{*2}e^{-2i\mathbf{k}\cdot\mathbf{x}}\right\}.\end{aligned} \tag{2.33}$$

With both of these terms, we can evaluate the variance of the electric field,

$$(\Delta\hat{E}_l)^2 = \langle\hat{\mathbf{E}}_l^2\rangle - \langle\hat{\mathbf{E}}_l\rangle^2 = \mathscr{E}_l^2\,. \tag{2.34}$$

Thus, the variance of the field is *independent* of the value of α, and equal to the variance of the field for a vacuum state since this is also a coherent state with $\alpha = 0$.

Now we turn to the variances in the quadrature components.

$$\langle\hat{a}_Q^2\rangle = \frac{1}{4}\left(\alpha^2 + \alpha^{*2} + 2\alpha\alpha^* + 1\right) \tag{2.35}$$

$$\langle\hat{a}_Q\rangle^2 = \frac{1}{4}\left(\alpha^2 + \alpha^{*2} + 2\alpha\alpha^*\right) \tag{2.36}$$

$$(\Delta\hat{a}_Q)^2 = \langle\hat{a}_Q^2\rangle - \langle\hat{a}_Q\rangle^2 = \frac{1}{4} \tag{2.37}$$

Similarly, the variance of the other quadrature component evaluates to

$$(\Delta\hat{a}_P)^2 = \langle\hat{a}_P^2\rangle - \langle\hat{a}_P\rangle^2 = \frac{1}{4} \tag{2.38}$$

Both quadrature amplitudes show the same variance, which is also the same as for the vacuum. Since there is an uncertainty relation between the quadratures, and the ground state is a minimal uncertainty state, this implies that the eigenstate of $\hat{a}$ is a minimum uncertainty state for the associated quadrature amplitudes of the electromagnetic field.

Without any proof, it should be noted that the coherent states represent the state typically emitted by a laser operating far above threshold, and assuming that the phase of the laser radiation is fixed by convention or a conditional measurement in an experiment.

It should also be noted that coherent states don't have a fixed number of photons in them, if the notion 'having n photons in a system' refers to the system being in the n-th excited energy eigenstate of the discrete field mode.

2.3 Tying it to the detection processes

So far, we have discussed observables and measurements only from a very formal point of view. In this section, we will have a somewhat closer look into various measurement techniques for light, and try to get an idea what we really measure in a particular configuration - and how this connects to the various "observables".

2.3.1 The photoelectric process

Until very recently, all optical measurement techniques relevant for the domain of quantum optics were based on various versions of the photoelectric effect. The effect of electron emission upon irradiation of a metallic surface was essential in the development of a quantum mechanical description of light.

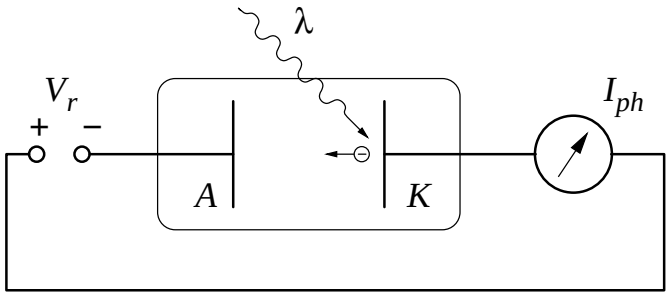

Figure 2.1: Experimental configuration to observe the photoelectric effect: Light at wavelength λ causes electrons leaving the metal surface with an energy independent of the intensity of the light.

The photoelectric effect refers to the phenomenon that upon exposure to light, electrons may be emitted from a metal surface and was experimentally observed in 1887 by H. Hertz [12] as a change in a spark intensity upon exposure of electrodes to ultraviolet light. More quantitative studies were carried out 1899 by J.J. Thomspon, who observed together with the discovery of electrons that the emitted charge increases with intensity and frequency of the light. In 1902, P. von Lenard carried out more quantitative measurements on the electron energy emitted by light exposure in an experimental configuration symbolized in Fig. 2.1 and found that the stopping potential V_r needed to suppress the observation of a photocurrent I_{ph} in a vacuum photodiode depended only on the wavelength of the light, and concluded that the kinetic energy of electrons after being liberated from the metal compound is determined by the frequency of the light, not its intensity. He also found a strong dependency of the liberation energy of the electrons, today referred to as *work function* , which depended strongly on the preparation of the metal.

This led to the spectacular interpretation in 1905 by A. Einstein that the electron emission was due to an absorption process of electrons in the metal, and

that absorption of light could only take place in well-defined packets or *quanta* of light, supplying another pillar in the foundation of a quantum mechanical treatment of the electromagnetic radiation besides M. Planck's description of blackbody radiation.

The numeric expression for the kinetic energy of the emitted electrons,

$$E_{kin} = hf - \Phi\,, \tag{2.39}$$

with f being the frequency of a monochromatic light field and Φ a material constant suggested a linear dependency between the excess energy of the electrons and the light frequency. This linearity was then quantitatively observed in experiments of R.A. Millikan in 1915.

Photomultiplier

The charge of the single photoelectron liberated in an absorption process is very small, and it is technologically challenging to detect this single charge directly. Therefore, the metallic surface generating the primary photoelectron is often followed by an electron multiplier. This is an arrangement of subsequent metal surfaces, were electrons are accelerated towards these metal surfaces (*dynodes*) such that upon impact, a larger number of electrons are emitted, which are subsequently accelerated towards the next plate:

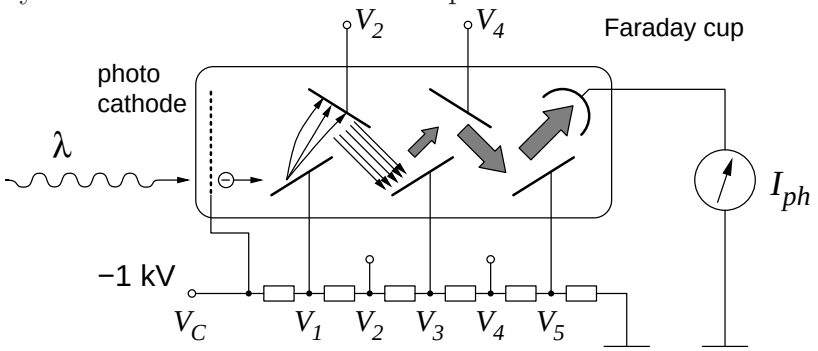

The photocathode, the dynode arrangement and a final Faraday cup to collect the secondary charge emission from the last dynode are kept in a small vacuum tube, and the cascaded accelerating potentials of the dynodes (a few 100 V) are derived via a voltage divider chain from a single high voltage source.

The overall gain of such an electron multiplication stage can be on the order of 10^6 to 10^8, leading to a charge pulse on the order of 10^{-11} As. Such a charge can be conveniently detected, leading to a measurable signal from a single single primary photoelectron.

The number of photoelectrons per unit time is proportional to the light power, as we will see later, so the photocurrent in such a device can be used to determine low light power levels.

A fundamental prerequisite for using the photoelectric effect to detect visible light is that the work function Φ of the photo cathode is sufficiently small. As the

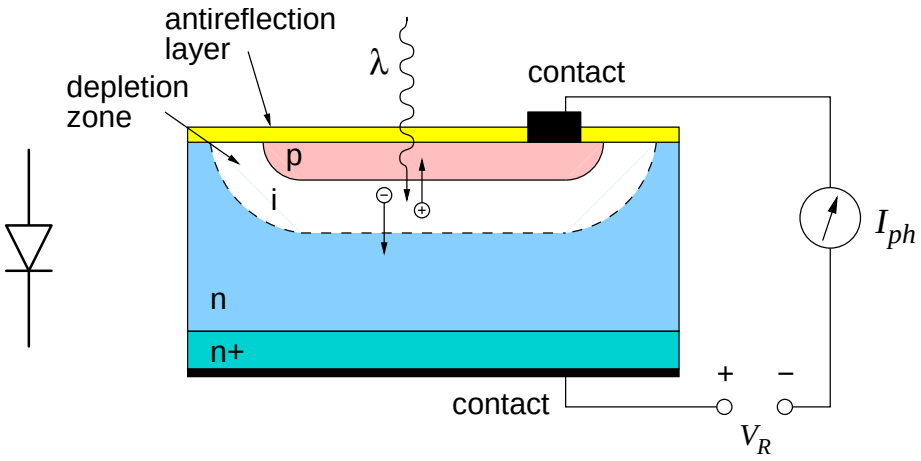

Figure 2.2: Schematic of a $p-i-n$ photodiode. Electron-hole pairs are generated in a depletion region with a low charge carrier density i, and separated by an electrical field so they can be detected as a macroscopic current.

binding energy of electrons in the metallic bulk can be on the order of a few eV, a careful choice of the photocathode material is necessary to observe the photoelectric effect with visible or infrared light. Typically, efficient photocathodes are made out of a combination of silver and several alkali metals and metal oxides.

Solid state photodiodes

Another important effect used for light detection utilizes the internal photoelectric effect in semiconductors, light is absorbed by an electron in the valence band, and transported into the conduction band. There, only the energy to bridge the band gap needs to be provided.

Such electron-hole pairs can then be separated with an electrical field in the semiconductor, leading to a detectable electrical current. Such photodetectors typically have the geometry of a semiconductor diode, with a depleted region of low conduction where the electron-hole pairs are generated by the absorbed light (see Fig. 2.2). These pin devices have a diode characteristic, and are operated in a reverse biased scheme. Typically, a large depletion volume is desired both to allow for an efficient absorption of the incoming light and to ensure a small parasitic capacity of the pn junction for a fast response of the photodetection process. The wavelength-dependent absorption coefficient is shown in Fig. 2.3. For a wavelength of $\lambda = 600\,\text{nm}$, the absorption length is on the order of $5\,\mu\text{m}$, which gives some constraints to the construction of Silicon photodiodes.

Various semiconductor materials are used for this type of photodetector, allowing to construct photodetectors for a large range of wavelengths. In a wavelength regime from 1000 nm to 200 nm, silicon is the most common semiconductor material with its band gap energy of 1.25 eV. For longer wavelengths, e.g. the typ-

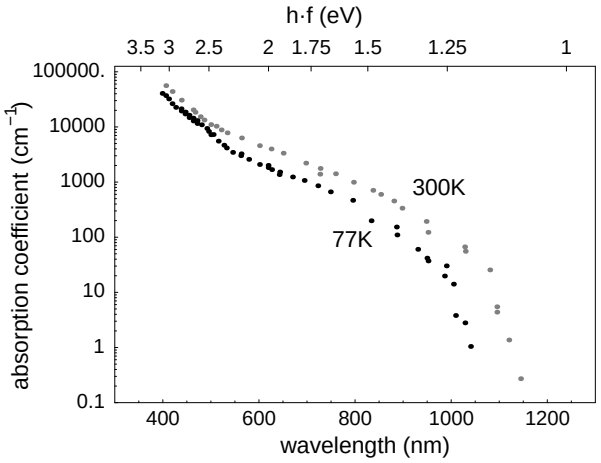

Figure 2.3: Absorption coefficient for silicon at room temperature and 77 K.

ical choice in optical fiber communication ($\lambda \approx 1300\,\text{nm}$ and $\approx 1550\,\text{nm}$) are III-V semiconductors like GaAs or InGaAs.

For some very fast photodetectors, the depletion region in a Schottky contact (i.e., metal-semiconductor interface) is utilized instead of a pn junction.

Semiconductor photodiodes typically exhibit a very high *quantum efficiency* η. This quantity describes the probability that light is converted into photoelectrons or electron/hole pairs, and detected. With appropriate anti-reflective coatings of the semiconductor to avoid the surface reflection at the large refractive index contrast interface, most of the light can be guided into the semiconductor. A proper dimension of the depletion region allows for a complete absorption of the light. It is not uncommon to find photodiodes with a quantum efficiency of η =95% or higher.

For a monochromatic light field at an optical frequency $f = c/\lambda$, there is a simple relationship between the observed photocurrent I_{ph} and the optical power P of the incident light. The rate of electron-hole pair creation, r_e, is just given by the rate of elementary absorption processes:

$$r_a = P/(hf) = \frac{P\lambda}{hc} \tag{2.40}$$

The resulting photocurrent, considering a quantum efficiency η, is simply given by the rate r_e and charge per electron:

$$I_{ph} = \eta e r_e = \eta e r_a = \eta \frac{e\lambda}{hc} P =: SP \tag{2.41}$$

For the wavelength of a HeNe laser, $\lambda = 633\,\text{nm}$, the *sensitivity* S of a photodiode with $\eta = 98\%$ is $S = 0.5\,\text{A/W}$.

One of the practical advantages of semiconductor photodiodes in comparison with photomultipliers is their low cost, a typically very small size and the absence

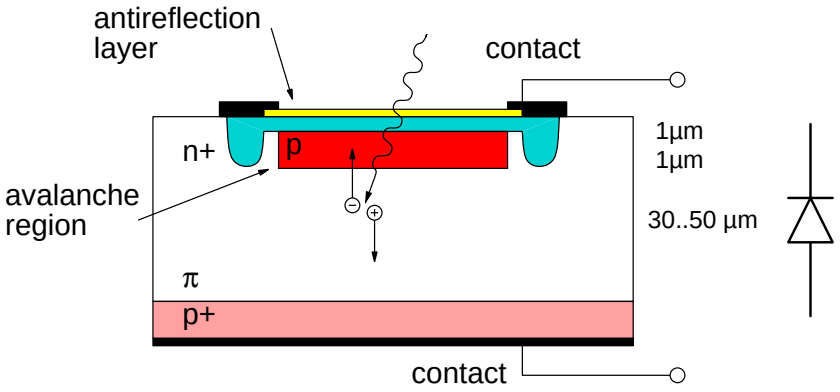

Figure 2.4: Structure of a reach-through Silicon avalanche diode. A large region where electron-hope pairs are created due to absorption of light is combined with a region of high electric field strength (p-n+ junction) where an avalanche of charge carriers are triggered.

of high voltages. On the physics side, we will see that many measurements of quantum states of light will require a high quantum efficiency, which is currently unparalleled with any other photodetection techniques.

Avalanche photodetectors

One of the shortcomings of a simple photodiode in comparison with a photomultiplier is the difficulty to observe single absorption processes, as the charge of a single electron-hole pair is hard to distinguish from normal electronic noise in a system.

However, it is possible to find an analogon to the electron multiplication process of a photomultiplier in a solid state device. In so-called avalanche diodes, a region with a high electrical field allows a charge carrier to acquire enough energy to create additional electron-hole pairs in scattering processes, similar to the ionization processes in an electrical discharge through a gas.

Such a semiconductor device can be combined with a charge-depleted region, where electron-hole pairs are generated as a consequence of light absorption (see Fig. 2.4). An avalanche photodiode with a built-in charge amplification mechanism can then also be used to detect a single absorption process.

The gain G of such photodiodes increases with the applied reverse bias voltage V_R. These devices are often operated in a regime where one photoelectron creates a charge avalanche of about 100 electron/hole pairs. In this regime, the avalanche photodiode is used in a similar way as a normal pin-photodiode. The gain of the multiplication region diverges at the so-called *breakdown voltage* V_{br}, where the stationary operation of the device leads to a self-sustaining conduction in reverse direction even without additional light from outside. Such a mode of operation is similar to an electrical discharge in a gas, where electrons and ions are accelerated

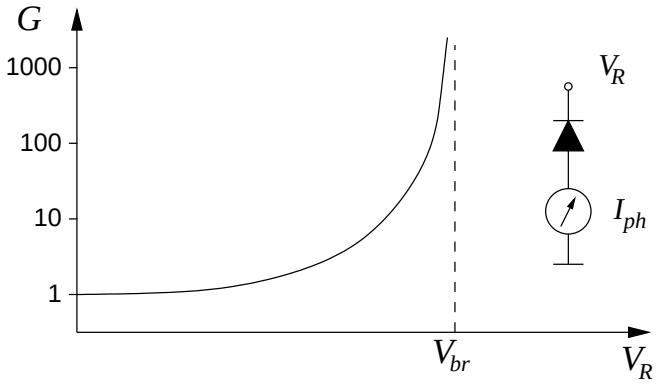

Figure 2.5: Gain G of an avalanche photodiode as a function of the reverse bias voltage V_R.

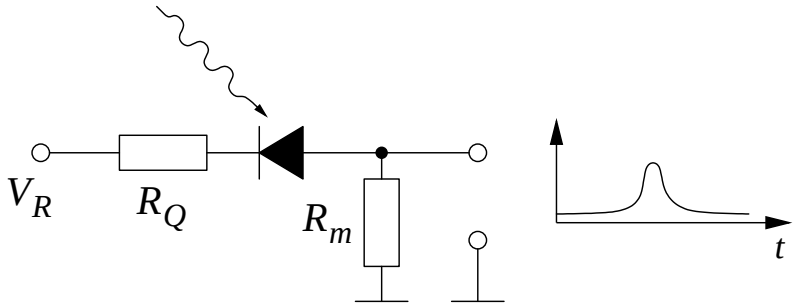

Figure 2.6: Operation of an avalanche photodiode to observe single absorption processes. The device is reverse-biased above its breakdown voltage V_{br} such that a single photoelectron can switch the device into a conducting mode. The subsequent voltage drop across the quenching resistor R_Q restores the non-conducting mode again.

in an electrical field and create more conduction carriers via impact ionization of the residual neutral gas. For semiconductor devices, such an operation over an extended time would deposit a destructive amount of heat into the device.

However, if the energy deposited in the device is limited, this operation regime can be used to identify individual photoelectrons, in a very similar way that a Geiger counter can be operated to observe the breakdown triggered by a few ions in a gas cell created by an incident particle. In a very simple approach, the discharge current during a breakdown of the diode is limited by a large resistor, which leads to a voltage drop below the breakdown voltage V_{br}.

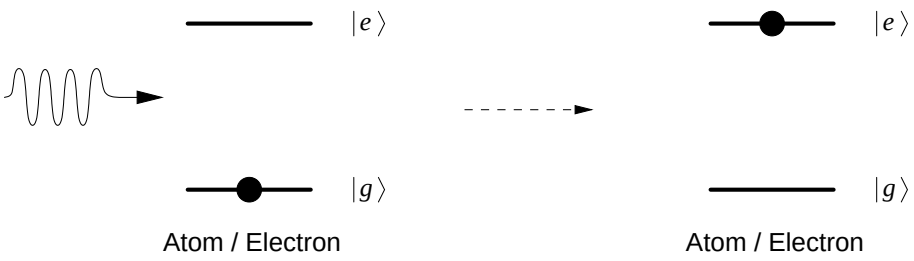

Figure 2.7: An atom gets into an excited state after absorption of light.

2.3.2 How to describe photodetection in terms of quantum mechanics?

We have seen several photodetector schemes so far - most of them rely on an elementary process of absorption of light, which is then detected by some other mechanism. Let us therefore consider the physical process of creating a photoelectron. We further simplify our detector to a two-level system instead of the more commonly found continuum of excitation states of usual photodetectors. The absorption process is then modeled by the following transition:

Energy conservation makes it necessary that the energy of the field and the detector system stays constant. Therefore the operator associated with the transition in the photodetector model has not only to "destroy" an energy quantum of the field, but also create an excitation of the detector. Restricting to a single field mode, we could represent this process by an operator

$$\hat{h} = \hat{a}\hat{d}^\dagger \,, \tag{2.42}$$

where $\hat{a}$ is our usual lowering operator for the field, and

$$\hat{d}^\dagger = |e\rangle\langle g| \tag{2.43}$$

describes the rising operator for the atom or electron. If the excitation operator $\hat{h}$ should be the outcome of a physical interaction process, it has to be derived from an interaction Hamiltonian of the form

$$\hat{H}_I = \text{const} \cdot (\hat{\text{a}}\hat{\text{d}}^\dagger + \hat{\text{a}}^\dagger\hat{\text{d}}) \tag{2.44}$$

To ensure hermiticity, with an atomic lowering operator $\hat{d} = |g\rangle\langle e|$. We will see such process later.

Single photoelectrons

Let's now consider the probability of observing a photoelectron. Assume the initial field before the creation of a photoelectron is in the state $|\psi_i\rangle$, and afterwards in the final state $|\psi_f\rangle$. The probability for such a transition is proportional to $|\langle\psi_f|\hat{a}|\psi_i\rangle|^2$.

If a photoelectron can be generated by a large bandwidth of frequencies from the electrical field, this probability can be expressed in terms of the sum over different modes of the electrical field operator $\hat{E}^{(+)}$ containing the lowering operators:

$$\tilde{w} \propto \left| \langle \psi_f | \hat{E}^{(+)}(\mathbf{x}, t) | \psi_i \rangle \right|^2 \tag{2.45}$$

This may be interpreted as the probability of creating a photoelectron at a position $\mathbf{x}$ and a time t – the usual model of light-matter interaction indeed justifies that, where we assign a well-defined location to the electron.

To use this probability to come up with some meaningful field measurement technique, let's keep in mind that for a given situation, we do not really do anything with the field state afterwards, and we consider only the photoelectron. We thus can obtain the probability of observing a photoelectron as a sum over all possible final field states,

$$\begin{aligned} w_1 &= \sum_f |\langle \psi_f | \hat{E}^{(+)}(\mathbf{x}, t) | \psi_i \rangle|^2 \\ &= \sum_f \langle \psi_i | \hat{E}^{(-)} | \psi_f \rangle \langle \psi_f | \hat{E}^{(+)} | \psi_i \rangle \\ &= \langle \psi_i | \hat{E}^{(-)} \hat{E}^{(+)} | \psi_i \rangle \,, \end{aligned} \tag{2.46}$$

where the completeness property has been used:

$$\sum_f |\psi_f\rangle\langle\psi_f| = \mathbb{I} \tag{2.47}$$

We end up with the probability w_1 of observing a photoelectron to be proportional to $\langle \hat{E}^{(-)} \hat{E}^{(+)} \rangle$. For stationary fields, this photoelectrons creation probability may be used to calculate a photo counting rate r.

However, the fact that we observe a number of discrete photoelectrons is not really an outcome of the field quantization procedure – you can derive a probability distribution for creating photoelectrons equally well assuming assuming a classical field interacting with a quantized detector system. There, the interaction Hamiltonian between field and system has a contribution

$$|e\rangle\langle g| E_{cl}^{(+)} d^{(+)} + |g\rangle\langle e| E_{cl}^{(-)} d^{(-)} \tag{2.48}$$

where $E_{cl}^{(+)}$ and $E_{cl}^{(-)}$ are components with positive and negative frequency respectively, and the $d^{\pm)}$ are the corresponding components of the electric dipole matrix elements of the considered transition. The photoelectron count rate then is proportional to

$$r = E_{cl}^{(-)} E_{cl}^{(+)} \propto I_{cl} \tag{2.49}$$

where I_{cl} is the classical intensity of the light field, derived out of the Poynting vector:

$$I = \left\langle \frac{1}{\mu_0} \mathbf{E} \times \mathbf{B} \right\rangle \cdot \mathbf{n}. \tag{2.50}$$

Photoelectron pairs

In the last section, we made the transition from a single photoelectron probability to a rate rather silently, assuming we can consider all photoelectron creation processes independently and summing them up, e.g. by assuming we evaluate the single photoelectron detection probability for infinitesimal time intervals Δt.

This may not always be appropriate. Let us therefore construct an expression for the probability w_2 of observing a pair of photoelectrons at two locations $\mathbf{x}_1$ and $\mathbf{x}_2$ at two times t_1 and t_2 (in the time intervals $[t_1, t_1 + \Delta t_1]$ and $[t_2, t_2 + \Delta t_2]$) similar to the single photoelectron case:

$$w_2(\mathbf{x}_1, \mathbf{x}_2, t_1, t_2) \propto |\langle \psi_f | \hat{E}^{(+)}(\mathbf{x}_2, t_2) \hat{E}^{(+)}(\mathbf{x}_1, t_1) | \psi_i \rangle|^2. \tag{2.51}$$

$\hat{E}^{(+)}(\mathbf{x}_1, t_1)$ and $\hat{E}^{(+)}(\mathbf{x}_2, t_2)$ refers to the creation of first and second photoelectrons respectively. Again, this should be summed over all the final field states, since we are only interested in the observation of the photoelectrons. This leads to

$$w \propto \langle \psi_i | \hat{E}^{(-)}(\mathbf{x}_1, t_1) \hat{E}^{(-)}(\mathbf{x}_2, t_2) \hat{E}^{(+)}(\mathbf{x}_2, t_2) \hat{E}^{(+)}(\mathbf{x}_1, t_1) | \psi_i \rangle. \tag{2.52}$$

Again, this probability may be associated with a count rate – this time, the observed quantity would be a coincidence count rate of detectors at $\mathbf{x}_1$ and $\mathbf{x}_2$ at times t_1 and t_2.

2.3.3 Correlation functions: First and second order

The expression for the single photodetection probability w_1 looks like an expectation value of a product of fields,

$$\langle \hat{E}^{(-)} \hat{E}^{(+)} \rangle \tag{2.53}$$

at the same position $\mathbf{x}$ and time t.

This concept can be generalized to different points $\mathbf{x}_1$, $\mathbf{x}_2$, t_1 and t_2 to a quantity

$$G^{(1)}(\mathbf{x}_1, \mathbf{x}_2, t_1, t_2) := \langle \hat{E}^{(-)}(\mathbf{x}_1, t_1) \hat{E}^{(+)}(\mathbf{x}_2, t_2) \rangle \tag{2.54}$$

which is called the *first order correlation function* of the field.

Similarly to the generalization of the simple photoelectron, this coincidence counting rate expression can be generalized into a definition of a *second order correlation function* for the electromagnetic field:

$$G^{(2)}(\mathbf{x}_1, \mathbf{x}_2, \mathbf{x}_3, \mathbf{x}_4, t_1, t_2, t_3, t_4) := \langle \hat{E}^{(-)}(\mathbf{x}_1, t_1) \hat{E}^{(-)}(\mathbf{x}_2, t_2) \hat{E}^{(+)}(\mathbf{x}_3, t_3) \hat{E}^{(+)}(\mathbf{x}_4, t_4) \rangle \tag{2.55}$$

Let's consider the case of a stationary field, where the two times involved in the definition of $G^{(1)}(\mathbf{x}_1, \mathbf{x}_2, t_1, t_2)$ are reduced to a time difference:

$$G^{(1)}(\mathbf{x}_1, \mathbf{x}_2, t_1, t_2) \to G^{(1)}(\mathbf{x}_1, \mathbf{x}_2, \tau) \qquad \text{with } \tau = t_2 - t_1 \tag{2.56}$$

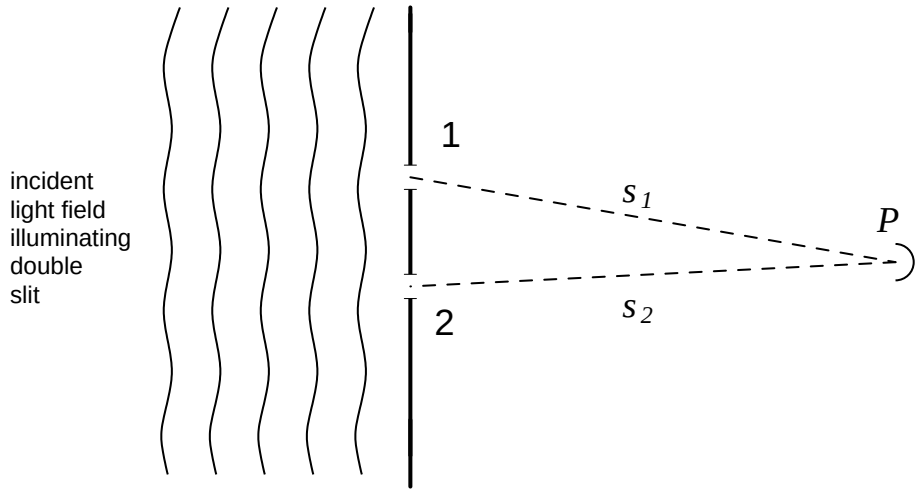

Figure 2.8: Double slit experiment. The field is detected at point P separated by distances s_1, s_2 from the two openings in the screen.

The count rate (or intensity) is then given by $G^{(1)}(\mathbf{x}, \mathbf{x}, 0)$ for a given position $\mathbf{x}$. We can perform a normalization of the correlation function using the intensities:

$$g^{(1)}(\mathbf{x}_1, \mathbf{x}_2, \tau) = \frac{\langle \hat{E}^{(-)}(\mathbf{x}_1, t)\hat{E}^{(+)}(\mathbf{x}_2, t+\tau)\rangle}{\sqrt{\langle \hat{E}^{(-)}(\mathbf{x}_1, t)\hat{E}^{(+)}(\mathbf{x}_1, t)\rangle \langle \hat{E}^{(-)}(\mathbf{x}_2, t+\tau)\hat{E}^{(+)}(\mathbf{x}_2, t+\tau)\rangle}} \tag{2.57}$$

Similarly for the second order correlation function,

$$g^{(2)}(\mathbf{x}_1, \mathbf{x}_2, \tau) = \frac{\langle \hat{E}^{(-)}(\mathbf{x}_1, t)\hat{E}^{(-)}(\mathbf{x}_2, t+\tau)\hat{E}^{(+)}(\mathbf{x}_2, t+\tau)\hat{E}^{(+)}(\mathbf{x}_1, t)\rangle}{\langle \hat{E}^{(-)}(\mathbf{x}_1, t)\hat{E}^{(+)}(\mathbf{x}_1, t)\rangle \langle \hat{E}^{(-)}(\mathbf{x}_2, t+\tau)\hat{E}^{(+)}(\mathbf{x}_2, t+\tau)\rangle}. \tag{2.58}$$

The normalization of this function is chosen such that the denominator contain two expressions $\langle \hat{E}^{(-)}(\mathbf{x}_i, t)\hat{E}^{(+)}(\mathbf{x}_i, t)\rangle$, which are intensities at the two locations, and independent of time for stationary fields.

These quantities are referred to as first order and second order *coherence functions*. They have a relatively simple interpretation for many optical experiments.

2.3.4 Double slit experiment

To understand the first order coherence function, we consider the double slit experiment as shown in Fig. 2.8.

Simple propagation of the field according to Huygens principle (under ignoring any fine emission structure due to diffraction, and attenuation at with distance from the openings in the screen) leads to an electrical field at the detector location P of

$$\hat{E}^{(\pm)}(\mathbf{r}, t) = \hat{E}^{(\pm)}\left(\mathbf{r}_1, t - \frac{s_1}{c}\right) + \hat{E}^{(\pm)}\left(\mathbf{r}_2, t - \frac{s_2}{c}\right) \tag{2.59}$$

For the intensity at the point P of observation behind the slit, we have

$$\begin{aligned} I(\mathbf{r},t) &= \langle \hat{E}^{(-)}(\mathbf{r},t)\hat{E}^{(+)}(\mathbf{r},t)\rangle \\ &= \langle \hat{E}^{(-)}\left(\mathbf{r}_1, t-\frac{s_1}{c}\right)\hat{E}^{(+)}\left(\mathbf{r}_1, t-\frac{s_1}{c}\right)\rangle \\ &\quad +\langle \hat{E}^{(-)}\left(\mathbf{r}_2, t-\frac{s_2}{c}\right)\hat{E}^{(+)}\left(\mathbf{r}_2, t-\frac{s_2}{c}\right)\rangle \\ &\quad +2\mathrm{Re}[\langle \hat{\mathrm{E}}^{(-)}\left(\mathbf{r}_1, \mathrm{t}-\frac{\mathrm{s}_1}{\mathrm{c}}\right)\hat{\mathrm{E}}^{(+)}\left(\mathbf{r}_2, \mathrm{t}-\frac{\mathrm{s}_2}{\mathrm{c}}\right)\rangle] \\ &= I_1 + I_2 + 2\mathrm{Re}[\sqrt{\mathrm{I}_1\mathrm{I}_2}\mathrm{g}^{(1)}(\mathbf{r}_1,\mathbf{r}_2,\tau)] \end{aligned} \tag{2.60}$$

with

$$I_{1,2} = \left\langle \hat{E}^{(-)}\left(\mathbf{r}_{1,2}, t-\frac{s_{1,2}}{c}\right)\hat{E}^{(+)}\left(\mathbf{r}_{1,2}, t-\frac{s_{1,2}}{c}\right)\right\rangle \tag{2.61}$$

and

$$\tau = \frac{s_2 - s_1}{c} \tag{2.62}$$

the time difference of propagation from the slits/holes to the detector position.

This can be rewritten using our new coherence function

$$g^{(1)}(\mathbf{x}_1,\mathbf{x}_2,\tau) = \left|g^{(1)}(\mathbf{r}_1,\mathbf{r}_2,\tau)\right| e^{i\varphi(r_1,r_2,t)}, \tag{2.63}$$

where the fastest change along the screen comes from the varying time difference. For a light field with a fixed frequency ω_0, the phase φ can be decomposed into

$$\varphi = \alpha(\mathbf{r}_1,\mathbf{r}_2,\tau) - \omega_0\tau, \tag{2.64}$$

where α is a slowly varying function[1].

With this, the intensity at the observation point P is given by

$$I(\mathbf{r}) = I_1 + I_2 + 2\sqrt{I_1 I_2}\cos\left(\alpha - \frac{s_1 - s_2}{c}\omega_0\right)|g^{(1)}(\mathbf{r}_1,\mathbf{r}_2,\tau)| \tag{2.65}$$

leading to the well-known interference pattern of a double slit[2], where the $|g^{(1)}(\mathbf{r}_1,\mathbf{r}_2,\tau)|$ term determines the "visibility" of the interference pattern. The quantitative definition of visibility of an interference pattern is given by

$$V := \frac{I_{\max} - I_{\min}}{I_{\max} + I_{\min}}, \tag{2.66}$$

which can be expressed in terms of the coherence function:

$$V = \frac{2\sqrt{I_1 I_2}}{I_1 + I_2}|g^{(1)}(\mathbf{r}_1,\mathbf{r}_2,\tau)| \tag{2.67}$$

[1] For infinitesimally small pinholes, α is a constant

[2] This expression includes Fresnel and Fraunhofer diffraction.

For $I_1 = I_2$, the visibility itself is equal to the modulus of the first-order coherence.

If light at two positions $\mathbf{r}_1$ and $\mathbf{r}_2$ is mutually incoherent, no interference pattern forms, or $V = 0$ and $g^{(1)}(\mathbf{r}_1, \mathbf{r}_2, \tau) = 0$. Maximal visibility of $V = 1$ occurs when $|g^{(1)}(\mathbf{r}_1, \mathbf{r}_2, \tau)| = 1$ or the fields are mutually coherent.

This is a result perfectly compatible with classical optics. In fact, the notion of a complex coherence function is very well established in classical optics, and can be used to describe incoherent or partially coherent light. For the first-order coherence describing field-field correlations, there are in fact no difference between the prediction of classical optics and the fact that we had to describe the field quantum mechanically.

2.3.5 Power spectrum

Another important coherence property is the connection between the power spectrum for different frequencies and the temporal coherence. One can show that the power density defined by

$$S(\mathbf{r}, \omega) = |\mathscr{E}(\omega)|^2 , \tag{2.68}$$

where

$$\mathscr{E}(\omega) = \frac{1}{\sqrt{\pi}} \int_{-\infty}^{\infty} E(\mathbf{x}, t) e^{-i\omega t} dt \tag{2.69}$$

is just the Fourier component of the electrical field at a given (angular) frequency ω.

The spectral power density is also related to the first order correlation function via

$$S(\mathbf{r}, \omega) = \frac{1}{\pi} \mathrm{Re} \int_{-\infty}^{\infty} \mathrm{G}^{(1)}(\mathbf{r}, \mathbf{r}, \tau) \mathrm{e}^{\mathrm{i}\omega\tau} \mathrm{d}\tau \tag{2.70}$$

Therefore, there is a close connection between the form of the power spectrum and the coherence length.

As an example, consider the green light component in common fluorescent lamps (resulting from mercury atoms emitting at around 546 nm). The atoms move with a velocity given by their thermal distribution, and thereby exhibit a Doppler effect for the emitted wavelength (which will dominate the spectral broadening). Assume the frequency distribution is Gaussian, with a center frequency ω_0 and a certain width σ:

$$S(\omega) = A e^{-\frac{(\omega - \omega_0)^2}{2\sigma^2}} \tag{2.71}$$

The corresponding coherence function is a Gaussian distribution again, this time centered around $\tau = 0$:

$$G(\tau) \propto e^{-\frac{t^2\sigma^2}{2}} = e^{-\frac{t^2}{2\tau_c^2}} \qquad \text{with } \tau_c = \frac{1}{\sigma} \tag{2.72}$$

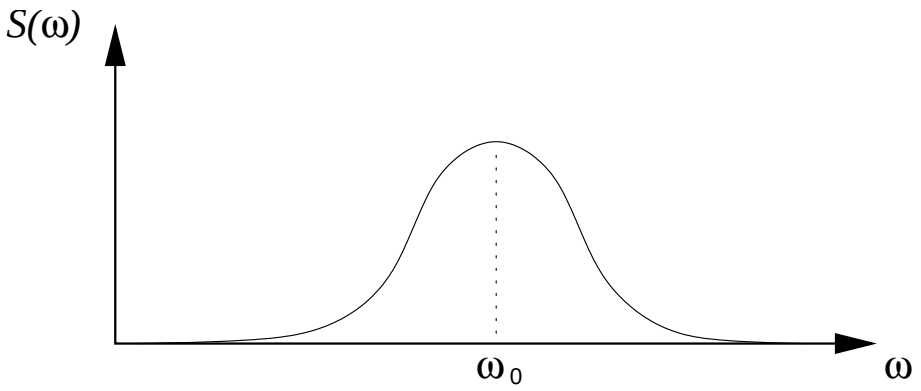

Figure 2.9: Spectral density of a light, with a Gaussian distribution centered around ω_0.

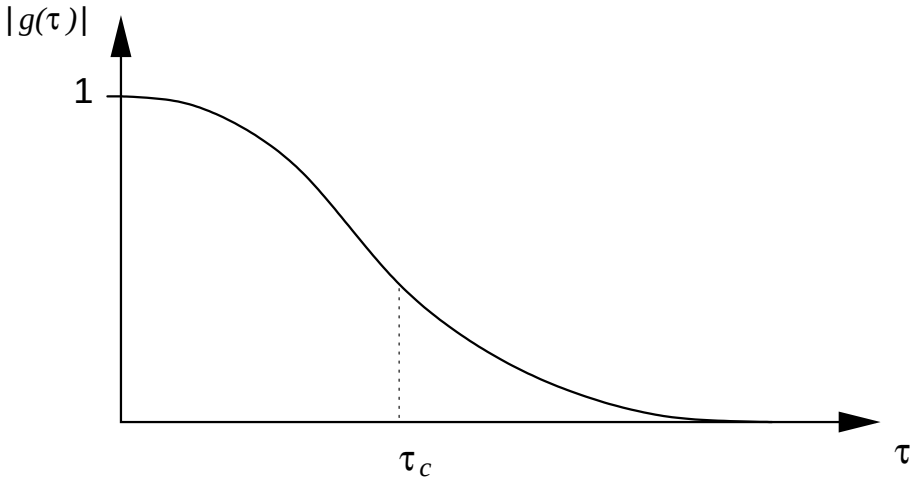

Figure 2.10: The coherence function of a light with a Gaussian frequency spectrum.

τ_c may be considered as the coherence time of the light field. Such a definition always makes sense if the whole distribution $G^{(1)}(\tau)$ can be characterized by a single number. Using the complex degree of coherence $g^{(1)}$, we obtain a function which is normalized to 1 for $\tau = 0$.

2.3.6 Coherence functions of the various field states

To get an understanding of the second order correlation function, we restrict ourselves to the case when only one mode present and evaluate them at a fixed location X. For comparison, we o the same thing also for the first order correlations. These simplified the correlation functions become

$$g^{(1)}(\tau) = \frac{\langle \hat{a}^\dagger(t)\hat{a}(t+\tau)\rangle}{\langle \hat{a}^\dagger\hat{a}\rangle} \tag{2.73}$$

$$g^{(2)}(\tau) = \frac{\langle \hat{a}^\dagger(t)\hat{a}^\dagger(t+\tau)\hat{a}(t+\tau)\hat{a}(t)\rangle}{\langle \hat{a}^\dagger\hat{a}\rangle^2}. \quad (2.74)$$

Let's now evaluate these functions for the three classes of states we have considered before. The first one that we consider is the number states:

$$g^{(1)}(\tau) = \frac{\langle \hat{a}^\dagger(t)\hat{a}(t+\tau)\rangle}{\langle \hat{a}^\dagger\hat{a}\rangle} = \frac{\langle n|\hat{a}^\dagger(t)\hat{a}(t)e^{-i\omega\tau}|n\rangle}{\langle n|\hat{a}^\dagger\hat{a}|n\rangle} = e^{-i\omega\tau} \quad (2.75)$$

$$g^{(2)}(\tau) = \frac{\langle \hat{a}^\dagger(t)\hat{a}^\dagger(t+\tau)\hat{a}(t+\tau)\hat{a}(t)\rangle}{\langle \hat{a}^\dagger\hat{a}\rangle^2} = \frac{\sqrt{n}\sqrt{n-1}\sqrt{n-1}\sqrt{n}}{n^2} = 1 - \frac{1}{n} \quad (2.76)$$

where we have made use of the following:

$$\hat{a}(t) = \hat{a}(t=0)e^{-i\omega t} \quad (2.77)$$

$$\hat{a}^\dagger(t) = \hat{a}^\dagger(t=0)e^{i\omega t} \quad (2.78)$$

Note that the first order coherence function of number states has the property that $|g^{(1)}(\tau)| = 1$. The second order coherence function has the property $g^{(2)}(\tau) < 1$ which implies that there is photon anti-bunching for number states. This means that given two detectors, if we detected a photon at the first detector, the probability of seeing another photon at the second detector at the same time is lowered.

Next, we proceed to coherent states where we have:

$$g^{(1)}(\tau) = \frac{\alpha^*\alpha e^{-i\omega\tau}}{\alpha\alpha^*} = e^{-i\omega\tau} \quad (2.79)$$

$$g^{(2)}(\tau) = \frac{\alpha^{*2}\alpha^2}{(\alpha^*\alpha)^2} = 1. \quad (2.80)$$

And finally we have for thermal states

$$g^{(1)}(\tau) = \frac{\sum_n p_n n e^{-i\omega\tau}}{\sum_n p_n n} = e^{-i\omega\tau} \quad (2.81)$$

$$g^{(2)}(\tau) = \frac{\sum_n (1-A)A^n n(n-1)}{(\sum_n (1-A)A^n n)^2} = 2 \quad (2.82)$$

Here, in contrast to the number states, we observe photon bunching due to $g^{(2)}(\tau) = 2$. We also note that the different states of the light field do not reveal themselves in the first order correlation function, but in the second order correlation function.

2.3.7 Interpretation of the $g^{(2)}(\tau)$ function

An interpretation of the $g^{(2)}(\tau)$ may be obtained if we go back to the definition of w_2. There, we find the probability w_2 of finding a photoelectron in the time interval $[t, t+\Delta t]$, and another one at the time interval $[t+\tau, t+\tau+\Delta t]$.

$g^{(2)}(\tau)$ is then simply the probability of finding two photoelectrons separated by a duration τ (in a given time interval Δt), compared to the squared probability of finding one photoelectron. Therefore, cases with $g^{(2)}(\tau) = 1$ correspond to the case where the pair probability is just the squared probability of a single count. The quasi-classical state $|\alpha\rangle$ shows exactly such a behavior.

For $g^{(2)}(\tau) < 1$, as seen for photon number states, this probability is *reduced*. This fact is referred to as "photon anti-bunching", i.e. for this state it looks like photons prefer to be detected separately. States of the light filed with $g^{(2)}(\tau) > 1$ are referred to as exhibiting photon bunching, with an increased probability of finding two photoelectrons at the same time.

We continue to discuss what happens to the $g^{(2)}(\tau)$ if light from two uncorrelated sources is detected. We use statistical argument here, where we denote the probability of seeing one photon from A and B to be P_A and P_B respectively, with

$$P_A + P_B = 1. \tag{2.83}$$

Now, we consider the case when two photons from source A are detected. This happens with a probability of P_A^2 with the corresponding $g_A^{(2)}(\tau)$ for source A. Similarly, we also have detection of two photons from source B with probability P_B^2 and $g_B^{(2)}(\tau)$. Finally, there is also a possibility that one photon is from source A, while the other one is from source B. The probability of this happening is $1 - P_A^2 - P_B^2$ and the $g_{AB}^{(2)}(\tau)$ associated is 1 for uncorrelated light source.

Now, the overall $g^{(2)}$ function for light from two uncorrelated sources is given by

$$g^{(2)}(\tau) = P_A^2 g_A^{(2)}(\tau) + P_B^2 g_B^{(2)}(\tau) + (1 - P_A^2 - P_B^2). \tag{2.84}$$

If the two sources A and B are similar, that is their $g^{(2)}$ functions are the same $g_A^{(2)}(\tau) = g_B^{(2)}(\tau)$, and $P_A = P_B$, we have

$$g^{(2)}(\tau) = \frac{1}{2} g_A^{(2)}(\tau) + \frac{1}{2}. \tag{2.85}$$

If the light is from two uncorrelated sources, the non-classical property of $g^{(2)} \neq 1$ is diluted.

2.3.8 Experimental measurements of photon pair correlations

With the second order correlation function $g^{(2)}(\tau)$ we have have seen a mathematical object or *measure* to distinguish between different quantum mechanical states of a light field, which classically is only characterized by an intensity and a frequency.

The differences between different states comes about in the probability of observing photoelectron pairs at a given time difference. Such experiments have

been pioneered by H. Hanburry-Brown and R. Twiss starting from 1956, and are now in widespread use.

The definition of $g^{(2)}(\tau)$ is already quite operational. The light of an optical mode under consideration is sent to two photodetectors using a beam splitter, and a photoelectron pair creation is detected as a coincidence count between the two outputs:

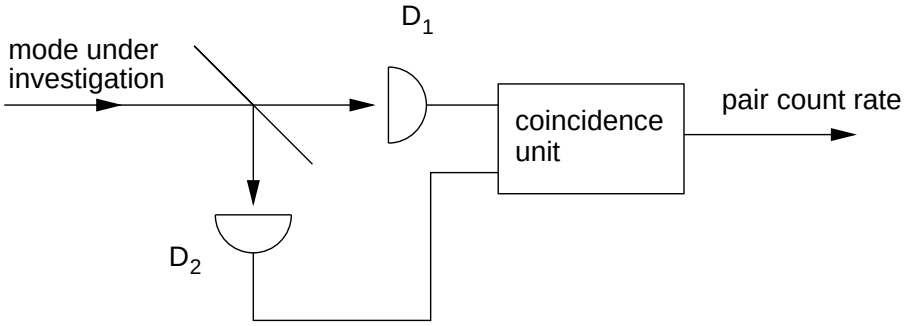

Figure 2.11: The mode under investigation is sent through a beam splitter where it is detected at the two detectors D_1 or D_2 before being sent through a coincidence unit.

By varying the time difference of the photodetection event, $g^{(2)}(\tau)$ can be measured. Furthermore, the observation of individual rates at detector D_1 and D_2 allow a proper normalization.

Such a setup is referred to as a Hanbury-Brown–Twiss configuration, according to the first experiments of this kind [13, 14, 15]. In initial experiments, the coincidence was obtained in a way by multiplying the photocurrents of the two photomultipliers.

This setup was first used to investigate light from a spectral line emitted by mercury, where intensity fluctuations have been found. Subsequently, this technique was applied to investigate light from stars, and to measure the transverse coherence length, allowing people to determine the diameter of a light source with a large virtual aperture and without running into phase stability problems.

Recently, this measurement technique was used to investigate and more or less *define* so-called single-photon sources as physical systems which exhibit a vanishing second order correlation function for $\tau = 0$, meaning that the probability of creating more than one photoelectron at any single time vanishes. We come back to this in Section 2.5.2.

2.3.9 Localized wave packets

So far, we have considered photodetectors which generate a single photoelectron, and described their outcomes in statistical terms. Such a description does not

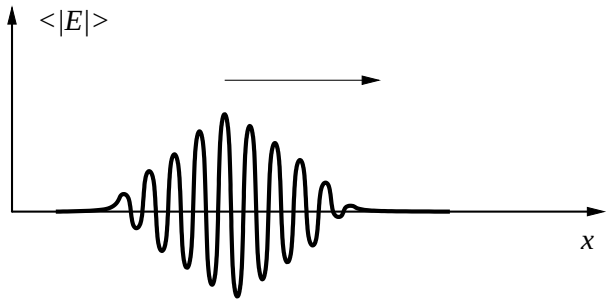

Figure 2.12: Wave packet, made up by modes with a similar wave vector k_0. Such a packet can be localizable in space and time, and present a light field which can lead to a localizable detection event.

imply the localization of a light field at all, but the observation of a single photoelectron or breakdown of an avalanche diode is a macroscopic signal, which one is tempted to give a localized light field as a physical reason. Later we will see that it is indeed possible to create light fields which are very well localized in time or space, and one would like to think of a light field which can generate exactly one photodetection event as a particle-like object - that would be our localized photon.

This concept, however, seems to be at odds with the definition of photons we encountered earlier, namely some sort of Fock states in well-defined discrete modes, which exhibit no localization in space or time, but are energy eigenstates of the field and thus stationary.

So how can we have a localization of a photon in time in a way that seems compatible with the observation of a single photodetection event, or a well-defined pair of them? The answer is reasonably simple: We can use a wave packet or a linear combination of different modes, and populate each of these modes with a certain state.

A simple example would be Gaussian wave packets. Take $f(\mathbf{k})$ as an amplitude for a component $\mathbf{k}$ of the field decomposition in plane waves indexed by $\mathbf{k}$, with

$$f(\mathbf{k}) = \frac{1}{A} e^{-\frac{(\mathbf{k}-\mathbf{k}_0)^2}{2\sigma_k^2}} \qquad \text{for } t = 0 \tag{2.86}$$

If $f(\mathbf{k})$ is the amplitude of a particular Fourier component of a classical electromagnetic field, this would result in an electric field $E(\mathbf{r})$ of

$$E(\mathbf{r}) = \int f(\mathbf{k}) e^{i\mathbf{k}\cdot\mathbf{r}} d\mathbf{k}. \tag{2.87}$$

If the time evolution is included, we have

$$E(\mathbf{r}, t) = \int f(\mathbf{k}) e^{i(\mathbf{k}\cdot\mathbf{r} - \omega_k t)} d\mathbf{k} \qquad \text{with } \omega_k = |\mathbf{k}|c \tag{2.88}$$

This is a localized moving wave packet with a well-defined center (in space) moving with the speed of light, c, and a constant spatial extent with a variance of $\frac{1}{\sigma_k^2} = \sigma_r^2$.

In order to write a creation operator for such a field state, we can just use the idea introduced with the beam splitter, where we expressed the lowering and raising operator at the output ports as linear combinations of the modes at the input:

$$\hat{c} = \sum_i \lambda_i \hat{a}_i \tag{2.89}$$

This linear combination of modes can be generalized for wave packets to

$$\hat{c}_{k_0} = \sum_k f(\mathbf{k}) \hat{a}_k. \tag{2.90}$$

Such an object would be able to generate exactly one photodetection event (assuming a wide band photodetector, i.e., that each of the contributing components $\hat{a}_k^\dagger|0\rangle$ would generate a detection event as well), and would exhibit a certain localization in time. If the distribution is reasonably restricted to a small number of mode indices k with a similar frequency, it still would appear to make sense to assign a center wavelength to the object $|\Psi\rangle = \hat{c}_{k_0}|0\rangle$ - which with some justification may be referred to as a localized photon.

2.4 Direct measurement of electric fields

Up to now, the optical measurements on quantized light fields we considered were related to detecting a photoelectron rates. In order to closer investigate the electrical field forming the light directly, we need to find a way to measure the electrical fields directly.

One approach of understanding how to measure fields connects to the basic setup in a Hanbury-Brown–Twiss measurement of photoelectron pairs, where two photodetectors are located behind a beam splitter. We used that beam splitter merely to divert a fraction of the light in a field mode of interest on each detector.

However, the beam splitter has not only two output modes c and d receiving contributions from one input mode a, but also from a second input port b, with the associated field fluctuations even if no light is entering this port. We therefore should consider this element more carefully.

2.4.1 Beam splitter

In classical optics, one can derive a relation between in and outgoing field amplitudes of a beam splitter; the outgoing fields are a linear combination of the

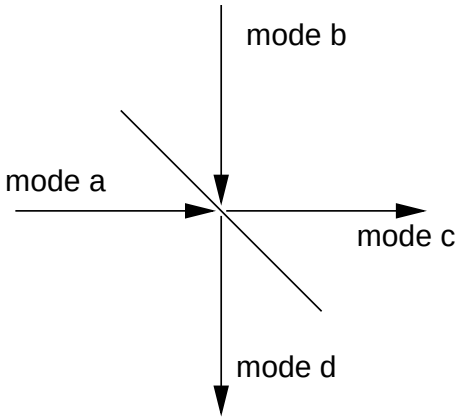

Figure 2.13: The beam splitter with two input modes a and b and two output modes c and d.

incoming fields of the form

$$\begin{pmatrix} E_C \\ E_D \end{pmatrix} = \begin{pmatrix} \sqrt{T} & i\sqrt{1-T} \\ i\sqrt{1-T} & \sqrt{T} \end{pmatrix} \begin{pmatrix} E_A \\ E_B \end{pmatrix} = S \begin{pmatrix} E_A \\ E_B \end{pmatrix} \tag{2.91}$$

where we define the "transfer matrix"

$$S := \begin{pmatrix} \sqrt{T} & i\sqrt{1-T} \\ i\sqrt{1-T} & \sqrt{T} \end{pmatrix}. \tag{2.92}$$

Here, we assume that we choose only one polarization, e.g. the polarization vector perpendicular to the plane of incidence. In this expression, T characterizes the fraction of transmitted *intensity*. For a balanced or symmetric beam splitter, $T = 0.5$, i.e. half of the light is transmitted and the other half reflected.

A somewhat surprising aspect of that transfer matrix is the i appearing on the reflection entries - where should that asymmetry come from? It can be understood when looking at a particular physical implementation of a beam splitter: One example would be a reflection from an air-glass interface, where the reflection from inside surface differs from the reflection on the outside surface by sign change in the electrical field. The choice of the phases of reflection is somewhat arbitrary and depends on the specific implementation, but it is always 180 degrees between the two reflections. The choice i for a model beam splitter is just a possibility which leads to a symmetric scattering matrix.

The linearity in fields carries simply over into a linear relationship between field operators, and the beam splitter itself may be regarded as an element which transforms creation and annihilation operators:

$$\begin{pmatrix} \hat{c} \\ \hat{d} \end{pmatrix} = S \begin{pmatrix} \hat{a} \\ \hat{b} \end{pmatrix} = \begin{pmatrix} \sqrt{T}\hat{a} & i\sqrt{1-T}\hat{b} \\ i\sqrt{1-T}\hat{a} & \sqrt{T}\hat{b} \end{pmatrix} \tag{2.93}$$

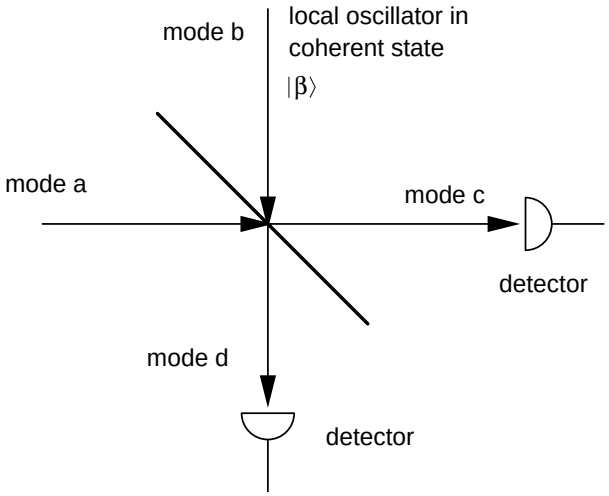

Figure 2.14: Basic homodyne detection configuration. The field in mode a gets superimposed with the field of a local oscillator in mode b in a coherent state $|\beta\rangle$.

We now can express the photocurrents or count rates recorded at detectors C and D as expectation values $\langle\hat{n}_C\rangle$ and $\langle\hat{n}_D\rangle$, where $\hat{n}_{C,D} = \hat{a}^\dagger_{C,D}\hat{a}_{C,D}$:

$$\langle\hat{n}_C\rangle = \langle\hat{c}^\dagger\hat{c}\rangle = T\langle\hat{a}^\dagger\hat{a}\rangle + (1-T)\langle\hat{b}^\dagger\hat{b}\rangle + i\sqrt{T}\sqrt{1-T}\langle\hat{a}^\dagger\hat{b} - \hat{b}^\dagger\hat{a}\rangle, \quad (2.94)$$

$$\langle\hat{n}_D\rangle = \langle\hat{d}^\dagger\hat{d}\rangle = (1-T)\langle\hat{a}^\dagger\hat{a}\rangle + T\langle\hat{b}^\dagger\hat{b}\rangle - i\sqrt{T}\sqrt{1-T}\langle\hat{a}^\dagger\hat{b} - \hat{b}^\dagger\hat{a}\rangle. \quad (2.95)$$

Both terms consists of intensities contributions $\langle\hat{a}^\dagger\hat{a}\rangle$ and $\langle\hat{b}^\dagger\hat{b}\rangle$, and a mixed term with $\langle\hat{a}^\dagger\hat{b}\rangle$ and $\langle\hat{b}^\dagger\hat{a}\rangle$.

2.4.2 Homodyne detection

Let's now assume that we have a "local oscillator field" in mode $\hat{b}$, where field b is in a coherent state $|\beta\rangle$. Such a situation can be realized using a classical light source. It turns out that a laser light source far above threshold may be considered as such a light source.

Assuming that the combined field state in modes a and b separates in the form

$$|\psi\rangle = |\psi_A\rangle \otimes |\beta\rangle\,, \quad (2.96)$$

the expectation value of the photon number in the detection mode c is given by

$$\langle\hat{n}_C\rangle = T\langle\hat{n}_A\rangle + (1-T)|\beta|^2 + i\sqrt{T}\sqrt{1-T}\langle\hat{a}^\dagger\hat{b} - \hat{b}^\dagger\hat{a}\rangle \quad (2.97)$$

If we interpret this as an expectation value of the number of detected photoelectrons, this vale refers to the expectation value of a discrete count rate (or photo current) at detector C. Using $\beta = |\beta|e^{i\varphi}$, this turns into

$$\langle\hat{n}_C\rangle = T\langle\hat{n}_A\rangle + (1-T)|\beta|^2 + i\sqrt{T}\sqrt{1-T}\,|\beta|\,\langle\hat{a}e^{i\varphi} - \hat{a}e^{-i\varphi}\rangle\,. \quad (2.98)$$

For $\varphi = 0$, the interference term t the end contains an expression for the expectation value for the field $\hat{E}$, so this method allows one to really measure the electric field.

We can define a generalized quadrature component along a phase angle φ by

$$\hat{a}_\varphi := \frac{1}{2}\left(\hat{a}^\dagger e^{i\varphi} + \hat{a}e^{-i\varphi}\right) = \hat{a}_Q \cos\varphi + \hat{a}_P \sin\varphi\,, \tag{2.99}$$

which can be used to simplify the expectation value in eqn (2.98):

$$\langle \hat{n}_C \rangle = T\langle \hat{n}_A \rangle + (1-T)|\beta|^2 + 2\sqrt{T(1-T)}\,|\beta|\,\langle \hat{a}_{(\varphi+\pi/2)} \rangle. \tag{2.100}$$

To compensate for the residual noise in the local oscillator, one often takes the difference of photocurrents in the two photodetectors, $i_C - i_D$, corresponding to an observable $\hat{n}_C - \hat{n}_D$. Then, only the interference term survives, and the noisy terms due to the local oscillator and the variance in the numbers of photons in the input state cancels out for $T = 0.5$:

$$\begin{aligned} \langle \hat{n}_C - \hat{n}_D \rangle &= 2i\sqrt{T(1-T)}|\beta|\langle \hat{a}^\dagger e^{i\varphi} - \hat{a}e^{-i\varphi} \rangle \\ &= -|\beta|\langle \hat{a}_{(\varphi+\pi/2)} \rangle \end{aligned} \tag{2.101}$$

This technique can now be used to measure the quadrature amplitude $\hat{a}_\varphi$ directly and get information about the variances of the light field directly, and is referred to as a *balanced homodyne detection*. It became an important detection tool for detecting squeezed states of light, with a reduced noise level in one of the quadrature components, as well as for more complex interacting systems in quantum information processing using continuous variables.

2.4.3 Heterodyne detection

The idea in a homodyning setup is to remove all the contributions containing intensities by looking for the difference in photocurrents, and extract the information about the electrical field out of that difference. In practice, the difference will always be a small contribution to the total photocurrent. Furthermore, the small difference will be contaminated by significant noise in the photodetection signal at low frequencies due to other sources than the photocurrent, which tends to be far above the shot noise limit corresponding to the photoelectron number fluctuation from the coherent state contributions.

To overcome the low frequency noise problem, another slightly modified configuration for field detection is typically used, referred to as *heterodyne detection*. The main idea behind this scheme is rather technical and takes the difference is not at low frequencies, but moves it to a frequency where (a) the photodetetors exhibit a low intrinsic noise, and (b) the necessary amplifiers can be built with better noise properties. The shift is realized by using a difference $\Omega/2\pi$ in the

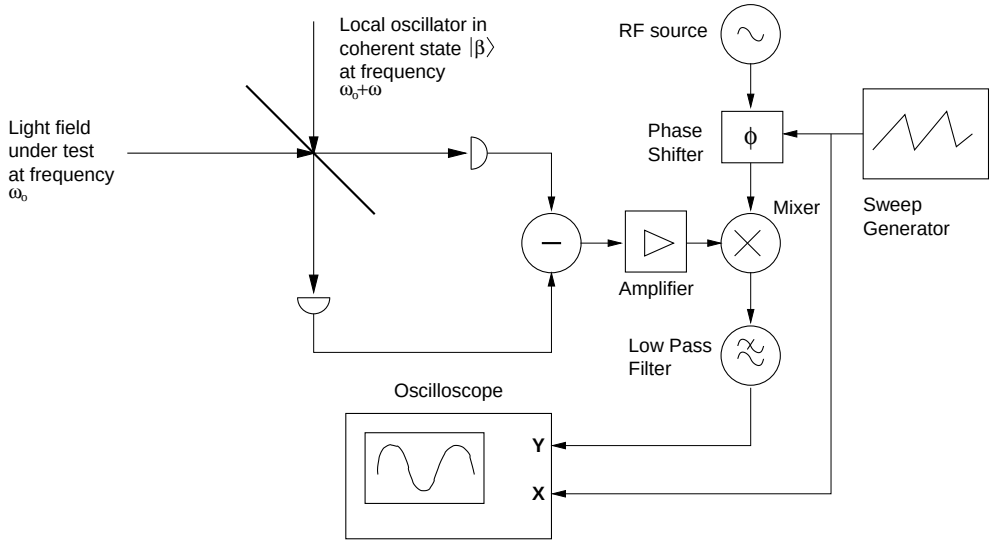

Figure 2.15: A setup for heterodyne measurement of a light field at frequency ω_0.

frequencies for the mode a under investigation and the local oscillator mode in the coherent state $|\beta\rangle$. Then, the photocurrent difference component containing information about the electrical filed in mode a is contained in a spectral component at $\Omega/2\pi$ in the photocurrent difference signal, which can be amplified without adding significant electronic noise. From there, the interesting spectral component can be brought back to a DC level with a second homodyning process, this time for classical electronic signals. The necessary element is just a mixer, which multiplies the amplified photocurrent difference with a sinusoidal signal at $\Omega/2\pi$. A phase shifter in the radio frequency path allows an easy access to both quadrature components of the electromagnetic field. A sketch summarizing this scheme is shown in Fig. 2.15.

In both homodyne- and heterodyne detection schemes the identification of a single photon is not exactly trivial; even the assignment of a well-defined value of α in a homodyne measurement is difficult. In practice, there is a time interval necessary, or a corresponding frequency window, over which a photocurrent or its fluctuations are registered. Only with this notion we arrive at well-localizable light states, which can be used as qubits or carrier of some information later on.

2.5 Tying "the photon" to the generation process

So far, we have seen how a photon can be defined via the detection scheme - in particular, the conversion into a single photoelectron seemed a very good candidate to define localizable photons. We are now looking for generation processes

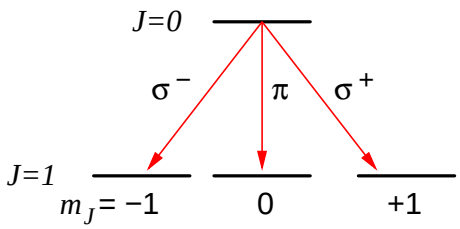

Figure 2.16: Three possible decay paths from $J = 0$ to $J = 1$.

which can provide us with a state that makes a photodetector give a localizable signal, and would be rightly described by a wave packet object generated by eqn (2.90).

2.5.1 Spontaneous emission

An explicit example for a compound "photon" is the light field emitted by spontaneous emission from an atom. Typically, the two levels can only be part of atomic levels, where there is a multiplicity in the levels. This allows interaction of the light field with the electronic states according to $\mathbf{E} \cdot \mathbf{p}$, where $\mathbf{E}$ is the electric field and $\mathbf{p}$ is the atomic electric polarization.

We also realize that there are a few possible decay paths in a typical atomic transitions, which is summarized in Fig. 2.16.

Now, for the spontaneous emission, Wigner and Weisskopf have given a closed expression for the state of the system [4]:

$$\begin{aligned} |\psi(t)\rangle &= a(t)|e\rangle_A \otimes |0\rangle_{field} \\ &\quad + \sum_\rho b_{\rho,-1}(t)|g_{-1}\rangle \otimes |n_\rho = 1, n_{\rho'\neq\rho} = 0\rangle \\ &\quad + \sum_\rho b_{\rho,0}(t)|g_0\rangle \otimes |n_\rho = 1, n_{\rho'\neq\rho} = 0\rangle \\ &\quad + \sum_\rho b_{\rho,+1}(t)|g_{+1}\rangle \otimes |n_\rho = 1, n_{\rho'\neq\rho} = 0\rangle \end{aligned} \tag{2.102}$$

with

$$a(t) = e^{-\gamma t/2}, \tag{2.103}$$

$$b_{\rho,m}(t) = \frac{w_{eg}}{\hbar} \frac{e^{-\gamma t/2} - e^{-i\Delta(\rho)t}}{i\gamma/2 - \Delta(\rho)} \mathrm{CG}\left[0, 0; 1, m|1, m\right] . \tag{2.104}$$

Therein, ρ, m is a mode index corresponding to a spherical vector harmonic and an outgoing radial part. The details and derivation of this expression are part of atomic physics, so we just mention that w_{eg} is some form of reduced electric dipole matrix element between the two levels, $\gamma = 1/\tau$ corresponds to the natural

line width of that transition, given by the lifetime τ of the excited state, $\Delta(\rho) = ck_\rho - \omega_0$ is the detuning of a particular radial mode from the atomic resonance frequency ω_0, CG is a Clebsch-Gordan coefficient corresponding to the angular momentum modulus of ground- and excited level (here chosen to be 0 and 1, respectively), and m is one of -1, 0 or +1, describing the type of transition (σ^-, π or σ^+).

For the spherical symmetry of the problem it is adequate to formulate the electrical field operator

$$\hat{\mathbf{E}}(\mathbf{x}) = i \sum_{k,m} \mathscr{E}_{\omega_k} \left(\hat{a}_{k,m} \mathbf{g}_{k,m}(\mathbf{x}) - \hat{a}^\dagger_{k,m} \mathbf{g}^*_{k,m}(\mathbf{x}) \right) \tag{2.105}$$

with two scalar mode indices k, m and a mode function $\mathbf{g}_{k,m}(\mathbf{x})$ expressing the position $\mathbf{x}$ in spherical coordinates r, θ, φ:

$$\mathbf{g}_{m,k}(r, \theta, \varphi) \approx \mathrm{Re}\left[\frac{\mathrm{e}^{-\mathrm{ikr}}}{\mathrm{kr}} \right] \frac{\mathbf{r}}{|\mathbf{r}|} \times \mathbf{X}_{\mathrm{l,m}}(\theta, \varphi) \tag{2.106}$$

An exact expression needs to include the field at the atom more cleanly; the above expression, however, is a good approximation a few wavelengths away from the atom [2].

The dominating part is a spherical wave propagating away from the atom at the coordinate origin, with a certain width due to the fact that the emission process takes only a finite time (see Fig. 2.17). The vector spherical harmonics $\mathbf{X}_{l,m}(\theta, \varphi)$ basically contain information of the polarization in the various directions. For example, along the z direction ($\theta = 0$, often referred to as quantization axis) the $m = \pm 1$ or $\sigma^\pm$ transitions correspond to left- and right circular polarization. This function also contains the emission pattern of the different transitions, e.g. the fact that for the $m = 0$ or π transition, the field in z direction vanishes.

We typically regard the outgoing state (a linear combination of single excitations in many modes) as a single photon, since the energy content of the field is limited by the initial atomic excitation. Moreover, we would expect typically only one photoelectron to be created in a detector. We also have a localized wave packet, centered around a frequency ω_0 corresponding to the initial energy difference $E_e - E_g = \hbar\omega_0$.

What we would like to do now is to combine the time dependencies of all the components $\{\rho, m\}$ in eqn (2.102) into simpler ones, corresponding to the three possible classes of transitions, $\sigma^\pm, \pi$ into a set of new mode functions $\tilde{\mathbf{g}}_m(\mathbf{r})$ in the very same way as we express the modes at the output of a beam splitter as a linear combination of modes at its inputs. This will be done more formally in Chapter 4, where we make the connection between photons and qubits.

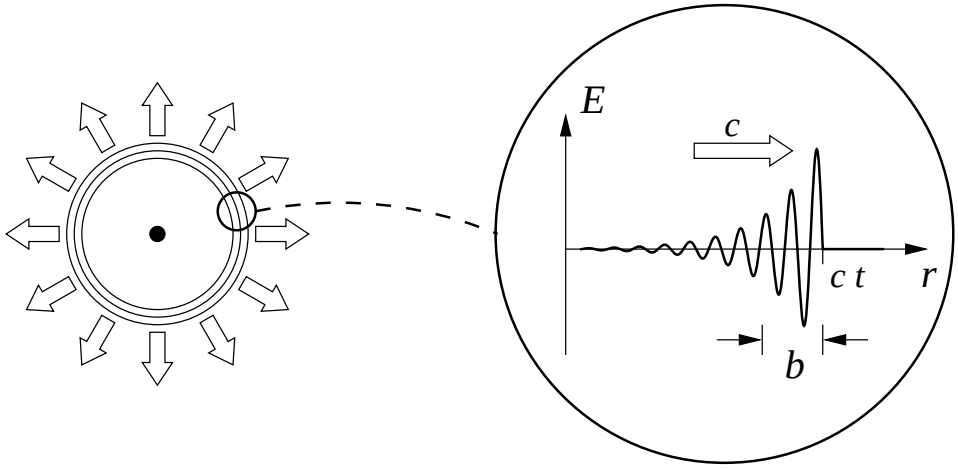

Figure 2.17: Mode function of the field around an atom after the radiative decay from an excited state: one on the role model examples of a localizable photon.

2.5.2 Single photon sources

Apart from the definition of what single photon states could be, we should consider specific physical implementations. While it is possible to prepare a single atom with a high probability into an excited state to establish the initial condition for a single photon emitted via subsequent spontaneous emission, it is not the simplest experimental approach. A much simpler approach is to excite an atomic system continuously, and observe the photodetection statistics of the scattered light of the microscopic system.

NV center single photon source

One of the perhaps simplest experimental implementations of such a single photon source is shown in Fig. 2.18, where a single charged nitrogen atom, which is embedded in a diamond lattice with an adjacent vacancy is used as the single quantum system. This nitrogen atom has an electronic transition which can emit light in the red wavelength range, and can be driven into the excited state by optical excitation with green light, by passing through some higher excited states and a subsequent relaxation to something close to a two-level system. Being embedded in a material with a high band gap, the electronic excitation is released with a high probability via a radiative decay, under additional broadening due to a change in the vibrational state of the atom/host lattice combination.

In an experimental setup, excitation light is focused down onto a single such color center, which can be done because these centers can be prepared with a very low density in a diamond host, such that the average distance between these centers is larger than a few optical wavelengths. Then, excitation light can be focused on a single color center, and the emitted light from the very same center

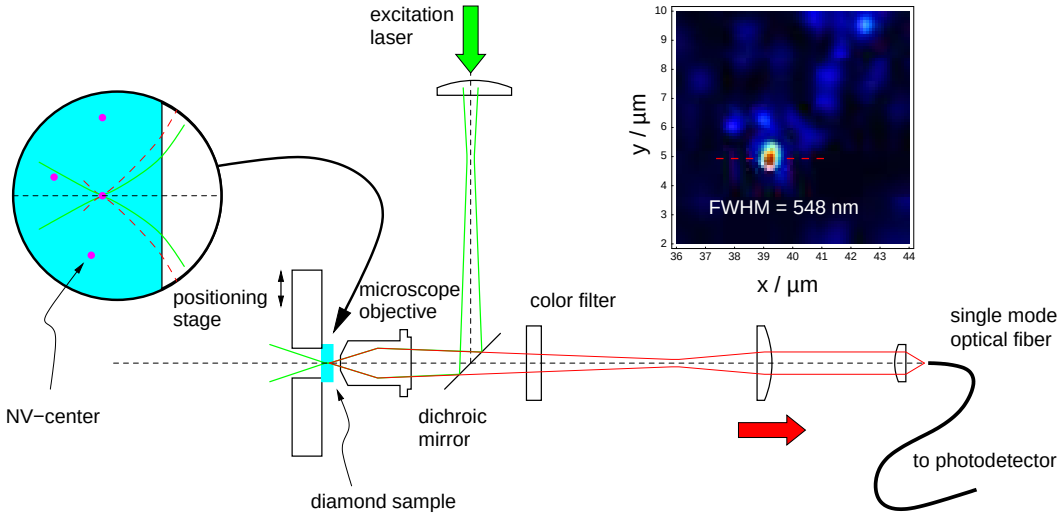

Figure 2.18: Experimental setup to observe single photon light from nitrogen-vacancy color centers in diamond. The excitation of the atom-like color center takes place with a short wavelength to an ensemble of states, which eventually lead to a spontaneous emission of a photon at a longer wavelength.

can be collected with a confocal microscope geometry. Since the spontaneous emitted light has wavelength which is far enough away from the excitation light (usually, a frequency-doubled Nd:YVO4 laser at a wavelength of 532 nm is used), color separation between the excitation light and the emitted light can be done with a high extinction ratio such that after spectral filtering, the photon statistics of the scattered light can be detected easily.

A typical photon statistics experiment following the setup of Hanbury-Brown and Twiss is shown in Fig. 2.19. The emitted light from the color center is directed onto a beam splitter, which distributes the field onto two photodetectors with a single photoelectron detection mechanism. The photoelectron detection signals are then histogrammed with respect of their arrival time difference to experimentally obtain a second order correlation function $g^{(2)}(\tau)$.

The experimental traces (c) in this figure shows a clear reduction of $g^{(2)}$ below 1 around $\tau = 0$ for low optical excitation powers, indicating that no two photoelectrons are generated at the same time. The interpretation of such an experimental signature is that the emitted light field is made up by isolated, or single photons. For larger excitation power levels, the "anti-bunching dip" gets narrower quickly, reflecting the fact that the NV center is transferred faster into the excited state again, ready for the emission of the next photon. The anticorrelation signature $g^{(2)}(\tau = 0) = 0$ gets more and more washed out, as the recovery time for the NV center excitation comes closer to the detector timing uncertainty.

The internal dynamics of the NV center guarantees that, once a photon has been emitted, the center is in the electronic ground state, and can only emit

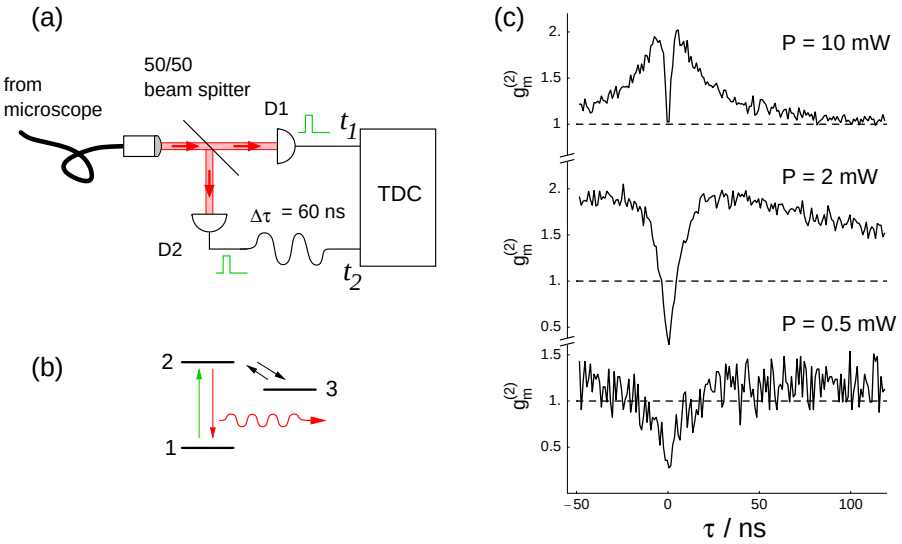

Figure 2.19: Observation of photon anti-bunching behavior in a Hanburry-Brown–Twiss geometry (a), where the time difference between photoevent pairs is analyzed. The corresponding level model of the NV center consists of three levels (b), and at room temperature the transitions between them can be well described using simple rate equations. The uncorrected measurement results (c) for different excitation powers reveal a characteristic signature of a photon anti-bunching for τ=0, thus indicating that there is a strong suppression of emission of more than one photon at the same time.

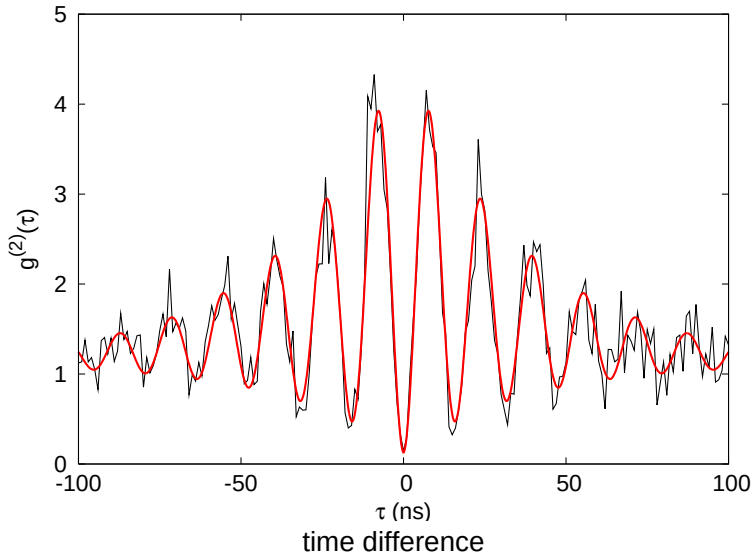

Figure 2.20: Second order correlation function for light scattered by a single atom under the exposure of near-resonant optical radiation. The atom was held in an optical tweezer, and the excitation light was driving a Rabi oscillation between ground- and excited state. The photon antibunching is still present for time differences $\tau = 0$ between photodetection events.

the next photon once the probability of being transferred into the excited state due to the presence of the excitation light has increased again. This particular experiment has been carried out at room temperature, where the presence of a huge phonon background in the diamond host leads to a very fast decoherence between ground- and excited state. Thus, the internal dynamics of the NV center is adequately described by a set of rate equations for the populations in the participating internal levels. From the presence of two exponential components in $g^{(2)}(\tau)$, it can be inferred that there are at least three participating levels.

Single photons from single atoms

A measurement on a physical system which shows much less decoherence between the internal electronic states is shown in Fig. 2.20. A single rubidium atom was trapped in an optical tweezer, while it was exposed to near-resonant excitation light. The atom undergoes occasionally a spontaneous emission, which is captured by a microscope objective onto a pair of photodetectors.

This time, the coherences between ground- and excited state can not be neglected, and $g^{(2)}(\tau)$ shows a damped oscillatory behavior together with a clear antibunching signature at $\tau = 0$. The damping time constant is related to the radiative lifetime of the excited state (26 ns for this transition), and the Rabi oscillation reflects the coherent population transfer under the electric field strength

of the excitation light.

This atomic single photon source, however, is far from being deterministic: While the probability of observing two photodetection events at the same time is very low, the probability of detecting a photon at a desired time is very small. This is due to the fact that the atom emits the photon in a spherical harmonics mode, but the collection optics manages to receive only a small fraction of the full solid angle. Furthermore, this particular excitation scheme is not deterministic at all, but driven by a continuous light source.

Deterministic single photon sources

To overcome the statistical nature of the single photons emitted in the previous two examples, two aspects need to be considered:

1. The excitation process has to happen at a well-defined time, and with a high probability. This can be achieved with an optical excitation either by a short pulse performing half a Rabi oscillation, or via an adiabatic transfer scheme. Both methods require a light pulse much shorter than the radiative lifetime of the excited state.

2. The collection process into a particular target mode has to be efficient. If the target mode should be mapped into a propagating beam, or into an optical fiber, the matching of the spontaneous emission mode in free space is very limited. A method to circumvent this problem is to enhance the electrical field strength of a particular target mode with an optical cavity, such that the spontaneous emission takes preferably place into that specific mode. This requires usually optical cavities with a high finesse. Implementations of such sources have been demonstrated both with atoms in free space as with single emitters (quantum dots) in a solid state matrix.

2.5.3 Heralded photon sources

Another method to prepare light fields into single photon states makes use that photon pairs can be generated with a strong temporal correlation via parametric down conversion. Then, one photon of a pair acts as a witness for the other photon, and an experiment can be triggered on a successful observation of the first photon. We will deal with this process in the next chapter.

Chapter 3

Parametric down conversion: A common workhorse

A key resource for many experiments in quantum information are sources of entangled photon pairs, based on parametric down conversion. In this process, energy from a pump field gets transformed into correlated photon pairs. In this lecture, we will present the underlying physical process for parametric down conversion.

We start with an extension of the electromagnetic field quantization into a regime of optical materials which respond to external fields. There is actually very little change in the field description to what we have seen so far. Then we will introduce a description of nonlinear optical materials, which allow for an interaction between the electromagnetic field in different modes. We tie this together to present one of the typical down conversion processes, and analyze quantitatively the generation rate of photon pairs.

3.1 Optics in media

Optical materials like glasses play an important role in manipulating electromagnetic fields: They allow us to change the mode structure. It should be of no surprise that they also play an important role in quantum optics. We quickly go through the ideas of how the interaction with such media is modeled, and how this affects the field quantization.

3.1.1 Macroscopic Maxwell equations

The response of an optical material to incoming fields is the combination of responses from a large number of atoms making up that material. In the optical regime, with wavelengths on the order of $10^{-7} \ldots 10^{-6}\,\mathrm{m}$ and a spacing of the atoms of $10^{-10} \ldots 10^{-9}\,\mathrm{m}$ can be well described by averaging over the material's

response, and by introducing new mean filed quantities connected to the electric and magnetic response of the material. The resulting Maxwell equations for these macroscopic fields can be written as:

$$\begin{aligned} \nabla \cdot \mathbf{D}(\mathbf{x},t) &= \rho_{\text{free}}(\mathbf{x},t)\,, && (3.1)\\ \nabla \times \mathbf{E}(\mathbf{x},t) &= -\frac{\partial}{\partial t}\mathbf{B}(\mathbf{x},t)\,, && (3.2)\\ \nabla \cdot \mathbf{B}(\mathbf{x},t) &= 0\,, && (3.3)\\ \nabla \times \mathbf{H}(\mathbf{x},t) &= \frac{\partial}{\partial t}\mathbf{D}(\mathbf{x},t) + \mathbf{j}(\mathbf{x},t)\,, && (3.4) \end{aligned}$$

with new quantitates of the dielectric displacement $\mathbf{D}(\mathbf{x},t)$ and a magnetic field strength $\mathbf{H}(\mathbf{x},t)$. In the simplest case, these quantities are linearly related to the electrical field $\mathbf{E}$ and the induction flux density $\mathbf{B}$ by

$$\begin{aligned} \mathbf{D}(\mathbf{x},t) &= \epsilon_\circ \epsilon_r \mathbf{E}(\mathbf{x},t)\,, && (3.5)\\ \mathbf{B}(\mathbf{x},t) &= \mu_\circ \mu_r \mathbf{H}(\mathbf{x},t)\,. && (3.6) \end{aligned}$$

There, the permittivity ϵ_r and the relative permeability μ_r summarize the material's response to electromagnetic fields. Most optical materials do not connect to the magnetic field component at optical frequencies, so we can set $\mu_r = 1$. They do, however, respond to the electrical field, so we will have a closer look at this part.

Firstly, the relationship in eqn (3.5) can be broken up into

$$\mathbf{D}(\mathbf{x},t) = \epsilon_\circ \mathbf{E}(\mathbf{x},t) + \mathbf{P}(\mathbf{x},t)\,, \tag{3.7}$$

with a contribution of the original electric filed $\mathbf{E}$ and a polarization $\mathbf{P}$, which characterizes the averaged induced electrical dipole moments of the material. For linear materials, this macroscopic polarization can be expressed as

$$\mathbf{P} = \epsilon_\circ \chi \mathbf{E}\,, \tag{3.8}$$

where χ is the susceptibility tensor characterizing the material, or simply a matrix connecting two vector quantities. For isotropic media like a gas or a glass, it is a scalar. We will later on drop this linear connection between electric field and material response.

For now, we consider the simple case that we have an isotropic, homogenous medium with no free charges, current densities and any magnetic susceptibility, i.e., $\rho_{\text{free}} = 0, \mathbf{j} = 0$, $\mu_r = 1$ and χ is constant for all $\mathbf{x}$. The dielectric permittivity is given by $\epsilon_r = 1 + \chi$, and the solutions to the macroscopic Maxwell equations can be derived from a wave equation similarly as in the vacuum case, but this time with a reduced speed of light,

$$c = \frac{1}{\sqrt{\epsilon_0 \epsilon_r \mu_0 \mu_r}} = \frac{1}{\sqrt{\epsilon_0 \mu_0}} \frac{1}{\sqrt{\epsilon_r}} = \frac{c_0}{n}\,, \tag{3.9}$$

with n being the refractive index of the media.

Note that the introduction of the new field quantities $\mathbf{D}$ and $\mathbf{H}$ did not introduce any new degrees of freedom - they just capture the presence of a material responding to the field in a way that averages over the response of a large number of atoms. Thus, the main strategy to quantize the electromagnetic field remains the same.

3.1.2 Energy density in dielectric media

The important quantity to carry out a field quantization in practice is an expression for the total energy in the electromagnetic field. With the quantities introduced to capture the material response, this quantity is given by

$$H = \frac{1}{2}\int d\mathbf{x}\left[\mathbf{E}(\mathbf{x})\cdot\mathbf{D}(\mathbf{x}) + \mathbf{B}(\mathbf{x})\cdot\mathbf{H}(\mathbf{x})\right], \tag{3.10}$$

which in media with dielectric response only can be reduced to

$$H = \frac{1}{2}\int d\mathbf{x}\left[\mathbf{E}(\mathbf{x})\cdot\mathbf{D}(\mathbf{x}) + \frac{1}{\mu_0}\mathbf{B}^2(\mathbf{x})\right] = \frac{\epsilon_0}{2}\int d\mathbf{x}\left[\mathbf{E}(\mathbf{x})(1+\chi)\mathbf{E}(\mathbf{x}) + c^2\mathbf{B}(\mathbf{x})^2\right]. \tag{3.11}$$

This equation has still the same structure as eqn 1.67 for the electromagnetic field in free space, i.e., the same mode decomposition strategy applies, leading to degrees of freedom which are governed by a harmonic oscillator-type dynamics. For an isotropic medium, the presence of the medium just leads to a modification of the electric field contribution to the total energy by the permittivity $\epsilon_r = 1+\chi$. For birefringent media, where the linear susceptibility depends on the direction of the electric field, the field decomposition can still be carried out as long as a proper polarization basis is chosen; the technical details are well-covered in books on light propagation in crystalline media (see e.g. [3]), but would exceed the scope of this lecture.

Similarly, the field operators can be written in the same way as for the vacuum case,

$$\hat{\mathbf{E}} = \hat{\mathbf{E}}(\mathbf{x},t) = i\sum_j \mathscr{E}_{\omega_j}\left(\mathbf{g}_j(\mathbf{x})\hat{a}_j(t) - \mathbf{g}_j^*(\mathbf{x})\hat{a}_j^\dagger(t)\right), \tag{3.12}$$

The presence of the medium manifests now in a modified constant $\mathscr{E}$ capturing the physical constants, and the connection between $\hat{\mathbf{E}}$ and $\hat{\mathbf{B}}$ needs to take care of the modified speed of light in the medium.

3.1.3 Frequency dependence of refractive index

Typically, the susceptibility χ of an optical medium dependent on the frequency of the exciting field. This is owed to the fact that the response of the medium in the optical domain may be considered as an off-resonant excitation of electrons bound

in the material. Typical binding energies of electrons in transparent materials are on the order of a few electron volts, corresponding to a resonance frequency corresponding to light in the ultraviolet regime. This is compatible with the fact that most materials transparent in the optical regime absorb ultraviolet light. The response of the medium in the visible regime then corresponds to the low-frequency tail of a resonance in the ultraviolet.

A semi-heuristic description of this behavior used to characterize the dispersion property of transparent materials is based on such a model, assuming that the susceptibility is due to one or several resonances in the material. This model is referred to as a Sellmeier equation of a given material, typically formulated as a dependency of the refractive index n from the vacuum wavelength λ_0:

$$n^2 - 1 = \sum_i \frac{A_i}{1 - B_i/\lambda_0^2} + \ldots + C_i/\lambda_0^i \tag{3.13}$$

Note that this is not a unique way of expressing the ultraviolet resonances, and serves mostly as an engineering tool where the coefficients A_i, B_i, C_i don't have an immediate physical interpretation, but are chosen to give an accurate (typically good to 10^{-6}) estimation of the refractive index in the visible regime, based on a few refractive index measurements at a few wavelengths. When you encounter a set of Sellmeier equations characterizing a particular material, make sure you are using the corresponding model function.

The general structure of this dispersion relation is that the refractive index *increases* with the frequency. If you encounter a birefringent material, the Sellmeier equations are typically given for electrical fields polarized in particular directions and propagation directions, where plane waves are solutions the set of Maxwell equations. Depending on the symmetry of the material, two or three sets of Sellmeier equations are required to give a full description of the dispersion properties for the optical medium. The resulting description is reasonably messy.

3.1.4 Nonlinear response of a medium

The linear response of a medium to an electric field has ensured that the complete electromagnetic field still can be decomposed into decoupled modes, and the field states in these individual modes evolve independently from each other.

We now consider a nonlinear response of the medium to an exciting field. Such a nonlinearity may be thought of as originating from a nonharmonic potential of the electrons in the media. As such a nonlinear response is usually a small effect, it can be captured well by a Taylor expansion of the polarization $\mathbf{P}$ of the material in the exciting electrical field $\mathbf{E}$:

$$\mathbf{P} = \epsilon_0 \left(\chi \mathbf{E} + \chi^{(2)} \mathbf{E}^2 + \chi^{(3)} \mathbf{E}^3 \ldots \right) \tag{3.14}$$

The newly introduced susceptibility tensors $\chi^{(n)}$ capture the higher order terms of the material response, and are tensor objects of higher order; as an example,

a contribution to the polarization vector due to the first higher order term $\chi^{(2)}$ can be written in components as:

$$P_j^{(2)} = \epsilon_0 \sum_{k,l=x,y,z} \chi_{jkl}^{(2)} E_k E_l \,, \qquad \text{with} \quad i = x, y, z \tag{3.15}$$

The second order nonlinear susceptibility tensor $\chi^{(2)}$ must reflect the symmetry of the underlying material; this usually reduces the number of independent entries in this tensor substantially. One of the most important symmetry constraints of this type is that the material must lack an inversion symmetry in order to have $\chi^{(2)} \neq 0$ (try to prove this!). Thus, all gases, amorphous materials like glass or polymers, and a large number of crystalline materials do not exhibit this type of nonlinear response to an external electrical field.

A typical signature of these higher order processes in classical optics is higher harmonics generation: If you consider a monochromatic electrical field (e.g. in form of a plane wave) at a frequency ω,

$$\mathbf{E}(\mathbf{x}, t) = \mathbf{E}_0 \, e^{i(\mathbf{k}\cdot\mathbf{x} - \omega t)} \,, \tag{3.16}$$

the second order nonlinear susceptibility will result in polarization components which oscillate at twice the original frequency,

$$\mathbf{P}^{(2)}(t) \;\propto\; \chi^{(2)} \mathbf{E}^2 \;\propto\; e^{-2i\omega t} \,. \tag{3.17}$$

This polarization component at a new frequency can be considered as a source term in the Maxwell equations, and will propagate through the medium according to the dispersion relation.

An example where such a process takes place are green laser pointers, which have a laser emitting light at a vacuum wavelength of 1064 nm, and a small piece of Potassium titanylphosphate (KTP) as a material with a nonlinear susceptibility to convert part of this light into radiation with a vacuum wavelength of 532 nm appearing as green. We will see later, however, that a nonlinear susceptibility alone is not enough to observe this process, but the dispersion properties of the material must allow the fundamental and second harmonic wave to propagate through the crystal with the same speed.

3.2 Nonlinear optics: Three wave mixing

To describe the energy transfer between different modes due to the nonlinear susceptibility quantitatively, we consider the Hamiltonian with the higher terms in the susceptibility:

$$\hat{H} \;=\; \frac{\epsilon_0}{2} \int d\mathbf{x} \, \left[\mathbf{E}(\mathbf{x}) \cdot \left(\epsilon_r \mathbf{E}(\mathbf{x}) + \chi^{(2)} \mathbf{E}^2(\mathbf{x}) \right) + c^2 \mathbf{B}^2(\mathbf{x}) \right] \tag{3.18}$$

$$= \frac{\epsilon_0}{2}\int d\mathbf{x}\,\left[\epsilon_r \mathbf{E}^2(\mathbf{x}) + c^2\mathbf{B}^2(\mathbf{x})\right] + \frac{\epsilon_0}{2}\int d\mathbf{x}\,\mathbf{E}(\mathbf{x})\cdot\chi^{(2)}\mathbf{E}^2(\mathbf{x}) \quad (3.19)$$

$$=: \hat{H}_0 + \hat{H}_I^{(2)} \quad (3.20)$$

There, we have split up the interaction with the medium into a part H_0 with decoupled harmonic oscillator modes, and an interaction term H_I containing the effects induced by the nonlinear susceptibility. Before we have a closer look to this interaction Hamiltonian, we quickly mention that in cases where higher order susceptibilities have to be considered, the interaction Hamiltonian takes a similar form. For example, a $\chi^{(3)}$ or Kerr nonlinearity leads to:

$$\hat{H}_I^{(3)} := \frac{\epsilon_0}{2}\int d\mathbf{x}\,\chi^{(3)}\hat{\mathbf{E}}^4(\mathbf{x}) \quad (3.21)$$

Returning to the $H_I^{(2)}$ again, we can gain some insight if we carry out the spatial integration. Recalling the electrical field operators from eqn (1.111),

$$\hat{\mathbf{E}}(\mathbf{x},t) = i\sum_j \mathscr{E}_{\omega_j}\left(\mathbf{g}_j(\mathbf{x})\hat{a}_j(t) - \mathbf{g}_j^*(\mathbf{x})\hat{a}_j^\dagger(t)\right), \quad (3.22)$$

the interaction Hamiltonian is an integral over space, and a generalized sum (i.e., sum and/or integral) over three mode indices:

$$\hat{H}_I^{(2)} = -i\int d\mathbf{x}\sum_j\sum_k\sum_l \{\mathscr{E}_j\mathscr{E}_k\mathscr{E}_l \quad (3.23)$$

$$\chi^{(2)}\left[\mathbf{g}_j(\mathbf{x})\hat{a}_j - \mathbf{g}_j(\mathbf{x})\hat{a}_j^\dagger\right]\left[\mathbf{g}_k(\mathbf{x})\hat{a}_k - \mathbf{g}_k(\mathbf{x})\hat{a}_k^\dagger\right]\left[\mathbf{g}_l(\mathbf{x})\hat{a}_l - \mathbf{g}_l(\mathbf{x})\hat{a}_l^\dagger\right]\} \quad (3.24)$$

This operator splits thus up into eight terms of the form

$$\hat{H}_I^{(2)} = C_0\,\hat{a}_j\hat{a}_k\hat{a}_l + C_1\,\hat{a}_j^\dagger\hat{a}_k\hat{a}_l + C_2\,\hat{a}_j\hat{a}_k^\dagger\hat{a}_l + C_3\,\hat{a}_j\hat{a}_k\hat{a}_l^\dagger + h.c.\,, \quad (3.25)$$

where the terms come in hermitian conjugated pairs. Each term has three ladder operators mediating transitions between population of modes - this gives the associated process the name *three-wave mixing*. The notion of waves is motivated by plane wave as mode functions $\mathbf{g}(\mathbf{x})$.

To illustrate the conditions under which the different terms contribute, we consider the prefactor C_1 for the second term in eqn (3.25) as an example, which mediates a process removing a photon in mode j and generates one in modes k and l each:

$$C_1 = i\frac{\epsilon_0}{2}\sum_j\sum_k\sum_l \mathscr{E}_j\mathscr{E}_k\mathscr{E}_l\int d\mathbf{x}\,\chi^{(2)}\mathbf{g}_j^*(\mathbf{x})\mathbf{g}_k(\mathbf{x})\mathbf{g}_l(\mathbf{x}) \quad (3.26)$$

Assuming plane waves as mode functions j,k,l of the form

$$\mathbf{g}(\mathbf{x}) = \hat{e_j}\,e^{i\mathbf{k}_j\cdot\mathbf{x}}\,, \quad (3.27)$$

where $\hat{e}$ is a polarization vector, the integral in the expression for C_1 becomes

$$C_1 = i\frac{\epsilon_0}{2}\sum_j\sum_k\sum_l \mathscr{E}_j\mathscr{E}_k\mathscr{E}_l(\hat{e}_j\chi^{(2)}\hat{e}_k\hat{e}_l)\int d\mathbf{x}\, e^{-i\mathbf{k}_j\cdot\mathbf{x}}\, e^{i\mathbf{k}_k\cdot\mathbf{x}}\, e^{i\mathbf{k}_l\cdot\mathbf{x}} \quad (3.28)$$

$$= i\frac{\epsilon_0}{2}\sum_j\sum_k\sum_l \mathscr{E}_j\mathscr{E}_k\mathscr{E}_l\chi^{(2)}_{\text{eff}}\int d\mathbf{x}\, e^{i(\mathbf{k}_k+\mathbf{k}_k-\mathbf{k}_j)\cdot\mathbf{x}} \quad (3.29)$$

$$(3.30)$$

With

$$\int d\mathbf{x}\, e^{i(\mathbf{k}_k+\mathbf{k}_l-\mathbf{k}_j)\cdot\mathbf{x}} = 2\pi\delta(\mathbf{k}_k+\mathbf{k}_l-\mathbf{k}_j) \quad \text{for a infinite integration volume,}$$
$$\approx 2\pi\delta(\mathbf{k}_k+\mathbf{k}_l-\mathbf{k}_j) \quad \text{for a } \textit{finite} \text{ integration volume,} \quad (3.31)$$

the coefficient C_1 only survives if the wave vectors of the removed photon matches the sum of the two created ones. This specific process is referred to as down conversion, and the above condition is referred to as the *phase matching condition* for the corresponding nonlinear optical process. For geometries which don't show a full translational symmetry, e.g. for an interaction region of finite size, the momentum conservation is only approximately fulfilled.

Remember that the terms in the interaction Hamiltonian always come in pairs: Hence, when the coefficient for a down conversion from mode j to modes k, l is non-vanishing, the reverse process is also possible. In this case, this would correspond to an upconversion process.

The modes in the phase matching conditions do not necessarily need to be distinct: The upconversion process with $k = l$, for example, corresponds to the SHG process mentioned earlier.

Keep in mind that the phase matching condition is only an overlap argument of various participating modes in a given interaction volume: It applies equally in a treatment of optical interactions in classical physics, and is not something which comes out of a quantum description of light. For many quantum optical experiments, it is nevertheless important to meet these phase matching conditions. Thus, we will elaborate a little on them in the next section.

3.3 Phase matching

Apart from the phase matching condition, which can be interpreted as momentum conservation in the limit of a large interaction region, the energy in conversion processes must be conserved. This puts another constraint on the processes taking place concurrently.

For the down conversion process introduced above, the three participating modes are traditionally labeled as *pump* (that's the mode which has the lowering

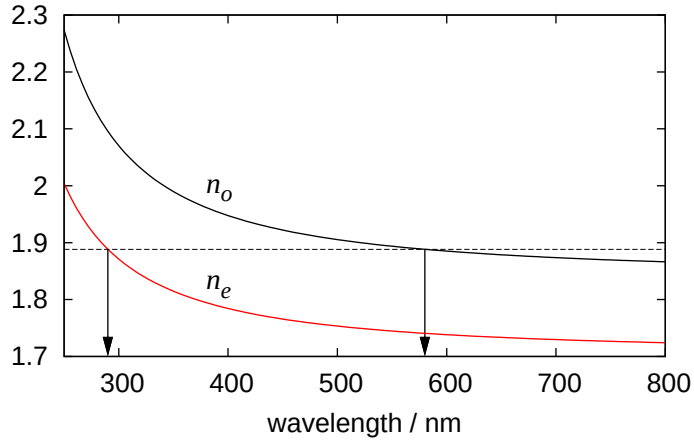

Figure 3.1: Non-critical phase matching in $LiIO_3$ for SHG or degenerate parametric conversion. An ordinarily polarized plane wave at 580 nm and an extraordinarily polarized wave at half the (vacuum-)wavelength have the same refractive index of $n = 1.88825$.

operator), and as *signal* and *idler* for the modes where photons are created in. The energy conservation then can then be written as

$$\omega_p = \omega_s + \omega_i \,. \tag{3.32}$$

In the limit of large conversion regions considered for understanding the concept, the momentum conservation becomes:

$$\mathbf{k}_p = \mathbf{k}_s + \mathbf{k}_i \tag{3.33}$$

Meeting both eqns (3.32) and (3.33) at the same time for a range of modes can be accomplished by choosing proper polarizations and engineering the dispersion relation

$$\omega = c|\mathbf{k}|/n \tag{3.34}$$

and adjusting refractive index n with various methods. We will go through a few examples for parametric down conversion from a pump frequency ω_p to a set of degenerate frequencies $\omega_s = \omega_i = \omega_p/2$ for the target modes. To meet eqn (3.33) in a collinear geometry (i.e., $\mathbf{k}_p \parallel \mathbf{k}_s \parallel \mathbf{k}_i$), the refractive indices for pump and target modes must be the same. As mentioned in Section 3.1.3, the refractive index for the pump (higher frequency) is larger than for the signal and idler frequencies. This problem is typically addressed by choosing different polarizations for the various modes since materials with non-vanishing $\chi^{(2)}$ are usually birefringent. Figure 3.3 shows this for the example of Lithium Iodate, $LiIO_3$, a negatively uniaxial birefringent material. A wave with a linear polarization parallel to the optical axis experiences the *extraordinary* refractive index n_e, while a plane wave

with a polarization vector in a plane orthogonal to the optical axis experiences the larger *ordinary* refractive index.

The refractive index n_e for a pump wavelength of 295 nm (this refers to the vacuum wavelength, a commonly used proxy measure for the frequency) matches the ordinary index n_o at a degenerate target wavelength of 580 nm. Thus, for a pump polarized parallel to the optical axis, parametric conversion into a mode copropagating with the pump but with orthogonal polarization would be allowed.

The combination of polarizations $(e - o - o)$ for pump, signal and idler is referred to as type-I phase matching. In this example, the propagation directions match the optical axes, which is referred to as non-critical phase matching.

The polarizations of the two target modes do not need to be the same; by choosing one of the target modes as e, and the other one as o-polarized, non-critical phase matching for a pump wavelength of 373.6 nm can be achieved in the $LiIO_3$, with the degenerate target modes at a wavelength of 747.3 nm. Such a polarization combination is referred to as type-II phase matching.

Obviously, the non-critical phase matching works only for very few wavelength combinations. There are, however, several efficient ways to extend the phase matching range: Refractive indices of a given material can be altered by material engineering, temperature, the propagation direction and an artificially introduced periodic reorientation. We will briefly discuss the last three methods.

3.3.1 Phase matching by temperature tuning

A number of materials have a strong dependency of their refractive index with temperature; a prominent example is potassium niobate, $KNbO_3$, a biaxial birefringent material with a strong optical nonlinearity and a strong temperature dependency of the refractive index (about 0.5% over 100K, [16]).

3.3.2 Phase matching by angle tuning

Another common way to ensure phase matching is to manipulate the refractive index of one or more modes by choosing propagation directions through the conversion crystals where the electric field vector is not parallel to one of the principal axes of the susceptibility tensor. We refer the reader to any textbook on classical optics in birefringent crystalline materials for details, and show the basic idea only for a simple example for this so-called critical phase matching.

For birefringent materials and a given propagation direction with respect to the principal axes of the material, there are always two orthogonal polarization vectors where the solutions of Maxwell equations can be written as plane waves with a well-defined propagation speed c/n. For uniaxial birefringent materials, two of the principal linear susceptibilities are the same, and correspond to the so-called ordinary refractive index $n_o = \sqrt{1 + \chi_o}$, while the response to a dielectric displacement along the optical axis is governed by the extraordinary refractive

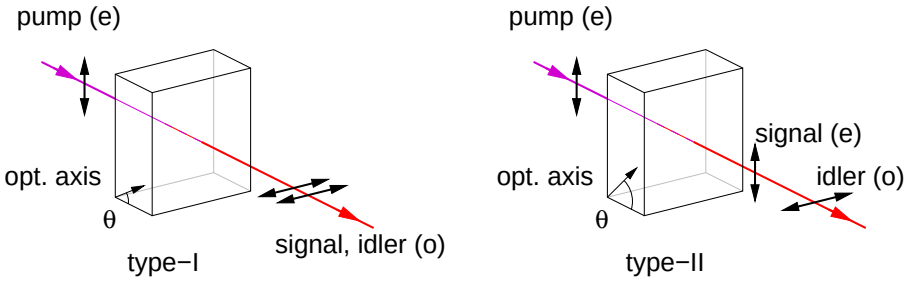

Figure 3.2: Critical phase matching (type-I and type-II) for a uniaxial birefringent crystal in a collinear configuration. The refractive indices of extraordinary beams are tuned by choosing an angle θ between the wave vectors and the optical axis of the crystal.

index n_e. A wave described by a propagation vector $\mathbf{k}$ which forms an angle θ with the optical axis has then one polarization mode ("ordinary wave") with the corresponding refractive index n_o and an electrical field vector in the plane normal the optical axis, while the other polarization mode ("extraordinary wave") has an orthogonal polarization and is n'_e is propagating corresponding to a refractive index

$$n'_e(\theta) = \frac{n_e n_o}{\sqrt{n_o^2 + (n_e^2 - n_o^2)\cos^2\theta}}\,. \tag{3.35}$$

Thus, by choosing a proper orientation angle θ, the refractive index for the extraordinary wave can be adjusted between n_e and n_o. Keep in mind that the refractive indices n_e and n_o still depend on the frequency. As an example, we consider the negatively uniaxial crystal BBO, and wavelengths of $\lambda_p = 351\,\mathrm{nm}$ for the pump, and $\lambda_s = \lambda_i = 702\,\mathrm{nm}$ for frequency degenerate target modes in a down conversion configuration. The refractive indices at these wavelengths are shown in the following table:

	n_e	n_o
$\lambda = 351\,\mathrm{nm}$	1.5784	1.7069
$\lambda = 702\,\mathrm{nm}$	1.5484	1.6648

This combination of refractive indices allows both for type-I and type-II phase matching for copropagating target and pump modes. For type-I, the target modes have to be both ordinary waves with $n = 1.66$, which lies between n_e and n_o for the pump wavelength. With an angle $\theta = 33.3°$, the extraordinary refractive index $n'_e(\theta)$ can be matched to the ordinary refractive index n_o of the target modes.

For type-II phase matching, one of the target modes is ordinarily, the other extraordinarily polarized. Since no combination of ordinary and extraordinary refractive index of the target modes can reach the ordinary refractive index at the pump wavelength, the pump wavelength is also extraordinarily polarized.

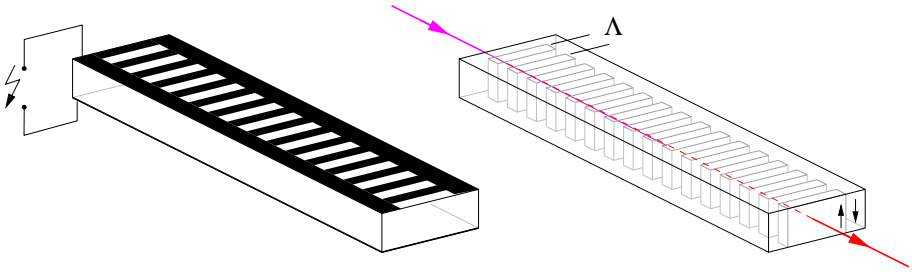

Figure 3.3: Engineered phase matching by electrically poling periodically various segments in a nonlinear optical material like KTP or Lithium niobate with a periode Λ. Additionally to the intrinsic wave vectors in the conversion material, an integer multiple of a quasi phase matching wave vector $2\pi/\Lambda$ is added to the phase matching condition.

The with the dispersion relation $c|k| = n\omega$, the phase matching condition for degenerate down conversion ($\omega_p/2 = \omega_s = \omega_i$) now reads

$$2n'_{e,351}(\theta) = n'_{e,702}(\theta) + n_{o,702}\,, \tag{3.36}$$

which has a solution for $\theta = 48.9°$. Such a configuration has been used for a large number of experiments with down-converted photon pairs. It should be mentioned, though, that the critical phase matching approach has the disadvantage that the wave vector and Poynting vector, describing the energy flow in a beam, are no longer parallel for the extraordinary waves. For modes with a finite transverse extent, this leads to a "transverse walk-off" between ordinary and extraordinary modes, which may have a number of undesirable consequences, among them a limitation of the possible geometric overlap of different modes. On the other hand, it allows usually to use popular laser wavelengths.

While the birefringent properties of a uniaxial crystal are completely determined by one angle θ, and thus the phase matching conditions are fully met, it should not be forgotten that the orientation of the nonlinear optical tensor elements may still depend on the other free orientation angle.

3.3.3 Phase matching by periodic poling

Another recent, very popular method to meet the phase matching condition in nonlinear optical materials is to engineer the optical properties of a material by breaking the translational symmetry of the conversion material, and modulate the optical property like the sign of the nonlinear optical susceptibility periodically. This can be achieved by applying strong static electrical fields in small portions of a nonlinear optical crystal under certain conditions. The field is applied to the material with the aid of microstructured electrodes, which later can be removed once the crystal is poled.

The new device has still a partial translational symmetry, since the optical properties repeat with the poling periode Λ. The phase matching condition is now replaced by a quasi-phase matching condition:

$$\mathbf{k}_p = \mathbf{k}_s + \mathbf{k}_i + \frac{2\pi\, m}{\Lambda}\,, \qquad m \in \mathbb{Z}_0 \tag{3.37}$$

By choosing the poling periode Λ and the quasiphasematching order m accordingly, wavelength combinations can be reached with materials with an intrinsic high nonlinear optical susceptibility. Materials which have been used for this type of phase matching include the very common $LiNbO_3$ (and is in this modification referred to as PPLN, periodically poled lithium niobate), as well as potassium titanylphosphate (KTP, or PPKTP).

While with these materials, a tremendous increase of brightness for photon pair sources have been observed, one needs to keep in mind that the engineered periodicity is subject to manufacturing uncertainties; particularly the duty cycle of the poling structures can be noisy across the conversion material. As a consequence, the material can be considered as a region with a distribution of poling periods beyond the single value given by $2\pi/\Lambda$, and allow for a small contribution of phase matching at a large number of modes. This may contribute to noise in a variety of nonlinear optical processes like upconverison or also parametric down conversion.

3.4 Calculating something useful: Absolute pair production rates

While many experiments with photon pairs from parametric down conversion can be and have been carried out with considering the rather qualitative phase matching criteria discussed in the previous section, it is helpful for developing these light sources better to get a quantitative expression on how many pairs can be expected in a particular geometry [17].

The example we consider in this chapter assumes that we generate photon pairs into modes which are defined by single mode optical fibers, which allows later on to manipulate the downconverted light conveniently in any interferometric arrangements - those typically require well-defined spatial modes, and an optical fiber acts as an efficient spatial mode filter for such purposes.

3.4.1 The model

To keep the calculation of an expected photon pair rate simple, we restrict ourselves to a geometry where the pump field is collinear with the target modes. Furthermore, we neglect all dispersion effects in the conversion crystal. The geometry of the model situation is shown in Fig. 3.4.1.

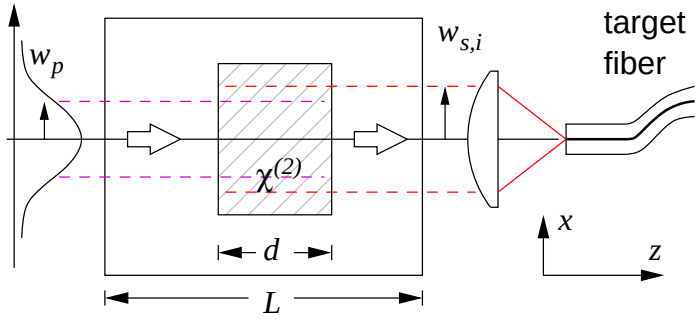

Figure 3.4: Model geometry to calculate pair generation rates in PDC collected by a single mode optical fiber. The pump and target modes are nearly collimated Gaussian beams with beam waists $w_{p,s,i}$, the conversion crystal should have a thickness d in propagation direction z and a size much larger than the beam waists in the transverse directions. For convenience, the nonlinear optical material is thought to be embedded in a material with the same refractive indices n_s, n_i, n_p as in the conversion region. We also introduce a quantization length L for the target modes.

The conversion is taking place in a crystal of thickness d in the main propagation direction of all modes, which we assume to have a Gaussian mode profile. For simplicity, we also neglect a possible transverse beam walk-off in case we use critical phase matching. Furthermore, we assume that we have chosen a type-II phase matching condition, such that the two target modes are distinct by their polarization. By embedding the conversion crystal in a surrounding with the same linear susceptibilities (and thereby refractive indices) as in the conversion region, we can make use of the expression (eqns 1.118-1.120) in Section 1.5 for the electrical field operator $\hat{\mathbf{E}}(\mathbf{x})_{s,i}$. The corresponding beam waists for signal and idler modes are w_s, w_i, and the corresponding refractive indices are $n_s = \sqrt{\epsilon_s}, n_i = \sqrt{\epsilon_i}$. The quantization length L should not influence the result of the pair rate and is just kept for conceptual convenience. With this, and keeping in mind that we still have the longitudinal wave vector k_s and k_i as a one-dimensional mode index for the target modes, the target field operators become

$$\hat{\mathbf{E}}_{s,i}(\mathbf{x}) = i \sum_{k_{s,i}} \mathcal{E}_{k_{s,i}} \boldsymbol{\varepsilon} e^{ik_{s,i}z} e^{-\rho^2/w_0^2} \hat{a}_{k_{s,i}} + h.c. \quad \text{with} \quad \mathcal{E}_{k_{s,i}} = \sqrt{\frac{\hbar\omega_{k_{s,i}}}{\pi w_{s,i}^2 L \epsilon_0 n_{s,i}^2}} \tag{3.38}$$

With the quantization length L and periodic boundary conditions, the mode indices $k_{s,i}$ are integer multiples of $2\pi/L$.

The pump field is assumed also to be monochromatic and in a Gaussian mode with waist w_p. The electrical field in the pump mode is treated as a classical amplitude, written in a similar form as the quantized field modes:

$$\mathbf{E}_p(\mathbf{x}, t) = iE_0 \left\{ \mathbf{g}_p(\mathbf{x}) e^{-i\omega_p t} - \mathbf{g}_p^*(\mathbf{x}) e^{i\omega t} \right\} \tag{3.39}$$

with the same Gaussian mode function $\mathbf{g}_p(\mathbf{x})$ from eqn 1.118 as the quantized fields, with a pump waist w_p. The optical power carried by this classical, real-valued electrical field is given by

$$P = E_0^2 n_p \pi w_p^2 \epsilon_0 c\,, \tag{3.40}$$

an expression which can be obtained by integrating the average Poynting vector, $\langle \mathbf{S} \rangle = \langle \mathbf{E}_p \times \mathbf{B}_p \rangle_t / \mu_0$ over the cross section of the beam.

3.4.2 Interaction Hamiltonian

To evaluate the rate of photon pairs generated in the spatial modes collected into the optical fiber, we need to consider the interaction Hamiltonian $\hat{H}_I$ as outlined in eqn 3.19, which is assumed to be a small perturbation to the free field. For a classical driving field, this Hamiltonian becomes explicitly time dependent.

$$\hat{H}_I(t) = \frac{\epsilon_0}{2} \int d^3\mathbf{x}\, \mathbf{E}_p(\mathbf{x},t) : \chi^{(2)} : \sum_{k_s} \hat{\mathbf{E}}_{k_s}(\mathbf{x}) : \sum_{k_i} \hat{\mathbf{E}}_{k_i}(\mathbf{x}) \tag{3.41}$$

Since we only want to consider processes where photon pairs are generated out of the vacuum of the target modes, it is sufficient to restrict the Hamiltonian to two terms for pair creation/annihilation, and we arrive at:

$$\begin{aligned} \hat{H}_I(t) &= i\frac{\epsilon_0}{2}(\boldsymbol{\varepsilon}_p : \chi^{(2)} \boldsymbol{\varepsilon}_s : \boldsymbol{\varepsilon}_i) E_0 \int_{-\infty}^{\infty} dxdy \int_{-d/2}^{d/2} dz \sum_{k_s,k_i} \frac{\hbar\sqrt{\omega_s\omega_i}}{\pi\epsilon_0 w_s w_i L n_s n_i} && (3.42) \\ &\quad \times e^{i\Delta\omega t} e^{-i\Delta k z} e^{-(x^2+y^2)/w_s^2} e^{-(x^2+y^2)/w_i^2} \hat{a}_{k_s}(0)\hat{a}_{k_i}(0) + h.c. && (3.43) \end{aligned}$$

We have introduced the detuning parameter $\Delta\omega = \omega_p - \omega_s - \omega_i$ and a wave vector mismatch $\Delta k = k_p - k_s - k_i$. With the effective nonlinearity d_{eff} (capturing the contraction of the nonlinear susceptibility for the polarizations used, $2d_{eff} = \boldsymbol{\varepsilon}_p : \chi^{(2)} \boldsymbol{\varepsilon}_s : \boldsymbol{\varepsilon}_i$), we can carry out the spatial integration of the mode function overlap and simplify the above expression:

$$\hat{H}_I(t) = i d_{eff} E_0 \sum_{k_s,k_i} \frac{\hbar\sqrt{\omega_s\omega_i}}{\pi w_s w_i L n_s n_i} \times e^{i\Delta\omega t} \Phi(\Delta k) \hat{a}_{k_s}(0)\hat{a}_{k_i}(0) + h.c.\,, \tag{3.44}$$

with

$$\begin{aligned} \Phi(\Delta k) &= \int_{-\infty}^{\infty} dxdy \int_{-d/2}^{d/2} dz\, e^{-i\Delta k z} e^{-(x^2+y^2)/w_s^2} e^{-(x^2+y^2)/w_i^2} e^{-(x^2+y^2)/w_p^2} && (3.45) \\ &= \pi \left(\frac{1}{w_p^2} + \frac{1}{w_s^2} + \frac{1}{w_i^2} \right)^{-1} d\,\mathrm{sinc}\,(\Delta k d/2) && (3.46) \end{aligned}$$

We observe that the interaction Hamiltonian does not vanish for a range of Δk due to the finite length d of the conversion crystal.

3.4.3 Fermi's Golden Rule and spectral rates

To make a quantitative statement on the number of photon pairs generated per unit time, we will use Fermi's Golden Rule for a transition rate $R(k_s)$ from a field in an initial vacuum state $|i\rangle = |0_{k_s}; 0_{k_i}\rangle$ into a final state $|f\rangle = |1_{k_s}; 1_{k_i}\rangle$ with one photon in each of the target modes k_s, k_i. Fermi's Golden Rule makes a statement about asymptotic scattering rates, thus energy must be conserved. We express this using the dispersion relation for signal and idler modes:

$$\Delta\omega = \omega_p - k_s \frac{c}{n_s} - k_i \frac{c}{n_i} = 0 \tag{3.47}$$

First, we consider now a transition rate $R(k_s)$ for photon pairs with a *fixed* target mode k_s. The density of states $\rho(\Delta E)$ per unit of energy $\Delta E = \hbar\Delta\omega$ is extracted out of the quasi-continuum of target modes k_i:

$$\rho(\Delta E) = \frac{\Delta m}{\Delta k_i} \cdot \frac{\partial k_i}{\partial(\hbar\Delta\omega)} = \frac{L}{2\pi} \cdot \frac{n_i}{\hbar c} \tag{3.48}$$

With the approximation that the frequencies ω_s, ω_i vary only little over the range where $\Phi(\Delta k)$ contributes, the transition rate is then given by

$$R(k_s) = \frac{2\pi}{\hbar} \left| \langle f | \hat{H}_I | i \rangle \right|^2 \rho(\Delta E) \tag{3.49}$$

$$= \left| \frac{d_{eff} E_0}{\pi w_s w_i} \Phi(\Delta k) \right|^2 \frac{\omega_s \omega_i}{n_s^2 n_i c L} \tag{3.50}$$

We would now like to map this transition rate into a fixed discrete mode k_s into a spectral rate density. For that, we just multiply the above expression with the number $L n_s / 2\pi c$ of modes k_s per frequency interval ω_s, and obtain

$$\frac{dR(\omega_s)}{d\omega_s} = \left[\frac{d_{eff} E_0 \Phi(\Delta k)}{\pi w_s w_i c} \right]^2 \frac{\omega_s \omega_i}{2\pi n_s n_i} \tag{3.51}$$

At this point, the earlier introduced quantization length L has vanished.

We still need to express the wave vector mismatch Δk as a function of the frequency ω_s. For that, we use dispersion relation for the different modes and arrive at

$$\Delta k = \frac{1}{c} \left(\omega_p (n_p - n_i) - \omega_s (n_s - n_i) \right) = \frac{n_s - n_i}{c} (\omega_s^0 - \omega_s) \tag{3.52}$$

The sinc function leads to a spectral distribution of the downconverted light in the signal mode around a center frequency $\omega_s^0 = \omega_p (n_p - n_i)/(n_s - n_i)$ with a width of $\Delta\omega_s = 4\pi c/(n_s - n_i)/d$ between the first two zeros. The thicker the conversion crystal length d, the narrower the spectrum of the collected light.

To quote typical numbers, we consider degenerate type-II down conversion in adequately aligned BBO from 351 nm to a center wavelength of 702 nm. There, $n_s - n_i \approx 0.111$. For a $d = 2\,\text{mm}$ thick crystal, the spectral width (between the zeros of the sinc function) would be $\Delta\omega = 2\pi \cdot 2.7\,\text{THz}$ corresponding to $\Delta\lambda \approx 4.4\,\text{nm}$.

3.4.4 Connecting it together

The spectral conversion rate of photon pairs can be integrated over all frequencies ω_s. Assuming that only a small spectral region around ω_s^0 contributes to the total pairs generated, the integration on over the spectral rate can be carried out over the mode overlap expression only; with $\delta\omega_s = \omega_s - \omega_s^0$ and

$$\int_{-\infty}^{\infty} d\delta\omega_s \, \Phi^2\left(\frac{n_s - n_i}{c}\delta\omega_s\right) = \frac{2\pi^3 cd}{n_i - n_s}\left(w_p^{-2} + w_s^{-2} + w_i^{-2}\right)^{-2} \tag{3.53}$$

we can finally write down the total pair rate R_T as

$$\begin{aligned} R_T &= \frac{d_{eff}^2 E_0^2}{w_s^2 w_i^2}\frac{\omega_s\omega_i cd}{n_s n_i(n_i - n_s)}\left(w_p^{-2} + w_s^{-2} + w_i^{-2}\right)^{-2} && (3.54)\\ &= \frac{d_{eff}^2 P d\omega_s\omega_i}{n_p n_s n_i(n_i - n_s)\pi\epsilon_0 w_s^2 w_i^2 w_p^2\left(w_p^{-2} + w_s^{-2} + w_i^{-2}\right)^2} && (3.55)\end{aligned}$$

With the common choice of waists, $w_s = w_i = w_p/\alpha$, we get

$$R_T = \frac{d_{eff}^2 P d\omega_s\omega_i}{n_p n_s n_i(n_i - n_s)\pi\epsilon_0 w_s^2\left(\alpha^{-1} + 2\alpha\right)^2}\,, \tag{3.56}$$

which for a fixed w_s maximizes for $\alpha = 1/\sqrt{2}$ to a value of

$$R_T = \frac{d_{eff}^2 P d\omega_s\omega_i}{8\pi\epsilon_0 n_p n_s n_i(n_i - n_s)w_s^2}\,. \tag{3.57}$$

A few observations on this expression should conclude this section:

- The rate of photon pairs grows linearly in the pump power and the crystal length;
- it also grows quadratically with the optical nonlinearity; therefore, it is very advantageous to look for materials with a strong optical nonlinearity; this makes it advantageous to consider waveguide structures in nonlinear optical materials, since there the mode can be confined to an area of about λ^2 over a long distance d;
- The total rate grows inversely proportional to the pump waist area, and maximizes if the ratio between target and pump mode waists are $\sqrt{2}$;
- While the spectral pair density is independent of the refractive index difference, the absolute rate grows inversely proportional to $n_i - n_s$, or the birefringence of the material.

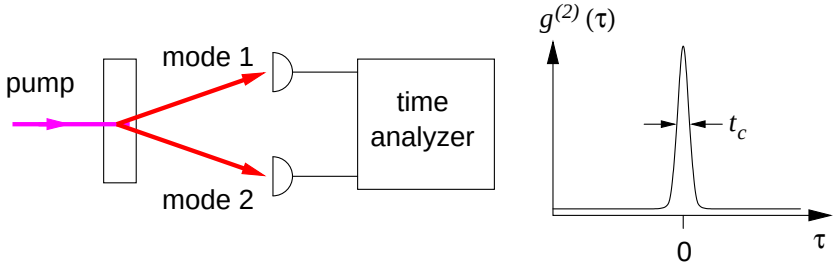

Figure 3.5: Temporal correlations in photodetection events in parametric down conversion. The second order correlation function shows a prominent peak for a detection time difference $\tau = 0$. Its width is usually limited by the timing resolution of the detectors.

3.5 Temporal correlations in photon pairs

One of the important aspects of light generated by parametric down conversion is its strong temporal correlation between photodetection events observed between light in signal and idler modes. An experimental schematic for this observation is shown in Fig. 3.5). First experimentally observed by Burnham and Weinberg [18], one usually finds a peaked pair correlation function for photodetection events where the width t_c is typically limited by the detector resolution. Thus, it appears that photoelectrons are preferably generated in coincidence.

This observation suggests that there are wave packets for signal and idler generated in a common "birth event"; it also leads to the view that each individual photon of a pair is a well-localized wave packet. More sophisticated measurements (see Hong-Ou-Mandel experiment in Section 4.2.3) indicate that the width t_c of the second order correlation function is indeed given by the coherence time of the corresponding spectral distribution for each photon, and that Fourier-limited wave packets would be appropriate descriptions for the photons in each mode.

For practical purposes, this allows to identify photon pairs by coincidence detection: A very powerful experimental method to take care of situations where one of the photons in a pair could not be detected, or was lost in either the collection or some optical elements between down conversion region and detectors. By looking for coincidences between two photodetectors, a selection of situations can be made where both of the photons made it through the entire experimental setup.

3.5.1 Heralded single photon source

This strong correlation in time can be utilized to "prepare by detection" of one of the photons a situation where there will be with a high probability a photon in the other mode. Hence, a photon pair source can in many cases be used to prepare single photon states.

The limitation of the heralding efficiency is typically given by the detection efficiency of both photodetectors, and by the collection efficiency in a particular down conversion setup. With many contemporary down conversion sources with a peak emission in the sensitive region of silicon avalanche detectors, a ratio between pair events and single detection events of about 30% can be reached; This efficiency is a product of both detection and collection efficiency. With detection efficiencies around 50% for silicon avalanche photodiodes, this corresponds to collection efficiencies around 60%. However, sources have been reported with a very good overlap of pump and target modes which seem to achieve collection efficiencies around 80%.

In any case, the very well localized wave packets associated with photoelectron pair detections in very good timing definition gives rise to try to treat these photons as distinguishable particles. In the next chapter we will see how such individual particles, with an additional set of degrees of freedom, can be used to encode information.

Chapter 4

Quantum information with photons

So far, we have treated photons – or more accurately, the electromagnetic field – with the aid of field operators and a variety of harmonic oscillator states. The electromagnetic field, similar e.g. to a position of a particle, is a continuous variable, and quantum mechanical properties in such a scenario are typically described and observed in terms of correlation functions between different continuous variables.

We have seen, however, that there is a set of physical phenomena where it makes sense to consider photons as localized electromagnetic fields, similar to how we perceive massive particles. We are used to the fact that particles can have "internal" degrees of freedom, which can be used to store or transport information. The simplest way of representing this concept in a quantum physics way is to think of such internal degrees as a qubit.

This chapter will review some of the practical considerations that arise when trying to select a physical system to perform quantum information tasks. Specifically, we will see how photons can be used as qubits, as they are virtually the universal choice when considering flying qubits used for quantum communication purposes. On the other hand, photons interact very weakly with each other and this limits the type of tasks that can be easily performed.

4.1 Single photons as qubits

Qubits are a convenient basic unit of storing or transporting information by a carrier governed by quantum physics. It is usually required that such a carrier is reasonably localized or otherwise distinguishable, such that it makes sense to talk about a system which is comprised by many qubits. In the previous chapters we have seen that in an attempt to generate and detect electromagnetic fields, photons can be often considered as fields which have this localizable property. We now need to find out how to make the transition from the field description to

a qubit implementation with single photons.

4.1.1 What is a qubit?

In principle any two level system could be chosen as the physical basis for qubits. In practice, all qubits are not created equal, and they may vary strongly in the ease of preparation, complexity of performing generalized rotations (single qubit gates), and their resistance to decoherence from interactions with the environment.

Whatever degrees of freedom we choose, a pure qubit state will be completely described by:

$$|\psi\rangle = \alpha|0\rangle + \beta|1\rangle \qquad \alpha, \beta \in \mathbb{C} \ , \ |\alpha|^2 + |\beta|^2 = 1. \tag{4.1}$$

Any system that we choose to implement our qubits should not only support the full range of qubits states, but also provide a mechanism to transform one qubit state into another (single qubit rotations).

4.1.2 Preliminaries: How an electron spin becomes a separable degree of freedom

In this section, we shall see how can we make connection between spin of an electron with internal, or much better, separable degree of freedom. As a first step, we should reconsider the way an electron spin is treated. This mechanism will help us understanding how to implement an equivalent with electromagnetic fields.

The spin of an electron is described by the spin wave function which arises naturally from the Dirac equation. In general, we can write the wave function of an electron as a vector quantity

$$|\Psi_e\rangle \equiv \begin{pmatrix} \phi_\uparrow(x) \\ \phi_\downarrow(x) \end{pmatrix} \quad , \tag{4.2}$$

where the two entries correspond to a spin up component and a spin down component. For completeness, it should be mentioned that in a relativistically correct description, this is a four-dimensional object, with the two additional entries corresponding to the two spin components of the positron mode, but we will not touch this further.

We may write this spin wave now as a superposition of two components,

$$|\Psi_e\rangle \equiv \phi_\uparrow(x) \begin{pmatrix} 1 \\ 0 \end{pmatrix} + \phi_\downarrow(x) \begin{pmatrix} 0 \\ 1 \end{pmatrix} , \tag{4.3}$$

with two terms written as a product of a spatial wave function and a vector with two components designating the spin state of the electron.

This re-writing of the spin wave function is an expression that, typically quoting observations of charge and mass conservation, we tend to consider the spatial aspects of the electron state as separable from its spin property. That process can be taken further by writing down a state in the form

$$\psi(x) \begin{pmatrix} \alpha \\ \beta \end{pmatrix} . \tag{4.4}$$

At this point, we would consider $\psi(x)$ as the spatial wave function governing the center-of-mass motion (and refer to it as an external degree of freedom), whereas the column vector represents the spin part of the wave function (which, as it is not subject to any spatial variation, we can refer to as an internal degree of freedom). The whole object (here: electron) is described as a tensor product of the from

$$|\Psi_e\rangle = |\psi_{ext}\rangle \otimes |\psi_{int}\rangle \, , \tag{4.5}$$

which resides in a product space for the external and internal degree of freedom. We should keep in mind, however, that this is not a restriction of the electron state to a particular subclass of separable states, as we always can have superpositions of states of the form eqn (4.5) which don't separate, and finally compose the most general state eqn (4.2).

For electrons, this treatment is reasonably familiar: For the external degree of freedom, we continue to use the description of a massive particle with a scalar wave function describing its position, while we use a simple two-dimensional space to describe the spin properties, typically decoupled from the position degree of freedom.

In many physical systems, we can manipulate this internal degree of freedom independent of the external wave function, although we often have to go for some length to suppress the coupling to the environment due to the charge, e.g. by using silver atoms with one unpaired electron spin to observe the Stern-Gerlach effect. Probably a better example is the nuclear spin of some atoms, where superposition states can last for hours without being affected by the position of the nucleus to the extent that spin-polarized can be prepared and then inhaled for medical imaging purposes without affecting the spin.

4.1.3 Generating "internal" degrees of freedom with photons

The concept we have seen in making the transition from a continuous Dirac state of an electron to a combination of internal and external degrees of freedom can easily be transferred to electromagnetic fields: First, we choose a light field which corresponds to a "single particle", as defined by the generation or detection process; in the previous chapter we have seen how this can be done for photons, and how they can be localized e.g. by wave packets.

We now simply try to find a set of wave packet modes, and populate them in a fashion that can be described like an internal degree of freedom similar to the spin state of an electron. We will present a few common choices for appropriate degrees of freedom: polarization, which-way and time-bin are among the most widely used.

Polarization qubits

Let us first consider the polarization of a spontaneously emitted photon from an atom localized at the origin. Two possible decay options, that are $\Delta m = +1$ and $\Delta m = -1$, have similar spatial distribution for the light fields. We shall consider how can we describe the light field as a combination of internal and external degree of freedom.

Besides this, we can also choose the basis for the photon's polarization as horizontal polarization ($|H\rangle$) and vertical polarization ($|V\rangle$). It is possible to use column vectors to represent the state:

$$|H\rangle \equiv \begin{pmatrix} 1 \\ 0 \end{pmatrix} \qquad |V\rangle \equiv \begin{pmatrix} 0 \\ 1 \end{pmatrix} \tag{4.6}$$

Similarly, we could equally well describe its polarization in terms of linear polarization along +45° and -45° directions or right handed and left handed circular polarization.

The states $|\pm 45°\rangle$ and circular polarization $|L\rangle$ and $|R\rangle$ for left and right handed polarization can be written in terms of $|H\rangle$ and $|V\rangle$ as follows:

$$|+45°\rangle = \frac{1}{\sqrt{2}} \begin{pmatrix} 1 \\ 1 \end{pmatrix} = \frac{1}{\sqrt{2}}(|H\rangle + |V\rangle), \tag{4.7}$$

$$|-45°\rangle = \frac{1}{\sqrt{2}} \begin{pmatrix} 1 \\ -1 \end{pmatrix} = \frac{1}{\sqrt{2}}(|H\rangle - |V\rangle), \tag{4.8}$$

$$|L\rangle = \frac{1}{\sqrt{2}} \begin{pmatrix} 1 \\ i \end{pmatrix} = \frac{1}{\sqrt{2}}(|H\rangle + i|V\rangle), \tag{4.9}$$

$$|R\rangle = \frac{1}{\sqrt{2}} \begin{pmatrix} 1 \\ -i \end{pmatrix} = \frac{1}{\sqrt{2}}(|H\rangle - i|V\rangle) \tag{4.10}$$

So we see that the polarization state of a single photon maps conveniently to a qubit. We now need to find out how to implement qubit rotations, i.e. , arbitrary unitary transformations of this degree of freedom. For polarization, these rotations or single qubit gates can simply be implemented by the use of birefringent materials. In these materials the refractive index is dependent on the polarization direction.

The optical elements that implement polarization rotations are known as wave plates and are constructed such that two orthogonal linear polarizations acquire a

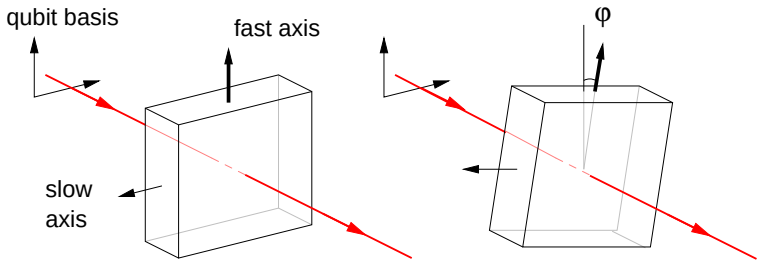

Figure 4.1: Plates of birefringent materials exerting different phase shifts for polarizations along different crystal axes. By rotating such a wave plate by an angle φ, a number of single qubit transformations can be implemented.

definite phase difference. Generally available wave plates implement a retardation of π ($\lambda/2$, half wave plate) or $\pi/2$ ($\lambda/4$, quarter wave plate) for polarizations parallel to their principal axes (see Fig. 4.1). For a half wave plate aligned with the basis vectors (referred sometimes to as "computational basis" in quantum information), the action on the qubit can be represented by the matrix

$$\hat{U}_{\lambda/2} = \begin{pmatrix} 1 & 0 \\ 0 & -1 \end{pmatrix} \tag{4.11}$$

Similarly, it is straightforward to consider the effect of a $\lambda/2$ plate rotated with respect to the computational basis by an angle φ (Fig. 4.1, right side) by concatenating rotation matrices and the retardation matrix:

$$\hat{U}_{\lambda/2}(\varphi) = \hat{R}(-\varphi) \cdot \hat{U}_{\lambda/2} \cdot \hat{R}(\varphi) \quad \text{with} \quad \hat{R}(\varphi) = \begin{pmatrix} \cos\varphi & \sin\varphi \\ -\sin\varphi & \cos\varphi \end{pmatrix} \tag{4.12}$$

One can show that a combination of $\lambda/2$, $\lambda/4$ and $\lambda/2$ plates which can be rotated individually is enough to transform any pure polarization into any other pure polarization.

An important component in qubit manipulation is also the detection or measurement process. We know how to detect a single photon already, but we do not yet have a way of measuring the qubit. Figure 4.2 shows how such a measurement is done for polarizations: the spatial mode carrying the photon with its two polarization components is sent on a polarization beam splitter (PBS), which transmits one and reflects the other polarization component. Both outputs of he PBS are now covered with single photon detectors. We will receive a binary answer (detector H or detector V) if there is a photon present, corresponding to measurement results seen in a Stern-Gerlach experiment.

Which-way qubits

Let's go back to the beam splitter shown in Fig. 4.3. There are two input ports, a and b, and two output ports, c and d. We can describe a photon passing through

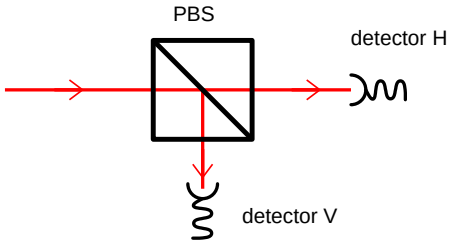

Figure 4.2: Measurement scheme for a polarization qubit, based on a polarizing beam splitter and two photodetectors.

this beam splitter from the input ports to output ports by artificially introducing an internal degree of freedom related to the ports of the beam splitter than the photon passes, together with an external degree of freedom associated with the propagation of a wave packet describing the extent of the non-vanishing field in the main propagation direction z:

Similarly to what we did with polarizations, we can represent the state of "internal" degree of freedom by column vectors. For example, a photon that enters the beam splitter through input port a can be represented by an internal state $|\Psi_i\rangle = \binom{1}{0}$.

In this image, we view the action of a beam splitter as a unitary operation acting on the states:

$$\hat{U}_{BS} = \frac{1}{\sqrt{2}} \begin{pmatrix} 1 & 1 \\ -1 & 1 \end{pmatrix}. \tag{4.13}$$

for an ideal symmetric beam splitter with a power transmission coefficient $T = 1/2$.

So, a photon in the initial state $|\Psi_i\rangle = \binom{1}{0}$ will pass through the beam splitter and "evolve" into the state

$$|\Psi_i'\rangle = \hat{U}|\Psi_i\rangle = \frac{1}{\sqrt{2}} \begin{pmatrix} 1 \\ -1 \end{pmatrix}. \tag{4.14}$$

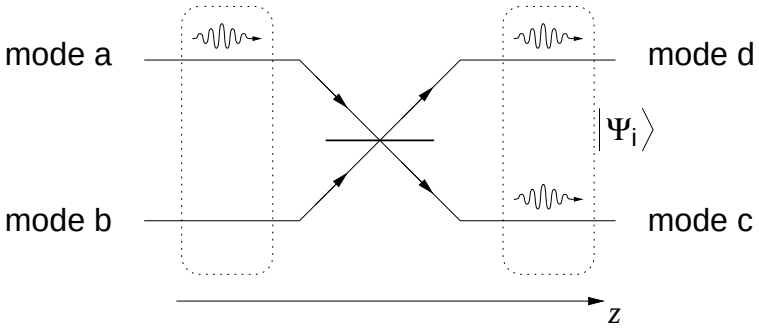

Figure 4.3: Two spatial modes can be used to represent a qubit, and transformations can be established using beam splitters.

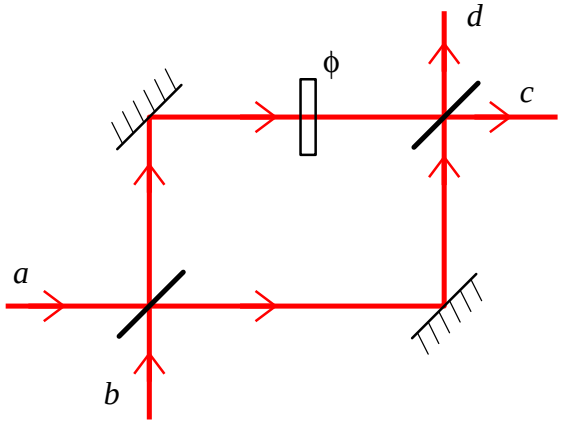

Figure 4.4: A balanced Mach-Zehnder interferometer can be used to create an arbitrary qubit state by controlling the splitting ratio of the beam splitters and the phase between the two possible paths.

The internal degree of freedom in this picture is just a combination of different propagation path possibilities, which could be implemented in a variety of ways. This method is not restricted to two-valued possibilities, equivalents to higher spin equivalents (or, in the language of quantum information, *qunits*, can be implemented using a larger base of possible propagation paths.

Typical elements to implement arbitrary unitary transformations in such a internal Hilbert space always involve beam splitters (to combine two modes) and phase shifters; a concatenation of such elements is e.g. a Mach-Zehnder interferometer. We can write the complete action of a Mach-Zehnder interferometer as:

$$|\psi\rangle_f = \hat{U}_{MZ}|\psi\rangle_i \tag{4.15}$$

$$\begin{pmatrix} c \\ d \end{pmatrix} = \frac{1}{\sqrt{2}}\begin{pmatrix} 1 & 1 \\ -1 & 1 \end{pmatrix}\begin{pmatrix} e^{i\phi} & 0 \\ 0 & 1 \end{pmatrix}\frac{1}{\sqrt{2}}\begin{pmatrix} 1 & 1 \\ -1 & 1 \end{pmatrix}\begin{pmatrix} a \\ b \end{pmatrix} \tag{4.16}$$

$$\begin{pmatrix} c \\ d \end{pmatrix} = \frac{1}{2}\begin{pmatrix} e^{i\phi}-1 & e^{i\phi}+1 \\ -e^{i\phi}-1 & -e^{i\phi}+1 \end{pmatrix} = \begin{pmatrix} a \\ b \end{pmatrix} \tag{4.17}$$

For detailed explanations on how to efficiently manipulate polarization and which-way degrees of freedom, have a look at the classic textbook from Hecht [19], or the very detailed matrix-centric [20].

Time-bin qubits

Time bin qubits exploit the time degree of freedom to implement a discrete basis [21]. The state of the photon is distributed into several distinguishable time of arrival "bins". These can be labeled as "early" and "late" or "long" and "short". The amplitude in each bin and the phase between the bins provide the

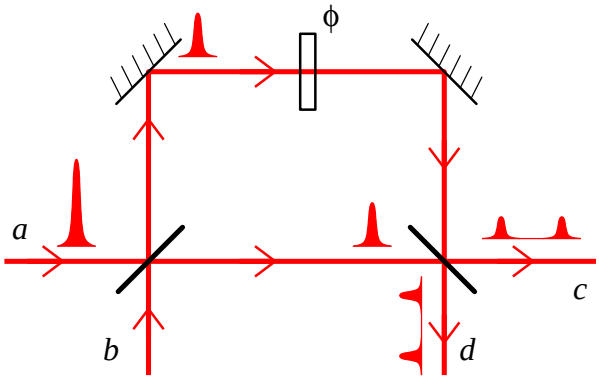

Figure 4.5: An unbalanced Mach-Zehnder interferometer can be used to create an arbitrary qubit state as the superposition of two time bins corresponding to propagation along either the long or the short path.

full Hilbert space for a qubit, and the scheme can in principle be extended to higher dimensional qunits.

The simplest implementation uses all passive elements in an asymmetric Mach-Zehnder interferometer as shown in Fig. 4.5. We can label the arms as *long* and *short*. If the beam splitters are balanced, a photon entering through path a and after passing through the interferometer and exiting through c will be described as

$$\psi = \frac{1}{\sqrt{2}} \left(|s\rangle + e^{i\phi} |l\rangle \right), \tag{4.18}$$

giving a photon which is in an equal superposition of arriving "early" or "late". To create a photon with different amplitudes in the two bins one can use a different splitting ratio in the first beam splitter. To measure the state in the $|s\rangle$ and $|l\rangle$ bases it is enough to record their times of arrival. To measure in the superposition basis it is necessary to use another interferometer and "reverse" the operation (See Fig. 4.6). On exit from the analysis interferometer, the photon will be distributed among three time bins. The first time bin clearly corresponds to a photon that has taken a short-short path. The last time bin equally clearly corresponds to a long-long path. However, the middle time bin has two contributions, that of a long-short path and that of a short-long path, and the two are indistinguishable, thus providing a projection onto the basis where the photon is in a superposition of the two time bins.

One disadvantage of this measurement scheme is that we only project onto the superposition basis with 50% probability. This could in principle be addressed by using active switches instead of the passive interferometers. In such a scenario, the early pulse would be directed towards the long path, and the late pulse through the short path. Both of them would arrive at the exit beam splitter simultaneously thus eliminating the satellite peaks.

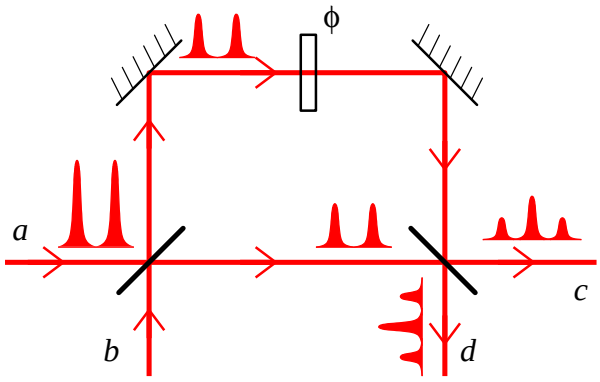

Figure 4.6: An unbalanced Mach-Zehnder interferometer with path differences that correspond exactly to the time bin encoding can be used as an analyzer to project the state into superpositions of different time bins.

4.1.4 Qubit tomography and the good old Stokes parameters

It has been known for a long time [22] that the state of polarization of light is fully characterized by four quantities, the Stokes parameters. These are defined in relation to the measured quantities used to estimate them and are often grouped together into a vector form.

$$S_0 = I_t \tag{4.19}$$
$$S_1 = I_H - I_V \tag{4.20}$$
$$S_2 = I_{45^\circ} - I_{-45^\circ} \tag{4.21}$$
$$S_3 = I_{C+} - I_{C-} \tag{4.22}$$

The first parameter is just the total intensity of the light. The others are respectively the difference in intensities in three orthogonal polarization basis. For example S_1 would be determined by the measuring the intensity of H and V polarized light and taking the difference. Equivalently for the S_2 and S_3 in the 45° and circular polarization basis. These four parameters form a complete basis of the space of all possible polarization states. It is also common to use a reduced normalized representation such that $\vec{S}_r = \frac{1}{S_0}(S_1, S_2, S_3)$. Using the reduced Stokes vector, any state of light can be visualized as a point in the Poincaré sphere.

The Stokes parameters are convenient because they take easily measurable quantities and reduce them to a minimal set that completely describes the light polarization; a corresponding experimental scheme is shown in Fig. 4.7, where a fraction of the original light is sent onto various measurement branches, each corresponding to one of the three Stokes parameters. These parameters are useful and conveniently based on a physical measurement, however, there is nothing

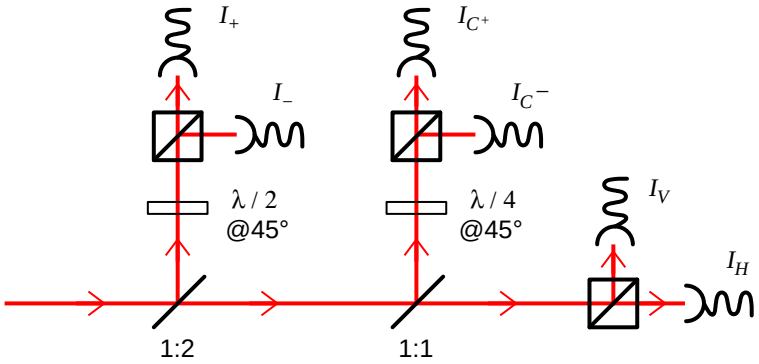

Figure 4.7: A simple setup to measure the Stokes parameters.

fundamental about them. It is possible to chose a different set of measurements and come up with an equally good equivalent representation.

Going back to qubits, consider now an arbitrary state of polarization written as a density matrix,

$$\rho = \begin{pmatrix} \rho_{HH} & \rho_{HV} \\ \rho_{VH} & \rho_{VV} \end{pmatrix} \quad \text{with} \quad \mathrm{tr}\rho = 1 \tag{4.23}$$

Quantum tomography tries to completely determine all the entries in the matrix so as to completely describe the quantum state. A not too deep examination shows that the number of independent parameters in the density matrix is the same as for the Stokes representation. Not surprisingly, the two representations are equivalent and related simply by a linear transformation. In this sense, classical polarimetry is equivalent to the state estimation of a single qubit. In the case of qubits encoded in polarization of single photons, this equivalence is exact.

An uncomfortable point about the measurement scheme in 4.7 is that we record six quantities that get instantaneously reduced to four independent parameters; we should be able to do better than that [23] and end up with a leaner alternative [24].

When considering tomography schemes it is useful to keep some conditions in mind. The measurement should be universal and unbiased; that is, it should be able to characterize any possible input state, and do so with equal accuracy, or nearly so, for all of them. Additionally, when working with photons, we should remember that measurements are destructive, and that, given the efficiency limitations of detectors, we cannot use the failure of a photon to arrive as a projective measurement.

A measurement that fulfills these conditions is made up of four detector readings corresponding to the overlap of the unknown Stokes vector with four non-coplanar vectors b_j that define a tetrahedron in the Poincaré sphere (see fig. 4.8). Each measurement operator B_j can be written as

$$B_j = \frac{1}{4}(\vec{b_j} \cdot \vec{\sigma}), \tag{4.24}$$

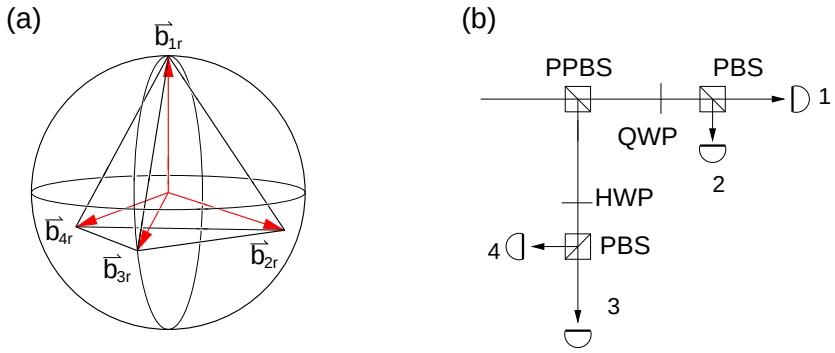

Figure 4.8: Efficient polarimetry. (a) Polarization measurements are carried out corresponding to four measurement states $\vec{b}_j$, which form a tetrahedron on the Poincaré sphere. (b) Experimentally, four photon counting detectors are used, each associated with the outcome of one of the measurements. The light is divided between the four detectors by a partially polarizing beam splitter (PPBS), half (HWP)- and quarter (QWP) wave plates, and polarizing beam splitters (PBS).

where $\vec{\sigma} = (\sigma_0, \sigma_1, \sigma_2, \sigma_3)$, σ_0 being the unit matrix and $\sigma_{1,2,3}$ the Pauli matrices. Figure 4.8 shows a possible experimental realization of these measurement operators. The average intensity falling on detector b_j is denoted as I_j. Expectation values of the tetrahedron operators are related to detected intensities as

$$\frac{I_j}{I_t} = \langle B_j \rangle = \frac{1}{4}(\vec{b_j} \cdot \vec{S}) \qquad \text{with} \qquad I_t = \sum_{j=1}^{4} I_j. \tag{4.25}$$

A bit of manipulation allows to relate the fractional intensities $\vec{I}$ directly to the components of the density matrix written in a vector form,

$$\vec{\rho} = \frac{1}{2}\Gamma_1 \Pi^{-1} \cdot \vec{I} = T \cdot \vec{I}. \tag{4.26}$$

Where $\vec{I} = \Pi \cdot \vec{S}$ and $\Gamma_1 = (\vec{\sigma_0}, \vec{\sigma_1}, \vec{\sigma_2}, \vec{\sigma_3})$. The matrix Π is sometimes referred to as the instrument matrix, as its exact values depend on the details of the experimental setup and will be adjusted during calibration. The relation between the fractional intensities and the entries in the density matrix is summarized in the so-called tomography matrix T.

4.2 Multi photon stuff

Photons as single qubits are only of moderate interest, the description is mostly a reformulation of phenomena that have been known in optics for more than 100 years into the language of quantum mechanics. The really fascinating effects

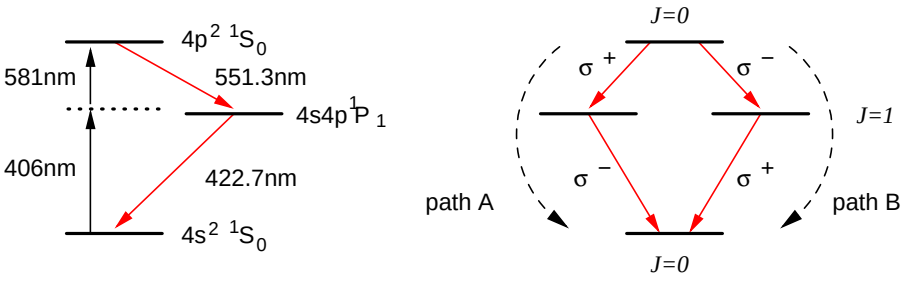

Figure 4.9: The relevant energy levels of calcium atom used to generate polarization entangled pairs of photons from an atomic cascade in Ca, and the two indistinguishable paths for a radiative decay of the upper excited state.

present themselves when considering multiphoton states. In particular those that arise from superpositions of multiphotons states, i.e. entangled states. Quantum physics allows the existence of states that cannot be described completely just in terms of their constituent parts. It was realized early on [25] that the existence of these states challenged the way we understood physical phenomena and the underlying physical theories accounting for them.

4.2.1 Entangled photon pairs

The theoretical implications of the existence of entangled states did not result in an experimental push to produce them until the formulation of Bell inequalities [26]. Until that point, it was understood that entanglement brought up philosophical questions about the underlying properties of our theories, but there was no experimentally relevant measurement that could discriminate between the options presented. With the formulation of Bell's theorem this changed radically. There was now an experiment that could be used to resolve the issues in the EPR paradox. The first step in any experiment of this type was to prepare a pure entangled state of two particles - photons seemed very promising, since the measurements could be carried out independently, and even in space-like separated settings.

4.2.2 Atomic cascades

In this subsection, we illustrate how we can produce pairs of entangled photons using atomic cascades. First of all, let us consider the following three energy levels in the calcium atom used in the experiment by Aspect [27].

First, photon pairs were generated by a cascade decay from an excited atomic state as shown in Fig. 4.9. Similarly to the single photon sources discussed earlier, this leads to photons which are well localized in time. The cascade decay ensures that there is a strong temporal correlation between the two photons as well.

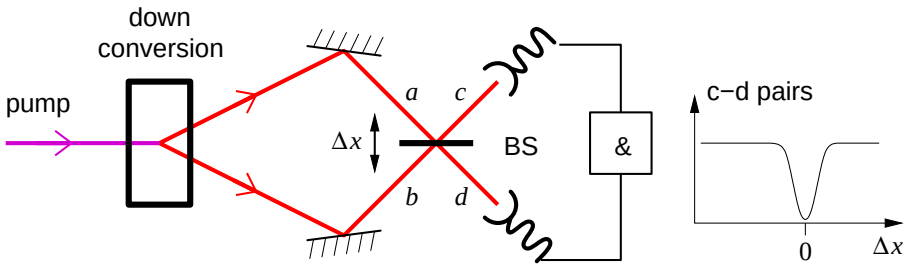

Figure 4.10: Hong-Ou-Mandel experiment on the indistinguishability of photons generated in parametric down conversion. Down-converted photons are superimposed on a beam splitter BS with an adjustable delay Δx, and photon pair coincidences between the two output ports are recorded.

The main idea to prepare an entangled state between this photon pair in a polarization degree of freedom is to consider the conservation of angular momentum for the complete decay process. As shown in Fig. 4.9, there are two possible paths for the decay to proceed, each involving different magnetic orientation states in the intermediate level. Each partial emission process conserves the angular momentum, so decay via path A leads first to emission of a σ^--polarized photon for the first stage, and a σ^+-polarized one for the second decay. For path B, the polarizations change accordingly.

The atom is initially and after the cascade in a $J = 0$ level, which does not allow to store any angular momentum information about the decay path. Since it is therefore impossible in principle to know which path the decay process actually has taken, the two photons are in an entangled state

$$|\psi^-\rangle = \frac{1}{\sqrt{2}}(|\sigma^+\rangle_1|\sigma^-\rangle_2 - |\sigma^-\rangle_1|\sigma^+\rangle_2). \tag{4.27}$$

In a practical experiment, a fraction of the emitted photons was captured into two opposite directions, and photon pairs were identified by a coincidence measurement with polarization analyzers under various angles.

After many hours of measurement time, the observed polarization correlations between the photon pairs violated the Bell inequality by 5 standard deviations.

4.2.3 Hong–Ou–Mandel interference in parametric down conversion

The observation of correlated photon pairs by parametric down conversion by [18] suggested that this process is able to deliver correlated photon pairs as well. In order to prepare this photon pair in an entangled state, it was also necessary to have two completely indistinguishable photon pair generation processes, similar to the different orientation paths for the atomic cascade decay.

An important step to demonstrate this indistinguishability was presented in a paper in 1987 [28] with a deceptive title: "Measurement of sub-picosecond time intervals between two photons by interference". The paper considered a scenario in which two photons enter the two input ports (a and b) of a 50:50 beam splitter (see Fig. 4.10). Classically we would expect a binomial distribution of the possible outcomes. That is we expect that 25% of the time both photons exit through port c, 25% through port d and 50% of the time the photons are distributed to different ports. However, the quantum behavior is very different.

In terms of operators for generating/removing photons from the vacuum, we can write the action of the beam splitter as

$$\hat{a} = \frac{1}{\sqrt{2}}\left(\hat{c} + \hat{d}\right) \quad , \quad \hat{b} = \frac{1}{\sqrt{2}}\left(\hat{c} - \hat{d}\right) \tag{4.28}$$

This implies that the two photons will never exit through different ports. A very simple way to see this is to express a two-photon state in modes a, b in terms of creation operators acting on the vacuum, and then reformulate the state in terms of creation operators on modes c, d using the operator transformation rule eqn (4.28):

$$\begin{aligned} |1_a; 1_b\rangle &= \hat{a}^\dagger \hat{b}^\dagger |0\rangle \\ &= \frac{1}{2}\left(\hat{c}^{\dagger 2} - \hat{d}^{\dagger 2}\right)|0\rangle = \frac{1}{\sqrt{2}}\left(|2_c; 0_d\rangle - |0_c; 2_d\rangle\right) \end{aligned} \tag{4.29}$$

This can be interpreted such that two photon interference effect gives complete cancellation of an outcome of a contribution $|1_c; 1_d\rangle$ leading to coincidence detection events. This simple description in terms of single modes needs to be completed to describe real systems: Each photon is a wave packet, e.g. described in a form of eqn (2.90). If the wave packets in the input modes do not perfectly overlap, the transfer relation eqn (4.28) for the input/output modes needs to be modified e.g. to include creation operators $\hat{a'}^\dagger$ which can take care of the part of wave packet mode a which does not overlap with the wave packet mode in b after superposition in the beam splitter. The overlap of the two wave packets that determines the degree of cancellation.

The right part of Fig. 4.10 a sketch and a corresponding experimental trace of this so-called Hong-Ou-Mandel dip. The H-O-M dips allow to judge the degree of indistinguishability of two photon wave packets and has become a common tool in photonic quantum information.

4.3 Entangled photon pairs from spontaneous parametric down conversion

The indistinguishability of the photons localized in time that originate from parametric down conversion as demonstrated in the Hong-Ou-Mandel experiments

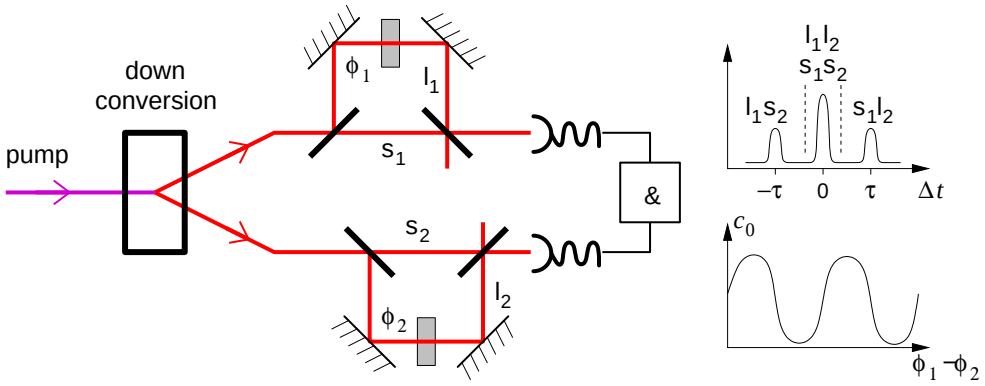

Figure 4.11: Observation of photon pairs which are entangled in time bin qubits. The detection post-selects on coincidences between the two detectors for a time difference $\Delta t = 0$, where both short/long path combinations become indistinguishable.

opened the path to generate entangled photon pairs via this process. The additional element needed to arrive at a photon pair were two indistinguishable processes. In the following, we highlight a few approaches to this problem.

4.3.1 "Energy-time" entanglement

Apart from the polarization entangled photon pairs generated in cascade decays, one of the early suggestions was related to what is now referred to as time-bin qubits, and was proposed still with an atomic cascade as a photon pair source [29]. The indistinguishability of two photon pair generation processes there comes from the fact that it is not known when a particular pair creation process takes place assuming the coherence length of the excitation light initiating the photon pair is long enough to not allow to infer when it happened.

A SPDC-based version of the original proposal is shown in Fig. 4.11. Each of two modes of target photons emanating from the nonlinear optical crystal are sent into asymmetric Mach-Zehnder interferometers with a path length difference corresponding to a time delay which can be resolved electronically (typically a few nsec) - such a configuration is referred to as "Franson interferometer". When looking for coincidences between the photodetectors at the output ports of the loops, the corresponding pair correlation function $g^{(2)}(\Delta t)$ has three distinct peaks, corresponding to the path combinations $s_1 l_2$, $s_1 s_2$ or $l_1 l_2$, and $l_1 s_2$. If the path length differences of the two asymmetric MZI is the same within the coherence length of the down-converted light (typically a few 100 μm for common down conversion sources), and if there is no possible indication of the pair generation time, then the possibilities $s_1 s_2$ and $l_1 l_2$ are indistinguishable. The necessary long coherence time for the pump mode implies a very narrow frequency distribution of the pump, or equivalently a well-defined energy of the pump photons - which

probably is the reason for the otherwise not so obvious choice of the common term "energy-time entanglement" for this idea.

By restricting the observation to photon pairs to a time difference $\Delta T = 0$, simply by carrying out a coincidence selection with a narrow time window, the observed pairs can be thought of having been in a time-bin entangled state. The entanglement, i.e., coherent superposition of the two early/late photon generation processes, can be verified by modulating the phases in both Mach-Zehnder interferometers. The detected coincidence pair rate c_0 then varies sinusoidally only according to the difference of the two phase shifts ϕ_1 and ϕ_2,and could be used to test a Bell inequality.

An experiment with almost the same scheme has been published by the Geneva group [21], but with a pulsed source. This pulsed source has a very short coherence time; in order to ensure the indistinguishability of the two photon pair generation processes – otherwise the to options $s_1 s_2$ and $l_1 l_2$ could be distinguished by looking at the detection time – the source path also had to include a Franson interferometer, preparing a coherent superposition of two pump pulses.

While preparing photons in a time-bin entangled state is not very demanding to the photon pair generation process, the asymmetric Mach-Zehnder interferometers can be a substantial technical challenge, as they have to kept stable within a fraction of the optical wavelength for a path length difference on the order of one meter to ensure proper electronic selection of the corresponding paths. Such a stability usually can only be maintained with relative elaborate active stabilization schemes.

4.3.2 Polarization entanglement from type-II non-collinear SPDC

Technically much less demanding than time bin qubits is the encoding into polarization states. An entangled photon generation scheme utilizing this degree of freedom was suggested and experimentally demonstrated [30]. For a long time, this was probably one of the most widely used schemes for generation of polarization- entangled photon pairs.

The basic idea there explores the angular dispersion properties in the birefringent conversion materials, and uses a non-collinear arrangement of pump- and target modes in a type-II phase-matching configuration. The geometry of pump- and target directions and polarizations is shown in Fig. 4.12(a). For a pump mode with a fixed wave vector k_p, there is a wide spectrum wave vectors of signal and idler to meet phase matching conditions and energy conservation. For a fixed target frequency, the possible combinations of signal- and idler modes form two cones, which – for type-II phase matching – have different main axes. For a proper choice of crystal orientations, these two cones intersect for two di-

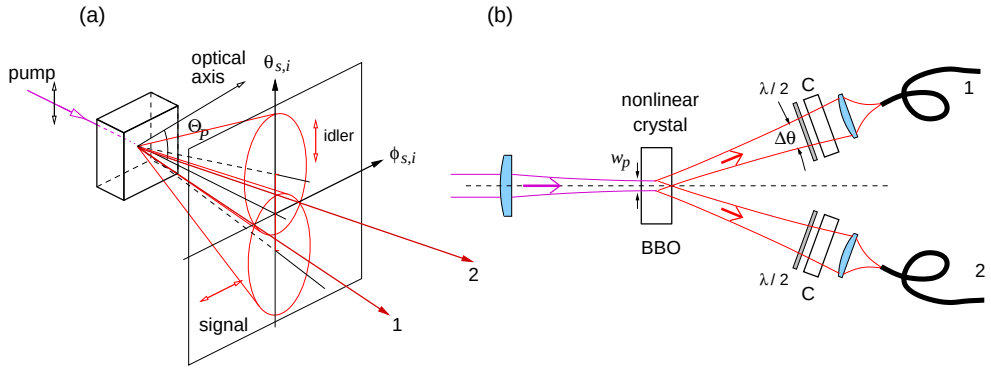

Figure 4.12: Type-II non-collinear parametric down conversion following (Kwiat et al. 1995).

rections (labeled 1 and 2). Parametric down conversion light collected into these two directions cannot clearly identified as being either the signal (ordinary polarization) or idler (extraordinary polarization. Transverse momentum conservation now requires that if a e-polarized photon is present in direction 1, the o-polarized twin photon from the same conversion process must be present in direction 2, and vice versa.

To make sure that the two corresponding down conversion possibilities leading to a photon pair in modes 1 and 2 are really indistinguishable, a residual distinguishability due to the birefringence in the conversion crystal needs to be removed, which would allow to infer the ordinary/extraordinary information from the delay between the two photons. This "longitudinal walk-off" can be compensated by birefringent media with half of the total retardation than the conversion crystal; often crystals made from the same material are used, preceeded by half wave plates to rotate the polarization before the modes enter the compensators as shown in Fig. 4.12 (b). This also partly reduces the effect of a transverse wall-off, which is present since the crystals are typically used in a critical phase matching scenario.

Such a source geometry allows to collect the down converted light efficiently into single mode optical fibers, which for a proper mode matching to the dispersion properties of the conversion crystal take care of the spectral filtering for the target modes [31]. With such an arrangement, a reasonably high brightness (around 1000 observed pairs per mW pump power for a 3 mm thick BBO crystal) can be achieved. The pair collection efficiency, quoted as observed pair events to single events (where one of the photons was not detected) for such a source is commonly around 30%, which would translate into a collection efficiency of 60% if a detector efficiency around 50% is assumed. For cw pumped source of this type, the desired singlet state $|\Psi^-\rangle = 1/\sqrt{2}(|H_1V_2\rangle - |V_1H_2\rangle)$ can be prepared with fidelities over 99.5%.

Such a geometry can also easily be used for generating pairs with ultrashort

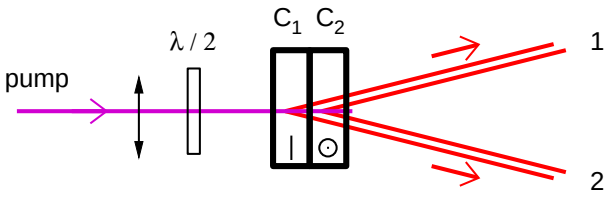

Figure 4.13: Polarization-entangled photon pair source based on two crystals C_1, C_2 cut for type-I phase matching conditions, tilted by 90° with respect to each other. The indistinguishable decay paths correspond to a pair generation in the first or second conversion crystal. By adjusting the pump polarization with the half wave plate $\lambda/2$, the balance between the two components $|HH\rangle$ and $|VV\rangle$ can be adjusted.

pump pulses, where the coherence length of the pump is on the order of the coherence length of the target photons. Such a pumping scheme is used for a large number of experiments where more than two photons needed to be generated.

4.3.3 Polarization entanglement from type-I SPDC

A somewhat simpler geometry to generate polarization-entangled photon pairs relies not on two different decay processes in one conversion crystal, but generates the two components with different crystals [32]. A schematic of this configuration is shown in Fig. 4.13.

By choosing crystals with type-I phase matching, down converted photon pairs are generated with the same polarization. The second decay process necessary to form an entangled state is provided by a second crystal located directly on top of the first one, but rotated by 90°. For collection into target modes 1,2 which are non-collinear with the pump beam, one needs to ensure that there is no distinction in any degrees of freedom from which of the crystals the pair emerged. Such a selection can either be done by spatial filtering, or by using single mode optical fibers, which efficiently remove any spatial information. This scheme is somewhat simpler than the type-II configuration discussed above, since it does not need any birefringence compensation as long as the coherence length of the pump field is larger than the physical extent of the two crystals. The photon pair is generated in a state

$$|\Psi\rangle = |H_1 H_2\rangle \cos\phi + |V_1 V_2\rangle \sin\phi\,, \tag{4.30}$$

where ϕ indicates the orientation of the polarization of the pump with respect to the extraordinary polarization for a given crystal. This pair state s different from a singlet state, but can easily be converted into one by applying local operations, i.e. , polarization transformations on one of the modes only. This scheme has therefore the advantage to generate non-maximally entangled states, while the

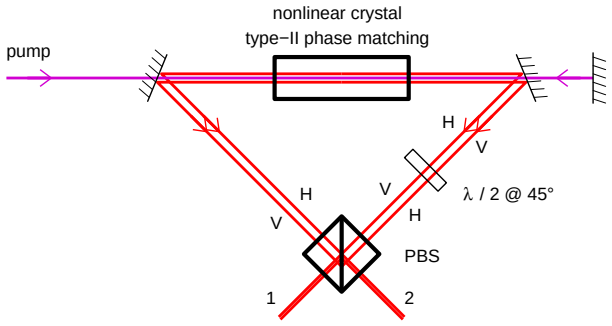

Figure 4.14: Type-II parametric down conversion in a Sagnac configuration. The two decay paths correspond to photon pairs generated in both directions in a collinear configuration; the pairs are combined via a beam splitter such that they form a polarization-entangled state.

type-II source discussed before has by construction a fixed ratio between H and V components.

Another advantage of this geometry is that for type-I phase matching in BBO, the material commonly used for this process, a larger optical nonlinearity can be used than in type-II phase matching. Since this enters in the source brightness quadratically, these sources have a potential of being intrinsically brighter than sources based on type-II phase matching.

Recently, a very bright source based on the same idea, but using a collinear arrangement of pump- and target modes was reported [33]. In this collinear configuration, the distinction between the two target modes is made by lifting the commonly used frequency degeneracy between the two target modes, and the photon pairs are separated with a wavelength division multiplexer. The collinear conversion geometry allows also for a very good mode overlap, resulting not only in a high brightness, but also into a pair/single ratio of up to 39%; correction with the usual detector efficiency of around 50% suggests that this source has an extremely high pair collection or single photon heralding efficiency, reaching up to 80%.

4.3.4 Sagnac geometry

Another approach to prepare polarization-entangled photon pairs in a collinear geometry makes use of a type-II phase matching process, but uses two different emission directions as the source for indistinguishable photon pairs [34]. A schematic of the experimental setup is shown in Fig. 4.14.

The conversion crystal has to be pumped from two directions, and to make the two pair processes indistinguishable, the coherence length of the pump must be longer than the path length difference; ideally it has a coherence length exceeding the one of the crystal or a few crystal lengths.

Each of the two pair generation processes leaves a H and a V polarized photon propagating in the same direction. In order to arrive at a polarization entangled state in two target modes 1 and 2, the polarization of pair photons from one direction is rotated by 90°, and then light from both conversion directions is combined on a polarization beam splitter. This distributes the photons from each conversion process onto the two output modes, resulting in a singled state for the photon pair.

Such sources have been implemented with periodically poled potassium titanyl phosphate (PPKTP), which leads to a very narrow spectral distribution of the photon pairs. An extremely high brightness of 28000 detected pairs per mW pump power for a 25 mm long crystal has been reported for such a source [35] after coupling into optical fibers, together with a fidelity of the targeted state comparable with the other bright sources described above. For this long crystal, a spectral bandwidth of 0.4 nm has been reported.

Such down conversion sources have actually a high enough spectral brightness that interactions with atoms have been observed.

4.4 Multiphoton Tomography

So far we have discussed the preparation of photonic qubit states - limited to single and two-photon states, but using higher order conversion processes, entangled states between up to 8 photons have been prepared.

Apart from techniques to prepare complex multiphoton states, we also need some tools to analyze such states. In this last section, we will visit a few common methods for state analysis if more than one photonic qubit is involved. While the techniques can be mapped onto most implementations of photonic qubits, here we focus on implementations with polarization.

4.4.1 Standard tomography

Following the same line of argument as in Subsection 4.1.4, we need to come up with a set of measurable quantities that can be used to determine all independent parameters necessary for a complete state description. A pure two-photon polarization state can be written as a linear combination of four product polarization states (we use H and V as our "computational basis"):

$$\begin{aligned} |\Psi_{12}\rangle &= \alpha_{HH}|H_1H_2\rangle + \alpha_{HV}|H_1V_2\rangle \\ &\quad +\alpha_{VH}|V_1H_2\rangle + \alpha_{VV}|V_1V_2\rangle\,, \quad \text{with} \quad \sum_{i,j=H,V} \alpha_{ij}^2 = 1 \end{aligned} \tag{4.31}$$

The density matrix of a two photon polarization state can consequently be written as a 4×4 matrix in the same basis, and has 15 independent parameters (assuming normalization). It is clear from this that it is not enough to do polarimetry on

the individual photons and just combine those results (3 free normalized Stokes parameters for each photon). This, in fact, is a reason why quantum information promises to be a powerful tool with not very complex systems.

To arrive at a sensible state description, we need to perform joint polarization measurements to fully account for the possible correlations present in the state. One way of doing this is to take the same basic measurements that are used for single photon tomography and combine them. The traditional measurement scheme for the stokes parameters with a measurement device as shown in Fig. 4.7 would require the recording of $6 \times 6 = 36$ detector correlations. A more sophisticated way of carrying out these measurements, and to reconstruct the photon pair state from them is given in [36]

There are a few issues with this procedure. One problem with this is that it does not estimate all states equally well. Another is that the estimation sometimes produces unphysical states. Additionally, the measurement is overdetermined and therefore apparently inefficient.

4.4.2 Efficient tomography

Alternatively we can use on the minimal tomography setup based on tetrahedron POVMs. What we would like to do is extend the concept of Stokes vector to a multiphoton state and extend the formalism presented in section 4.1.4 to an arbitrary number of photons.

The simplest multi-photon system is a photon pair identified by coincident time of arrival. In this scheme, each component photon is passed through a four-output polarimeter like the one described in 4.1.4. Given two polarimeters 1 and 2, each with four detectors b_{i_1} and b_{i_2}, respectively, $(i_1, i_2 = 0, 1, 2, 3)$, there are 16 possible coincidence combinations. Each coincidence rate is governed by an operator composed from the individual detectors' measurement operators. If we denote again the measurement operator of detectors b_{i_1} and b_{i_2} as B_{i_1} and B_{i_2}, and the coincidence count between them as c_{i_1,i_2}, we can express the coincidence rates as a linear function of a 2-photon polarization state vector S_2:

$$\begin{aligned} \frac{c_{i_1,i_2}}{c_t} = \langle B_{i_1} \otimes B_{i_2} \rangle &= (\frac{1}{4}\vec{b_{i_1}} \otimes \frac{1}{4}\vec{b_{i_2}}) \cdot \vec{S_2}, \\ \text{with } c_t &= \sum_{i_1,i_2=1}^{4} c_{i_1,i_2} \end{aligned} \tag{4.32}$$

Here, $\vec{S_2}$ is the Stokes vector equivalent for a 2-photon system and c_t is the total number of observed coincidences. We now have the set of measurement operators governing the coincidence pattern. The sixteen coincidences c_{i_1,i_2} can be written in column vector format $\vec{C_2} = (c_{1,1}, c_{1,2}, ..., c_{4,4})$. If we define the 2-polarimeter instrument matrix as Π_2, we obtain an instrument response:

$$\vec{C_2} = \Pi_2 \cdot \vec{S_2} \Leftrightarrow \vec{S_2} = \Pi_2^{-1} \cdot \vec{C_2} \tag{4.33}$$

Thus the 2-photon density matrix is given by:

$$\vec{\rho_2} = \frac{1}{2^2}\Gamma_2 \cdot \vec{S_2} = T_2 \cdot \vec{C_2} \tag{4.34}$$

Each column of Γ_2 is the product of two Pauli operators $\sigma_{i_1} \otimes \sigma_{i_2}$ $(i_1, i_2 = 0, 1, 2, 3)$ written in column vector format and T_2 is the complete tomography matrix for the 2-photon state.

Similarly, the procedure is generalized to states containing an arbitrary number of photons,

$$\vec{S_N} = \Pi_N^{-1} \cdot \vec{C_N}, \tag{4.35}$$

$$\vec{\rho_N} = \frac{1}{2^N}\Gamma_N \cdot \vec{S_N} = T_N \cdot \vec{C_N}. \tag{4.36}$$

Each row of the instrument matrix Π_N is given by $(\frac{1}{4}\vec{b_{i_1}} \otimes \frac{1}{4}\vec{b_{i_2}} ... \otimes \frac{1}{4}\vec{b_{i_N}})$ and each column of Γ_N is the product of N Pauli matrices $\sigma_{i_1} \otimes \sigma_{i_2} ... \otimes \sigma_{i_n}$ $(i_n = 0, 1, 2, 3$ and $n = 1, 2, ..., N)$.

A few more comments about multi-qubit tomography. The procedure just described uses the minimal number of measurements and thus is efficient in an experimental sense. It is also known to be optimal for single qubits, but it is an open question whether this holds for multi-qubit states. We are only considering here methods that are "simple" and efficient from an experimental point of view. For example, we limit ourselves to individual measurements per photon rather than the in principle more powerful global POVMs for the simple reason that these are a by themselves a challenge to implement. We have however extended our dictionary of available measurements beyond naive projective measurements, and expanded into simple POVMs. It is interesting to note that the classical optics community converged in very similar protocols for polarimetry [37].

4.5 Bell state analysis

The four Bell states are a complete orthogonal basis of the state of two qubits:

$$|\Psi^{\pm}\rangle = \frac{1}{\sqrt{2}}\left(|H_1V_2\rangle \pm |V_1H_2\rangle\right), \qquad |\Psi^{\pm}\rangle = \frac{1}{\sqrt{2}}\left(|H_1H_2\rangle \pm |V_1V_2\rangle\right), \tag{4.37}$$

They play a fundamental role in protocols such as teleportation, entanglement swapping and many others. None of these states can be identified b simply doing single qubit measurements; each of them would result in a completely random result. A Bell state measurement is now defined as a measurement, where an arbitrary two-photon state is projected onto the four Bell states, and the measurement result is one out of four values, indicating one of the four states in eqn 4.37.

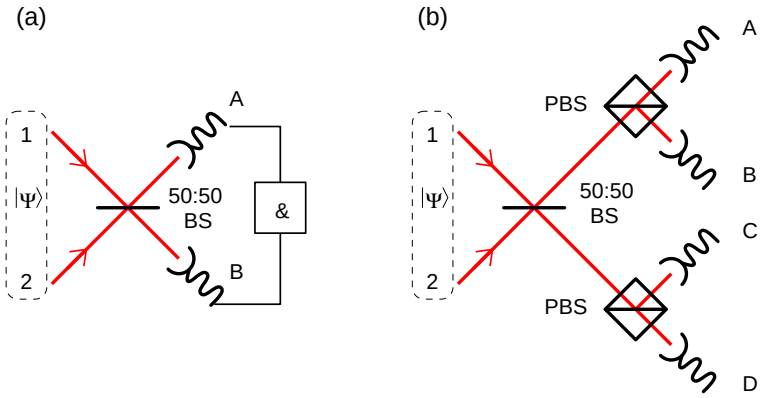

Figure 4.15: Simple partial Bell state analyzer, using the symmetry of photons entering a symmetric beam splitter(a). For most physical beam splitters, the photon pair gets distributed onto the two detectors A,B only for $|\Psi_{12}\rangle = |\Psi^+\rangle$. Another Bell state $|\Psi^-\rangle$ can be identified if each output port is further analyzed with polarizing beam splitter (b).

Being orthogonal states, in principle it should be possible to distinguish the unambiguously. Unfortunately, it can be be shown that it is not possible to distinguish all four Bell states using only linear optics. This problem is equivalent to the difficulty of implementing a universal two-qubit gate with linear optics [38], since a Bell state measurement can be implemented with a CNOT gate and a (cheap) one qubit Hadamard gate.

4.5.1 Partial Bell state analysis

The basic idea behind a partial Bell state analysis makes use of the fact that both photons of pair entering the input ports of a normal 50:50 beam splitter will leave the beam splitter at different output ports if the photon pair is in a $|\Psi^+\rangle$ state, as shown in Fig. 4.15(a). This can be seen by extending the simple beam splitter matrix eqn (4.13) to a 4×4 matrix for both polarization modes. One caveat for most beam splitters is that they change the helicity of the polarization upon reflection; this means that the transfer matrix has the phase shift between the two reflections at the other ports. We leave it to the reader to generate the full transfer matrix, and to work out its action on various Bell states.

Most of the proof of principle experiments implementing a Bell state analysis only perform this relatively simple part by looking for coincidences at detectors A and B behind beam splitter to identify $|\Psi^+\rangle$ [39].

A simple extension of this method allows to identify one more Bell state if the configuration shown in Fig. 4.15 is used, where each of the output ports of the beam splitter is followed by a polarizing beam splitter, leading to a unique detector pattern in case both a H and V polarized photon was present. The

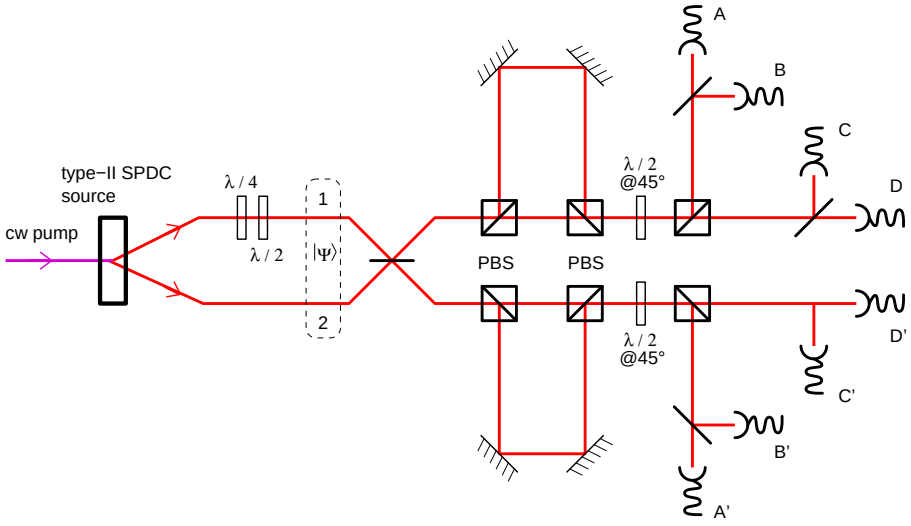

Figure 4.16: Setup to perform a complete Bell state measurement. This scheme relies on the fact that a polarization-entangled photon pair generated in a cw-pumped SPDC process exhibits also a time-bin entanglement. The larger Hilbert space this pair is embedded in allows then to carry out a complete Bell state analysis with linear optical elements.

identification of the Bell state can be obtained from the following lookup table:

detector coincidence	state
A-C or B-D	$\|\Psi^+\rangle$
A-B or C-D	$\|\Psi^-\rangle$

There have been several attempts to get around this limitation. Some invoke non-linear optical effects (ref), probabilistic identification (ref) or heralded detection (ref).

4.5.2 Complete Bell state analysis

Surprisingly there are ways to get around this limitation [40, 41] if one takes advantage of additional entanglement which is present "for free" in the usual PDC sources used to produce Bell states.

When preparing entangled states via PDC (see Section 4.2.1f), the photons are not only in a polarization entangled state but also in an energy-time entangled state, i.e. , they were generated at an unknown but identical time. This property, sometimes called hyper-entanglement, can be exploited to implement a full and deterministic Bell state analyzer using only the tools of linear optics. Consider the setup in Fig. 4.16. A PDC source produces pairs which are then combined into a beam splitter. At zero delay, H-O-M interference will result in the state

$|\psi^+\rangle$ split between the two output modes, thus can be uniquely identified. The other three states will send the two photons together either through a' or b'. Of these, $|\psi^-\rangle$ has its two photons in orthogonal polarizations. By sending this state into a delay line based on a pair of PBSs the two photons will be split deterministically with the V photon taking the long path (l) and the H photon taking the short path (s). This state can be uniquely identified by the different time of arrival given by the delay. Finally the $|\phi\rangle$ states both have their photons in superpositions of identical polarizations with only the phase differentiating them. When going through the delay line the two photons will stick together and take either the long or the short path depending on their polarization, resulting in a state,

$$|\phi^\pm\rangle = \frac{1}{\sqrt{2}}(|H_s, H_s\rangle \pm e^{2i\phi}|V_l, V_l\rangle). \tag{4.38}$$

When $\phi = 0$, these two states can be easily distinguished by analyzing in the 45° basis.

$$|\phi^+\rangle = \frac{1}{\sqrt{2}}(|+45°, +45°\rangle + |-45°, -45°\rangle) \tag{4.39}$$

$$|\phi^-\rangle = \frac{1}{\sqrt{2}}(|+45°, -45°\rangle + |-45°, +45°\rangle) \tag{4.40}$$

Bibliography

[1] C Cohen-Tannoudji, J Dupont-Roc and G Grynberg. *Photons and Atoms: Introduction into quantum electrodynamics*. Wiley Interscience, 1997.

[2] J D Jackson. *Classical Electrodynamics*. John Wiley & Sons, 1999.

[3] B E A Saleh and M C Teich. *Fundamentals of Photonics*. John Wiley & Sons, 2007.

[4] V Weisskopf and E Wigner. Berechnung der natürlichen Linienbreite auf Grund der Diracschen Lichttheorie. *Z. Physik* 63, 54, 1930.

[5] W E Lamb. Anti-photon. *Appl. Phys. B* 60, 77, 1995.

[6] P Lenard. Ueber die lichtelektrische wirkung. *Ann. Physik* 313, 149, 1902.

[7] Albert Einstein. Über einen die Erzeugung und Verwandlung des Lichtes betreffenden heuristischen Gesichtspunkt. *Ann. d. Phys.* 17, 132, 1905.

[8] R A Millikan. Einstein's photoelectric equation and contact electromotive force. *Phys. Rev.* 7, 355, 1916.

[9] G Wentzel. Zur Theorie des photoelektrischen Effekts. *Zeitschr. Phys.* 40, 574, 1926.

[10] G N Lewis. The conservation of photons. *Nature* 118, 874, 1926.

[11] R Glauber. Coherent and incoherent states of the radiation field. *Phys. Rev.* 131, 2766, 1963.

[12] H R Hertz. Ueber einen einfluss des ultravioletten lichtes auf die electrische entladung. *Ann. Phys.* 267, 983, 1887.

[13] R Hanbury-Brown and R Q Twiss. A new type of interferometer for use in radio astronomy. *Phil. Mag.* 45, 663, 1954.

[14] R Hanbury-Brown and R Q Twiss. A test of a new type of stellar interferometer on Sirius. *Nature* 178, 1046, 1956.

[15] R Hanbury-Brown and R Q Twiss. Interferometry of the intensity fluctuations in light. i. basic theory: the correlation between photons in coherent beams of radiation. *Proc. Roy. Soc.* A242, 300, 1957.

[16] B Zysset, I Biaggio and P. Guenter. Refractive indices of orthorhombic KNbO3. I. Dispersion and temperature dependence. *JOSA B* 9, 380, 1992.

[17] Alexander Ling, Antia Lamas-Linares and Christian Kurtsiefer. Absolute emission rates of spontaneous parametric down conversion into single transverse gaussian modes. *Physical Review A* 77, 043834, 2008.

[18] David C Burnham and Donald L Weinberg. Observation of simultaneity in parametric production of optical photon pairs. *Physical Review Letters* 25, 84, 1970.

[19] Eugene Hecht and Alfred Zajac. *Optics*. Addison Wesley, 1997.

[20] A Gerrard and J M Burch. *Introduction to Matrix Methods in Optics*. Dover, 1994.

[21] J Brendel, Nicolas Gisin, Wolfgang Tittel and Hugo Zbinden. Pulsed energy-time entangled twin-photon source for quantum communication. *Phys. Rev. Lett.* 82, 2594, 1999.

[22] George Gabriel Stokes. On the composition and resolution of streams of polarized light from diferent sources. *Transactions of the Cambridge Philosophical Society* 9, 399, 1856.

[23] Jaroslav Řeháček, Berthold-Georg Englert and Dagomir Kaszlikowski. Minimal qubit tomography. *Phys. Rev. A* 70, 052321, 2004.

[24] Alexander Ling, Soh Kee Pang, Antia Lamas-Linares and Christian Kurtsiefer. Experimental polarization state tomography using optimal polarimeters. *arxiv/quant-ph* 0603126, 2006.

[25] Albert Einstein, B Podolsky and Nathan Rosen. Can quantum-mechanical description of physical reality be considered complete? *Physical Review* 47, 777, 1935.

[26] John S Bell. On the Einstein–Podolsky–Rosen paradox. *Physics* 1, 195, 1964.

[27] Alain Aspect, Philipe Grangier and G Roger. Experimental tests of realistic local theories via Bell's theorem. *Phys. Rev. Lett.* 47, 460, 1981.

[28] C. K. Hong, Z. Y. Ou and L. Mandel. Measurement of subpicosecond time intervals between two photons by interference. *Phys. Rev. Lett.* 59, 2044, 1987.

[29] J D Franson. Bell inequality for position and time. *Phys. Rev. Lett.* 62, 2205, 1989.

[30] Paul G. Kwiat et al. New high-intensity source of polarization–entangled photon pairs. *Phys. Rev. Lett.* 75, 4337, 1995.

[31] Christian Kursiefer, Markus Oberparleiter and Harald Weinfurter. High efficiency entangled photon pair collection in type ii parametric fluorescence. *Physical Review A* 64, 023802, 2001.

[32] Paul G Kwiat, Edo Waks, Andrew G White, Ian Appelbaum and Philippe H Eberhard. Ultra-bright source of polarization-entangled photons. *Phys. Rev. A* 60, R773, 1999.

[33] Pawel Trojek and Harald Weinfurter. Collinear source of polarization-entangled photon pairs at non-degenerate wavelengths. *Appl. Phys. Lett.* 92, 211103, 2008.

[34] T Kim, M Fiorentino and F N C Wong. Phase-stable source of polarization-entangled photons using a polarization sagnac interferometer. *Phys. Rev. A* 73, 012316, 2006.

[35] Alessandro Fedrizzi, Thomas Herbst, Andreas Poppe, Thomas Jennewein and Anton Zeilinger. A wavelength-tunable fiber-coupled source of narrowband entangled photons. *Optics Express* 15, 15377, 2007.

[36] Daniel F V James, Paul G Kwiat, William J Munro and Andrew G White. Measurement of qubits. *Phys. Rev. A* 64, 052312, 2001.

[37] R Azzam and A De. Optimal beam splitters for the division-of-amplitude photopolarimeter. *J. Opt. Soc. Am. A* 20, 955, 2003.

[38] T Sleator and H Weinfurter. Realizable univeral quantum logic gates. *Phys. Rev. Lett.* 74, 4087, 1995.

[39] K Mattle, H Weinfurter, P G Kwiat and A Zeilinger. Dense coding in experimental quantum communication. *Phys. Rev. Lett.* 76, 4656, 1996.

[40] Paul G Kwiat and Harald Weinfurter. Embedded Bell-state analysis. *Physical Review A* 58, R2623, 1998.

[41] Carsten Schuck, Gerhard Huber, Christian Kurtsiefer and Harald Weinfurter. Complete deterministic linear optics Bell state analysis. *Phys. Rev. Lett.* 96, 190501, 2006.